

**Self-Reversal of Remanent
Magnetisation of Basalts — Origin,
Mechanisms and Consequences**

*Inaugural-Dissertation
zur Erlangung des Doktorgrades
der Fakultät für Geowissenschaften der
Ludwig-Maximilians-Universität München*

vorgelegt von

David Krása

15. September 2003

1. Berichterstatter: Prof. Dr. N. Petersen
2. Berichterstatter: PD Dr. T. Kunzmann

Tag der mündlichen Prüfung: 17.11.2003

Contents

Abbreviations and symbols	6
Preamble	9
Zusammenfassung	10
1 Introduction	14
1.1 Magnetomineralogy of basalts	15
1.2 Processes leading to self-reversal of the remanent magnetisation .	19
1.3 Scientific aims	24
2 Rock magnetic properties	26
2.1 Samples	26
2.2 Methods	27
2.3 Measurements of magnetic hysteresis and thermomagnetic curves	28
2.3.1 Olby and Laschamp samples	28
2.3.2 Vogelsberg samples	32
2.4 Low-temperature measurements	36
2.5 Conclusions	43
3 Microscopic observations	45
3.1 Reflected light microscopy	45
3.2 Electron microprobe analysis	53
3.3 Magnetic force microscopy	60
3.3.1 Imaging technique	60
3.3.2 Sample preparation	61

3.3.3	Results and comparison to microprobe and light micro- scopic observations	63
3.4	Conclusions	69
4	Self-reversal of TRM	71
4.1	Continuous thermal demagnetisation	72
4.2	NRM demagnetisation results	75
4.3	Experiments with laboratory thermoremanent magnetisation . . .	85
4.4	The Laschamp event: Geomagnetic origin or self-reversal?	94
4.5	Conclusions	95
5	Numerical modelling	97
5.1	The analytical model of a spherical two-phase grain	98
5.2	Numerical model for arbitrary geometries	102
5.3	Conclusions	111
6	Thellier experiments	112
6.1	Relevant properties of multidomain and partially self-reversed thermoremanence	113
6.2	Sample description and experimental methods	115
6.3	Results	120
6.4	Conclusions	125
7	Summary	127
	Bibliography	130
	Acknowledgements	142
	Curriculum Vitae	144

List of Figures

1.1	Temperature dependence of f_{O_2} in basalts	17
2.1	M_{RS}/M_S versus H_C of Olby/Laschamp samples	29
2.2	$M_S(T)$ curves of Olby/Laschamp samples	30
2.3	Rock magnetic properties of samples from Vogelsberg	33
2.4	M_{RS}/M_S versus H_C of Vogelsberg samples	36
2.5	Typical low-temperature hysteresis loops	38
2.6	Temperature dependence of M_S (Olby/Laschamp)	39
2.7	Temperature dependence of M_S (Vogelsberg)	40
2.8	SIRM measurements on sample V23-1	41
2.9	Temperature dependence of coercive force (Olby/Laschamp)	42
2.10	Temperature dependence of coercive force (Vogelsberg)	43
3.1	Polished section of sample L-1A covered with magnetic colloid . . .	46
3.2	Polished section of sample O-1E	47
3.3	Microscopic detail of sample V25-5	48
3.4	Titanomagnetite grain from sample O-1C	49
3.5	Titanomagnetite grain from sample O-1G	51
3.6	Titanomagnetite grain from sample V28-5	52
3.7	Element distribution of a grain from sample O-1G	55
3.8	Schematic view of the proposed model for partial oxidation	57
3.9	Element distribution of a grain with unfilled crack	59
3.10	Magnetic force microscope at the IRM in Minneapolis	60
3.11	Composite MFM micrograph of grain 2 of sample V27	64
3.12	Micrograph of sample O-1C	65

3.13	Grain from sample O-1G represented by MFM and microprobe . . .	66
3.14	Detail of sample O-1E viewed with different microscopic techniques	67
3.15	Detail of sample V27 viewed with different microscopic techniques	68
4.1	Continuous thermal demagnetisation	73
4.2	Results of single phase samples L-1A and O-2C	76
4.3	Results of sample O-1G	77
4.4	Results of sample V27-0	78
4.5	Results of sample V25-5	79
4.6	Results of sample O-1R	80
4.7	Results of sample O-1C displaying total self-reversal	83
4.8	Results of sample O-1E	84
4.9	Continuous demagnetisation of TRM acquired in varying H_{ext} . . .	86
4.10	Continuous demagnetisation of pTRM(500 °C,220 °C,25 μ T) . . .	87
4.11	Continuous demagnetisation of pTRM(600 °C,210 °C,25 μ T) . . .	89
4.12	Continuous demagnetisation of pTRM(600 °C,210 °C,25 μ T) for samples with high $T_C(1)$	91
4.13	Alternating field demagnetisation of pTRM(600 °C,210 °C,25 μ T)	92
5.1	Spherical two-phase model	99
5.2	Results for spherical model	100
5.3	Results for spherical model with blocking condition for phase B .	102
5.4	Results of numerical calculations for spherical model	105
5.5	Magnetisation structure for the spherical grain	106
5.6	Result for spherical model with phase A consisting of one cell . .	107
5.7	Rectangular two-phase model grain	108
5.8	Results of numerical calculations for rectangular model	109
5.9	Magnetisation structure for the rectangular grain	110
6.1	Low-temperature SIRM warming curves of the synthetic samples .	117
6.2	Viscous decay of SIRM for sample W1	118
6.3	Scheme of the proposed additivity check	119
6.4	Results of the Thellier experiments	121
6.4	(<i>continued</i>)	122

List of Tables

2.1	Rock magnetic parameters of Olby and Laschamp samples	31
2.2	Rock magnetic parameters of Vogelsberg samples	34
3.1	Microprobe analysis: Elements, spectrometers, analysis crystals .	54
4.1	Results of pTRM(600 °C,210 °C,25 μ T) demagnetisation	90
6.1	Rock magnetic parameters of synthetic magnetite samples	116
6.2	Results of the palaeointensity experiment	123

Abbreviations and symbols

Abbreviations

AC	additivity check
AF	alternating field
CRM	chemical remanent magnetisation
FC	field cooled
FFT	fast Fourier transformation
Hem	hematite
HI	hemoilmenite
Ilm	ilmenite
IRM	isothermal remanent magnetisation
LT	low-temperature
MD	multi-domain
MFM	magnetic force microscopy
MOKE	magneto-optical Kerr effect
MPMS	Magnetic Properties Measurement System
Mt	magnetite
NRM	natural remanent magnetisation
OP-S	amorphous silica polishing liquid
PSD	pseudo single-domain
pTRM	partial thermoremanent magnetisation
QFM	quartz-fayalite-magnetite buffer
RGB	red-green-blue colour space
RT	room temperature
SD	single-domain
SEM	scanning electron microscopy

SIRMsaturation isothermal remanent magnetisation
SP superparamagnetic
TD two-domain
TM titanomagnetite
TCRM thermochemical remanent magnetisation
TRM thermoremanent magnetisation
Usp ulvospinel
VFTB Variable Field Translation Balance
VSM Vibrating Sample Magnetometer
ZFC zero field cooled

Symbols and constants

a_0 [Å]lattice parameter
f_{O_2} [Pa] oxygen fugacity
H [T] magnetic field
H_C [T] coercive force
H_{CR} [T]remanence coercivity
H_{ext} [T] external field
H_{int} [T] internal field
J_S [$\frac{A}{m}$]saturation magnetisation
K [$\frac{J}{m^3}$]magnetocrystalline anisotropy constant
m [Am^2] magnetic moment
M [$\frac{Am^2}{kg}$] specific magnetisation
M_R [$\frac{Am^2}{kg}$] remanent magnetisation
M_{rem} [$\frac{Am^2}{kg}$]remaining magnetisation (after demagnetisation)
M_{RS} [$\frac{Am^2}{kg}$] specific saturation remanence
M_S [$\frac{Am^2}{kg}$] specific saturation magnetisation
N_d (<i>w/o dimension</i>) demagnetising factor
Q_{nt} (<i>w/o dimension</i>) KOENIGSBERGER (1936) ratio
S_d (<i>w/o dimension</i>)viscous decay coefficient
T_b [°C] blocking temperature
T_C [°C] Curie temperature

T_k [K]	isotropic point of magnetocrystalline anisotropy
T_K [°C] or [K]	compensation temperature
T_{ub} [°C]	unblocking temperature
T_V [K]	temperature of Verwey transition
x (<i>w/o dimension</i>)	composition parameter of titanomagnetites
y (<i>w/o dimension</i>)	composition parameter of hemoilmenites
z (<i>w/o dimension</i>)	oxidation parameter
κ (<i>w/o dimension</i>)	magnetic volume susceptibility
λ [Å]	wavelength
λ_s (<i>w/o dimension</i>)	magnetostriction constant
μ [$\frac{Vs}{Am}$]	magnetic permeability
$\mu_0 = 4\pi \cdot 10^{-7} \frac{Vs}{Am}$	vacuum permeability

Preamble

Parts of this thesis are based on, or directly taken from papers published or to be published in scientific journals. Below, these papers are listed in order of their appearance in the text:

Krása, D., 2002. Partial Self-reversal of the NRM in Basalts: Identifying the Responsible Mineral Phases, *IRM Quarterly*, 12(2):3–4.

Krása, D., Heunemann, C., Leonhardt, R. and Petersen, N., 2003. Experimental Procedure to Detect Multidomain Remanence During Thellier-Thellier Experiments, *Phys. Chem. Earth*, 28(16–19):681–687

Heunemann, C., Krása, D., Gurevitch, E.L., Soffel, H.C. and Bachtadse, V. Directions and Intensities of the Earth's Magnetic Field During a Reversal: Results from the Permo-Triassic Siberian Trap Basalts, Russia, submitted to *Earth Planet. Sci. Lett.* (in review)

Zusammenfassung

Die natürliche remanente Magnetisierung (NRM) von Gesteinen stellt die wichtigste Informationsquelle über das Verhalten des Erdmagnetfeldes in der geologischen Vergangenheit dar. Insbesondere Vulkanite bieten die Möglichkeit, hochgenaue Daten über die Richtung und vor allem auch die Intensität des Magnetfeldes zur Zeit ihrer Platznahme zu gewinnen. Allerdings bedarf eine derartige, verlässliche Rekonstruktion des Erdmagnetfeldes einer genauen Kenntnis der Minerale, welche die remanente Magnetisierung tragen. Besonders für die Bestimmung der Intensität des Erdmagnetfeldes gelten sehr spezifische Voraussetzungen bezüglich des Remanenzserwerbs, der thermischen Stabilität und des magnetischen Domänenzustands der Magnetominerale.

Der Schwerpunkt der vorliegenden Arbeit wurde auf die Untersuchung von Basalten gelegt, die eine Selbstumkehr der NRM aufweisen. Der Terminus *vollständige* Selbstumkehr umschreibt hierbei das auf den ersten Blick kontraintuitive Phänomen, daß die NRM entgegengesetzt zur Richtung des äußeren Feldes, in dem die Remanenz erworben wurde, gerichtet ist. Eine vollständige Selbstumkehr tritt, wie wir heute wissen, nur äußerst selten auf. Im Gegensatz dazu beobachtet man sehr viel häufiger eine sogenannte *partielle* Selbstumkehr. Hierunter versteht man die Tatsache, daß nur ein Teil der Gesamtremanenz antiparallel zum äußeren Erdmagnetfeld ausgerichtet ist. Partielle wie vollständige Selbstumkehr lassen sich durch die Standarduntersuchungsmethoden der Paläomagnetik nicht identifizieren und bleiben daher üblicherweise verborgen.

In dieser Arbeit wurde in einem ersten Schritt eine große Anzahl von Basalten vermessen, um Proben, bei denen partielle Selbstumkehr auftritt, für weitere Untersuchungen auszuwählen. Die einzige Methode, mit der eine Selbstumkehr

der remanenten Magnetisierung unzweideutig nachgewiesen werden kann, ist die kontinuierliche Messung der Temperaturabhängigkeit der natürlichen remanenten Magnetisierung. Für die weitergehende Untersuchung des Phänomens der Selbstumkehr wurden dann Proben von Basalten der Chaîne de Puys nahe Olby (Frankreich) und von Basalten des Vogelsbergs ausgewählt.

Die Träger der NRM dieser Proben wurden daraufhin mit gesteinsmagnetischen, sowie mikroskopischen und mikroanalytischen Methoden untersucht. Die magnetische Mikrostruktur der magnetischen Erzkörner wurde mittels einer in der Gesteinsmagnetik neuen Methode, der magnetischen Kraftmikroskopie (MFM) analysiert. Diese Methode verfügt im Vergleich zu bisherigen Techniken der Beobachtung des mikromagnetischen Zustands über eine sehr viel höhere Auflösung und Empfindlichkeit.

Die Besonderheiten des Remanenzzerfalls der Proben wurden untersucht, indem das Entmagnetisierungsverhalten künstlich im Labor aufgeprägter thermoremanenter Magnetisierungen (TRM) mit dem Entmagnetisierungsverhalten der NRM verglichen wurde.

Auf der Basis dieser experimentellen Befunde wurde ein numerisches Modell entwickelt, welches bestätigt, daß die mikroskopisch beobachtete Struktur der Magnetominerale eine Selbstumkehr verursachen kann.

Die folgenden Ergebnisse der vorliegenden Arbeit liefern einen wesentlichen Beitrag zum Verständnis der Selbstumkehr und deren Einfluß auf paläomagnetische Daten:

- Das Phänomen der Selbstumkehr wird in den untersuchten Proben durch zwei gekoppelte magnetische Phasen mit unterschiedlichen Blockungstemperaturen T_b verursacht. Bei dem Mineral mit geringerer T_b handelt es sich um den primären, aus dem basaltischen Magma kristallisierenden Titanomagnetit (primäre Phase). Die höhere T_b entspricht einem Titanomaghemit (sekundäre Phase) der durch partielle Tieftemperatur-Oxidation des primären Titanomagnetits entsteht. Die sekundäre Mineralphase bildet schmale Streifen ($\approx 5 \mu\text{m}$ breit) entlang von Rissen, die die ansonsten unveränderte primäre Phase durchziehen. Hierdurch entstehen Kristalle aus innig verwachsenem Titanomagnetit und Titanomaghemit. Es treten also ausgesprochen unterschiedliche magnetische Eigenschaften in ein

und demselben Kristall auf. Indem die verschiedenen mikroskopischen Untersuchungsverfahren auf einzelne Erzkörner angewendet wurden, konnte eine direkte Korrelation zwischen Magnetomineralogie und magnetischen Eigenschaften hergestellt werden.

- Numerische Modellierungen des Remanenzserwerbs zeigen, daß die beobachtete räumliche Verteilung zweier magnetisch unterschiedlicher Phasen innerhalb eines Partikels und die magnetischen Eigenschaften der zwei Phasen dazu führen, daß sowohl partielle als auch vollständige Selbstumkehr auftritt. Durch die numerischen Simulationen und weitere experimentelle Ergebnisse konnte nachgewiesen werden, daß die beiden in den untersuchten Proben vorhandenen magnetischen Mineralphasen durch magnetostatische Wechselwirkung gekoppelt sind.
- Die Untersuchungen deuten darauf hin, daß der Prozess der Tieftemperatur-Oxidation und damit die Bildung der sekundären magnetischen Phase während des primären Abkühlens bei Temperaturen im Bereich der Blockungstemperatur dieser sekundären Phase oder darüber stattfindet. Diese Titanomagnetit-Phase ist daher der Träger der stabilen magnetischen Remanenz in Richtung des äußeren Erdmagnetfeldes. Obwohl Titanomagnetit die primäre Phase darstellt, trägt er nicht die primäre Remanenz, sondern ist zumindest zum Teil magnetostatisch an die sekundäre Mineralphase gekoppelt. Durch diesen Prozess der magnetischen Kopplung ist seine Remanenz – zumindest in Teilen – entgegengesetzt zum äußeren Feld gerichtet.
- Beobachtungen mittels magnetischer Kraftmikroskopie zeigen, daß sich die primäre Mineralphase im magnetischen Mehrbereichszustand befindet. Infolgedessen ist die von dieser Phase getragene Remanenz nicht stabil, sondern wird bei Raumtemperatur durch eine viskose Magnetisierung ersetzt. Im Vergleich dazu ist die Remanenz der sekundären Phase aufgrund ihrer höheren Koerzivität sehr viel stabiler.

Für die Proben von Olby ergeben sich aus den magnetomineralogischen Untersuchungen neue Argumente, die für die Existenz des sogenannten *Laschamp* Events sprechen: Wenn die sekundäre Mineralphase mit hoher Blockungstem-

peratur eine stabile Remanenz in Richtung des äußeren Magnetfeldes trägt, besaß das lokale erdmagnetische Feld – im Gegensatz zu den Schlußfolgerungen von HELLER UND PETERSEN (1982a,b) – während der Eruption dieser Basalte tatsächlich inverse Polarität.

Aufgrund ihrer komplexen Magnetomineralogie und des komplexen Remanenzenerwerbs eignen sich Proben, die eine Selbstumkehr aufweisen, nicht für eine Bestimmung der Paläointensität des Erdmagnetfeldes. Um derartige Proben während solcher Experimente zu erkennen und von der weiteren Untersuchung ausschließen zu können, wird eine Erweiterung der bestehenden THELLIER UND THELLIER (1959) Methode vorgeschlagen. Mit Hilfe dieser Modifikation können auch von Mehrbereichsteilchen getragene Remanenzen erkannt werden. Dies bedeutet eine entscheidende Verbesserung der Verlässlichkeit und damit Qualität der gewonnenen Ergebnisse, da Mehrbereichsteilchen einen der häufigsten Gründe für fehlerhafte Paläointensitätsbestimmungen darstellen.

Chapter 1

Introduction

Ainsi, du point de vue physique, il n'est pas absurde d'imaginer que l'aimantation permanente des roches éruptives ou sédimentaires soit dirigée en sens inverse du champ magnétique qui régnait au moment de leur formation (NÉEL, 1951).

Thus, from the physical point of view, it is not absurd to imagine that the permanent magnetisation of eruptive or sedimentary rocks is directed oppositely to the magnetic field at the time of their formation.

This is the first sentence of the conclusions of Néel's study *L'inversion de l'aimantation permanente des roches* published in 1951. Néel develops several mechanisms in this study which could cause a remanent magnetisation directed antiparallel to an applied external magnetic field, a so-called *self-reversed* magnetisation. At that time a number of previous publications had shown that some rocks carry a magnetisation which is reversed with respect to today's Earth's magnetic field. A long standing discussion had evolved if such records of reversed magnetisation are caused by any hypothetical mechanisms of self-reversal inherent to the studied rocks and their magnetic remanence carriers or if the Earth's magnetic field could indeed reverse its polarity. Néel was the first to propose specific physical or magnetomineralogical mechanisms for self-reversal of magnetisation. However, he stressed that these mechanisms were purely theoretically justified and that by the time of publication of his article no actually proven instance of such a self-reversal was found in nature.

Only one year later NAGATA ET AL. (1952) was the first to report on an impressive example of self-reversal of the natural remanent magnetisation in hypersthene hornblende dacite samples from Mt Haruna (Japan). In the following decades several other examples for self-reversal in igneous rocks were discovered. However, for the vast majority of rocks carrying reversed magnetisations it became clear that this magnetisation is indeed caused by a reversed geomagnetic field. Evidence for this conclusion came from the fact that almost all rocks carrying reversed magnetisations could be correlated with other rocks – both sedimentary and igneous – of the same age but different locality and magnetomineralogy which also carried a reversed magnetisation. This demonstrated that complete self-reversal occurs rather scarcely.

However, a more frequent phenomenon especially in basalts is *partial* self-reversal. This term describes the situation that only part of the remanent magnetisation is directed antiparallel to the magnetic field in which remanence was acquired. The net magnetisation, however, remains more or less parallel to this field and only the intensity of remanent magnetisation is reduced. As a result, palaeodirectional studies on rocks exhibiting this behaviour are not necessarily affected whereas determinations of the palaeointensity of the Earth's magnetic field on these rocks are presumably severely biased. Thus, the principal aim of this work is to elucidate the exact magnetomineralogical conditions and physical mechanisms leading to this phenomenon.

1.1 Magnetomineralogy of basalts

The dominant magnetic remanence carrier in basalts is ferrimagnetic titanomagnetite $\text{Fe}_{3-x}\text{Ti}_x\text{O}_4$ ($0 \leq x \leq 1$: composition parameter). It is a member of the magnetite (Fe_3O_4) – ulvospinel (Fe_2TiO_4) solid solution series and has a cubic inverse spinel crystallographic structure. In many cases rhombohedral hemoilmenite ($\text{Fe}_{2-y}\text{Ti}_y\text{O}_3$, $0 \leq y \leq 1$: composition parameter) as a second iron-titanium oxide coexists with the titanomagnetite. Other magnetic minerals like chromium spinel or iron sulfides may also be present in minor amounts but can be neglected with regard to the bulk magnetic properties of basalts. The primary composition and crystallisation temperature of the iron-titanium (Fe-Ti) oxides

depends on the composition of the parent magma and the oxygen fugacity f_{O_2} present in the melt. These relationships were investigated by BUDDINGTON AND LINDSLEY (1964), TAYLOR (1964), CARMICHAEL AND NICHOLLS (1967) and HARGRAVES AND PETERSEN (1971) in great detail. Generally, the crystallisation of Fe-Ti-oxides depends on the following factors:

- The concentrations of FeO, Fe₂O₃, and TiO₂ have to exceed a certain minimum value.
- Furthermore, the concentration ratio $C(\text{Fe}_2\text{O}_3)/C(\text{FeO})$ has to be above a specific threshold value.

If these prerequisites are not met, no Fe-Ti-oxides will precipitate from the melt as was shown by CARMICHAEL AND NICHOLLS (1967) for some samples from the *Cascade Volcanic Province*.

The ratio $C(\text{Fe}_2\text{O}_3)/C(\text{FeO})$ is controlled by the following relationships:

- For a given temperature, $C(\text{Fe}_2\text{O}_3)/C(\text{FeO})$ increases with increasing f_{O_2} .
- With increasing temperature $C(\text{Fe}_2\text{O}_3)/C(\text{FeO})$ is decreasing.
- Increasing basicity yields increasing f_{O_2} and thus rising $C(\text{Fe}_2\text{O}_3)/C(\text{FeO})$.

It follows from the second point, that the Fe-Ti-oxides only crystallise below a certain temperature which is depending on the magma composition. This temperature is higher for alkali basalts (up to 1200 °C) than for tholeiitic basalts (between 1000 and 1100 °C).

The Fe-Ti-oxides are among the first minerals to crystallise from alkali basaltic magmas and thus form euhedral crystals. In tholeiitic magmas the crystallisation temperature of Fe-Ti-oxides lies just above the basalt solidus (WRIGHT AND WEIBLEN, 1968) and therefore the crystals have a skeletal shape.

The composition of the oxide minerals depends on the equilibrium f_{O_2} of the basaltic melt at crystallisation temperature. This dependence is shown in Figure 1.1. The range of equilibrium f_{O_2} in basaltic magmas is represented by the vertically hatched area. The f_{O_2} temperature dependence of an average basalt can be approximated experimentally by a quartz-fayalite-magnetite (QFM) buffer

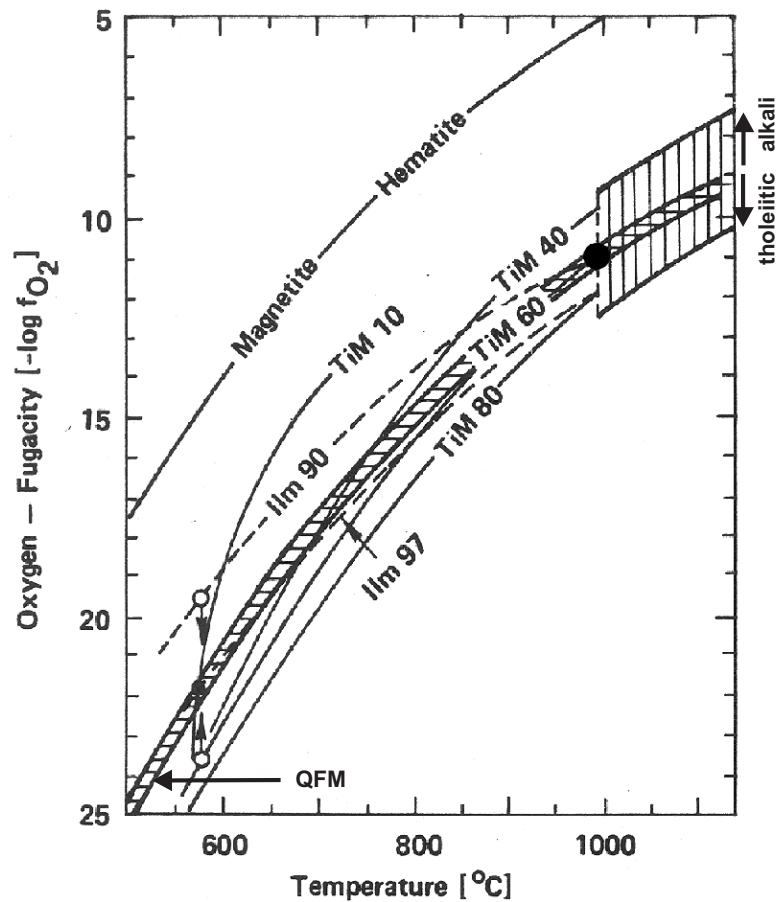


Figure 1.1: Temperature dependence of equilibrium oxygen fugacity f_{O_2} in basaltic magmas (vertically hatched). The area of f_{O_2} in equilibrium with a QFM buffer is hatched horizontally. Depicted are also the f_{O_2} equilibrium lines of coexisting titanomagnetites (black lines) and hemoilmenites (dashed lines). The difference of f_{O_2} in tholeiitic and alkali basaltic magmas is shown schematically by arrows at the right-hand side. Modified after HARGRAVES AND PETERSEN (1971).

which is indicated by the horizontally hatched area. For a crystallisation temperature of 1000 °C, titanomagnetite with 60% ulvospinel (TM60) and hemoilmenite with 90% ilmenite content (HI90) are in equilibrium with the QFM buffer. Generally, for basalts the primary composition of titanomagnetite lies between TM40 and TM85 and the composition of hemoilmenite between HI80 and HI99 (HARGRAVES AND PETERSEN, 1971). However, it has to be noted that this composition is only maintained if the basalt is cooled very rapidly. The reason for that is that the temperature variation of f_{O_2} of the basalt does not coincide

with the temperature dependence of the equilibrium f_{O_2} of the Fe-Ti-oxides. As a consequence, the primary magnetominerals are not in equilibrium with the basalt oxygen fugacity below the crystallisation temperature.

For the case of a primary assemblage of TM60 and HI90 which is cooled to 600 °C, the equilibrium ulvospinel content in the titanomagnetite decreases to 10% and the ilmenite content in hemoilmenite increases to 97% (Figure 1.1). If the system is cooled slowly and the phases are thus able to reach equilibrium, the TM60 will be oxidised to TM10 and titanium will be expelled from the crystal lattice to form ilmenite lamellae pervading the titanium depleted titanomagnetite. These grow preferentially parallel to the {111} planes of the spinel lattice. In turn, the HI90 will be reduced to HI97 and the excess iron will be incorporated in magnetite needles forming within the hemoilmenite. This phenomenon takes place above ≈ 500 °C and is thus termed high-temperature or deuteric oxidation.

At room temperature, unchanged primary titanomagnetites in rapidly cooled basalts are in an extreme state of non-equilibrium. They are thus also subject to oxidation. This process is different from high-temperature oxidation and is called low-temperature oxidation or maghemitisation and the product is labelled titanomaghemite. Low-temperature oxidation is proceeding gradually over geological timescales. The degree of oxidation is quantified by the oxidation parameter z which is defined by the number of Fe^{2+} ions oxidised to Fe^{3+} ions divided by the number of originally present Fe^{2+} ions (READMAN AND O'REILLY, 1972). The oxidised titanomagnetite retains its cubic crystal structure and no second crystallographical phase does evolve. However, the Fe/O ratio decreases in the course of maghemitisation due to Fe migration out of the spinel lattice. Lattice sites formerly occupied by Fe cations are then partially void in titanomaghemite thus forming lattice vacancies. Therefore, titanomaghemite is also termed *non-stoichiometric*. Low-temperature oxidation raises the Curie temperature and lowers the lattice parameter. It has been shown, that low-temperature oxidation proceeds by Fe cations migrating out of the crystal lattice and simultaneous oxidation of the remaining Fe^{2+} ions to Fe^{3+} ions (e.g. GALLAGHER ET AL., 1968; PETERSEN ET AL., 1979, iron migration model). This led to the important conclusion, that the Fe/Ti ratio is decreasing during maghemitisation. With rising number of lattice vacancies, the spinel lattice of the titanomaghemite gets more

and more unstable and eventually may invert to form an intergrowth between Ti-poor titanomagnetite and ilmenite.

The two different oxidation processes significantly affect the magnetic properties of titanomagnetites. High-temperature oxidation produces titanomagnetite with a lower Ti content (composition close to that of magnetite) compared to the primary composition. This in turn leads to an increase of saturation magnetisation M_S and Curie temperature T_C . Additionally, high-temperature oxidation effectively subdivides the crystals into smaller volumes, thus causing an increased coercive force H_C . All these changes take place during or shortly after the extrusion of the basalt.

Low-temperature oxidation gives rise to gradual variations of magnetic parameters. With increasing oxidation state, the Curie temperature increases. However, other parameters like M_S and H_C change in a more complicated, non-monotonic manner (e.g. PETERSEN ET AL., 1979; MATZKA ET AL., 2003). Low-temperature oxidation generally occurs after acquisition of the primary magnetic remanence. As a consequence, the latter is also affected by maghemitisation.

1.2 Processes leading to self-reversal of the remanent magnetisation

As mentioned above, NÉEL (1951) was the first to propose theoretical mechanisms leading to self-reversal of the remanent magnetisation. These mechanisms can be subdivided into two classes: Single-phase models and models with two participating magnetic mineral phases. For the case of only one magnetic phase, the author noted that the peculiar properties of ferrimagnetic minerals can lead to a self-reversed remanent magnetisation. A ferrimagnetic mineral is defined as having two magnetic sublattices consisting of magnetic moments m_A on tetrahedrally coordinated lattice sites (A-sublattice) and magnetic moments m_B on octahedrally coordinated lattice sites (B-sublattice). The moments m_A and m_B are directed antiparallel. If the spontaneous magnetisation of the two sublattices is unequal, the material is called ferrimagnetic.

The behaviour of these substances can be grouped into different types, depending on the different temperature dependence of spontaneous magnetisation of the two sublattices $M_{SA}(T)$ and $M_{SB}(T)$, respectively (NÉEL, 1948). Significant for self-reversal is the so-called Néel N-type: In this case the total spontaneous magnetisation $M_S(T) = M_{SA}(T) + M_{SB}(T)$ reverses sign at a specific compensation temperature T_K , as e.g. $M_{SA} > M_{SB}$ above this temperature and $M_{SB} > M_{SA}$ below this temperature. The same applies in principle for the acquisition of thermoremanent magnetisation (TRM) in a weak external field. Under the assumption that both the blocking temperature T_b of TRM and the compensation temperature T_K are above room temperature and additionally $T_b > T_K$, the N-type mineral will acquire a TRM in an applied external field which is directed parallel to the external field above T_K and reverses sign below T_K . This mineral will thus possess a self-reversed magnetisation at room temperature directed opposite to the external field. The first and so far only example for this type of self-reversal above room temperature was described by SCHULT (1976) in the weathered rim of an alkali basalt hand sample. All other cases of N-type self-reversal reported in the literature have a T_K below room temperature and are thus of minor significance for palaeomagnetism.

Additionally, NÉEL (1951) proposed a second single-phase model for self-reversal: In a ferrimagnetic mineral, the net magnetisation as the sum of the sublattice magnetisations points in direction of the stronger sublattice magnetisation vector. If, by some chemical process, the cations on this stronger sublattice are substituted or removed from the crystal, the antiparallel magnetisation of the previously weaker sublattice outweighs the previously stronger sublattice. Thus, the net magnetisation will change sign. In principle, such a process could occur at ambient temperatures and therefore might account for a self-reversed magnetisation. NÉEL (1951) noted that this type of self-reversal would not be reproducible by laboratory acquisition of thermoremanence. This is because in this case the polarity of remanent magnetisation is a function of time (the reversal being of chemical origin) as opposed to the above mentioned N-type self-reversal where the polarity is a function of temperature.

A third model for self-reversal discussed by NÉEL (1951) involves two different ferro- or ferrimagnetic minerals. Assume that these two phases have the blocking

temperatures T_{bA} and T_{bB} with $T_{bA} > T_{bB}$. Phase B shall consist of randomly oriented single-domain (SD) grains with the shape of a prolate ellipsoid with a demagnetising factor $N_p < \frac{1}{3}$ (SI-units) in direction of the long axis. These are embedded in a spherical region (demagnetising factor $N_s = \frac{1}{3}$) of SD grains of phase A. If this assemblage is cooled from above T_{bA} in an external field H_{ext} , the phase A grains acquire a TRM along the direction of H_{ext} . On further cooling, the temperature will eventually fall below T_{bB} and phase B will thus acquire a TRM in direction of the effective field H_{eff} at the location of phase B grains. H_{eff} consists of the external field H_{ext} , the demagnetising field resulting from the poles on the surface of the spherical phase A region and the demagnetising field from the poles on the inner surface of the cavities filled by phase B grains:

$$H_{\text{eff}} = H_{\text{ext}} - (N_s - N_p) \cdot M_A(T_{bB}) \quad (1.1)$$

where $M_A(T_{bB})$ is the magnetisation of phase A (assumed to be uniform) at T_{bB} . For phase B grains with the long axis parallel to H_{ext} , the term in parentheses becomes positive. The demagnetising field is thus acting opposite to H_{ext} . If this term outweighs H_{ext} , the phase B grain becomes magnetised in H_{eff} antiparallel to H_{ext} . Assuming that the particles of both phases are in the SD range, the temperature dependence of remanent magnetisation $M_A(T)$ and $M_B(T)$ of both phases is proportional to their respective M_S . For $M_A(T_0) < M_B(T_0)$ (T_0 : room temperature), the assemblage will have a self-reversed magnetisation at T_0 , as the reverse magnetisation of phase B outweighs the normal magnetisation of phase A. In the case of $M_A(T_0) > M_B(T_0)$, the remanent magnetisation of the assemblage will decrease below T_{bB} as phase B acquires a remanence but will not change sign. This situation is called partial self-reversal of remanent magnetisation. Note however, that this so-called negative coupling of the two phases is only effective for grains aligned with H_{eff} . The demagnetising factor of phase B grains perpendicular to their long axis is $N_p > \frac{1}{3}$. For grains oriented perpendicular to H_{ext} , the term in parentheses becomes negative and H_{eff} is therefore always directed parallel to H_{ext} leading to positive coupling of the two phases. Nevertheless, NÉEL (1951) proved that an assemblage with randomly oriented phase B grains can acquire a self-reversed magnetisation under the assumption that elongated SD particles can only carry a magnetisation aligned with their

long axis. Phase B grains perpendicular to H_{ext} will only contribute with an induced magnetisation which is in this case negligible compared to the remanent magnetisation of phase A particles and phase B particles oriented parallel to H_{ext} .

Finally, another two-constituent model was proposed by NÉEL (1955). In this model the two magnetic phases with different blocking temperatures are coupled negatively by superexchange interaction across the boundary between the two phases. For this mechanism, the two phases have to be in close contact to each other. Moreover, as UYEDA (1958) pointed out, the crystal lattices of both minerals have to be in good agreement as superexchange interaction is acting on the molecular length scale. In oxide ferri- and antiferromagnets, superexchange interaction between two phases is thought to be mediated via O^{2-} ions which are shared by both crystal lattices at the interface (e.g O'REILLY, 1984). Due to the strict confinement to the boundary layer, this type of interaction is only effective if the low- T_b phase is in the SD range as then the bulk of this phase is coupled to the boundary layer by the ferrimagnetic ordering or in very fine intergrowths with large interfacial surfaces of the two phases.

The first experimental evidence for superexchange interaction between different phases was found for cobalt crystallites which were covered with a fine oxidation layer of CoO (MEIKLEJOHN AND BEAN, 1956, 1957). If one of the two constituents is antiferromagnetic, superexchange interaction can be detected by rotational hysteresis measurements (MEIKLEJOHN, 1962). As a result, a non-vanishing rotational hysteresis loss even in very high fields, a $\sin \theta$ term in torque curves and, under certain circumstances, a shifted magnetic hysteresis loop can be found. In contrast to magnetostatic interaction where the maximum interaction field is in the range of the demagnetising field $N \cdot M$, superexchange interaction yields a very high field in the range of several Tesla which is needed to suppress the coupling (e.g. NAGATA, 1961).

Regarding materials of geological importance, the self-reversal of natural remanent magnetisation (NRM) of the Mt Haruna dacite was finally attributed to superexchange interaction between different disordered and ordered hemoilmenite phases with composition parameter $y \approx 0.5$ (NAGATA AND UYEDA, 1959; MEIKLEJOHN AND CARTER, 1960). A host of other acidic igneous rocks (e.g. andesitic pumice from Nevado del Ruiz (Colombia), dacitic pumices from Mt Shasta (USA)

and Pinatubo (Philippines)) exhibiting self-reversal were studied by several authors (e.g. HAAG ET AL., 1988, 1990a,b; LAWSON ET AL., 1987; PRÉVOT ET AL., 2001; OZIMA AND FUNAKI, 2003) who also determined superexchange coupled hemoilmenite phases as the carriers of self-reversed magnetisation.

In basalts, hemoilmenites are generally paramagnetic at room temperature due to their composition with $y \approx 0.9$ (see section 1.1). They are thus not contributing to the remanent magnetisation at or above room temperature and cannot account for a possibly self-reversed magnetisation. Therefore, the self-reversed magnetisation must in some way reside in the titanomagnetite phase responsible for the remanent magnetisation of basalts. HAVARD AND LEWIS (1965) and OZIMA AND OZIMA (1967) were the first to describe complete and partial self-reversal of magnetisation in basalts after treating them thermally in laboratory experiments. CREER AND PETERSEN (1969) and CREER ET AL. (1970) performing similar experiments, concluded that originally stoichiometric titanomagnetite is gradually oxidised by the heat treatment. They found that after a certain heating time at 400 °C the basalts exhibit two T_C ; the lower one close to the T_C of the unaltered titanomagnetite and a higher T_C near 500 °C. It was shown, that the low- T_C phase can acquire a reversed thermoremanence if the oxidation process is performed in an applied weak magnetic field.

Following these studies, similar heating experiments were performed on a variety of natural (e.g. AGABEKOV AND METALLOVA, 1972; BOL'SHAKOV ET AL., 1973; RYALL AND ADE-HALL, 1975) and synthetic Fe-Ti spinel phases (e.g. PETERSEN AND BLEIL, 1973; TEPLYAKOV ET AL., 1973; PETHERBRIDGE ET AL., 1974; TUCKER AND O'REILLY, 1980). Later, HELLER ET AL. (1979) detected partial self-reversal of the NRM in some basalts from Mt Etna (Italy) without prior thermal treatment, and HELLER (1980) and HELLER AND PETERSEN (1980) found evidence for complete self-reversal in basalts from Olby and Laschamp (France) containing two magnetic phases. Most of the above mentioned authors agreed that the two observed Curie temperatures are caused by some kind of oxidation of the primary spinel phase. However, discussion arose as to the exact nature of the two magnetic phases. The hypotheses brought forward were splitting of phases due to ionic reordering (OZIMA AND OZIMA, 1967), ultrafine exsolution or “unmixing” of the primary titanomagnetite (CREER

AND PETERSEN, 1969; PETHERBRIDGE, 1977), and low-temperature oxidation transforming part of the titanomagnetite to titanomaghemite (HELLER AND PETERSEN, 1982a,b). Similarly, it is still under debate, if the coupling of the two phases is caused by superexchange interaction as in the case of the hemoilmenites in dacitic pumices or by magnetostatic interaction resembling the above described two-constituent model of NÉEL (1951). These discrepancies are partly due to the fact, that the assumed mineral assemblages are difficult to observe directly by microscopic techniques: Either the inferred structures are too small for conventional light-optical microscopy (in the case of ultrafine exsolution) or the two phases (titanomagnetite/titanomaghemite) are hardly discernible due to their very similar optical and chemical properties.

1.3 Scientific aims

This study aims at resolving the ambiguities regarding the phases involved in the phenomenon of complete and partial self-reversal of remanent magnetisation in basalts and their mode of interaction. The sample set used to answer these questions consists of basalts from Olby and Laschamp which are known to exhibit partial self-reversal. Additionally, samples from a lava flow from Vogelsberg (Germany) are studied which show broad variations in their magnetomineralogy. The latter samples were not studied previously regarding their ability to acquire a self-reversed magnetisation. In particular the following points will be addressed:

- Correlation of the phenomenon of self-reversal with the magnetomineralogy and rock magnetic properties of the studied basalts.
- Characterisation of the carriers of magnetic remanence by different microscopic and microanalytical techniques. Of special interest here is the geometry and spatial arrangement of possibly multiple magnetic phases. This information will contribute to the determination of the actual coupling mechanism.
- Comparison of the behaviour of natural remanent magnetisation on the one hand and laboratory induced thermoremanent magnetisation on the other hand.

- Development of a theoretical model which is capable of explaining self-reversal with the observed rock magnetic and microstructural properties. The validity of this model will be checked by numerical calculations.
- Determination of the influence of self-reversal on the reliability of palaeomagnetic information and development of criteria which allow to identify self-reversal by standard palaeomagnetic techniques.

Chapter 2

Rock magnetic properties of self-reversing basalts

2.1 Samples

The basalts investigated in this study originate from two different volcanic provinces: The quaternary *Chaîne de Puys* (France) and the *Vogelsberg* (Germany).

The Vogelsberg volcanic complex covers a surface area of about 2500 km² and consists of both olivine tholeiites and alkaline olivine basalts of Miocene to Pliocene age (WIMMENAUER, 1974). These have been emplaced as lava flows and sheets as well as dykes and vent fillings. The studied samples were taken from a drill core which penetrates a single, \approx 30 m thick basalt flow. The magnetic properties of this drill core were first described by ANGENHEISTER AND TURKOWSKY (1964) and subsequently studied by PETERSEN (1976) due to the large variability in the composition of magnetominerals within a single flow.

The Chaîne de Puys is a range of quaternary volcanoes in the French Massif Central. The composition of the lava flows belongs to the alkaline series olivine poor basalt–trachyandesite–trachyte–rhyolite (WIMMENAUER, 1974). The sample collection of the present investigation was previously studied by HELLER AND PETERSEN (1982a,b) and consists of 25 trachybasalt samples from a single flow near Olby and 4 trachyandesitic samples from an outcrop near Laschamp. BONHOMET AND BABKINE (1967) and BONHOMET AND ZÄHRINGER (1969)

found reversed palaeomagnetic directions in samples from these sites and concluded that the lavas comprise a very recent record of a reversed geomagnetic field. HELLER (1980) and HELLER AND PETERSEN (1982b) contested this hypothesis by demonstrating that the remanence carriers, at least of samples from Olby, exhibit self-reversal of natural remanent magnetisation, a phenomenon which will be studied in detail in the present work.

Volcanic activity in the Chaîne de Puys began around 70 ka BP (VERNET ET AL., 1998). The K-Ar dating for samples with a reversed NRM direction from Laschamp and Olby by BONHOMMET AND ZÄHRINGER (1969) yielded ages between 8000 and 20000 yr. However, HELLER AND PETERSEN (1982b) argued that this first determination was biased by excess argon. Due to the potential importance of the “Laschamp geomagnetic polarity event” as a stratigraphic marker, samples from Laschamp and Olby were subject to a large number of age determinations. An overview of these studies is given in THOUVENY AND CREER (1992). Thermoluminescence ages range from 29.8 ± 3.3 to 35.0 ± 3.0 ka for Laschamp samples and 37.3 ± 3.5 to 44.1 ± 6.5 ka for Olby samples (THOUVENY AND CREER, 1992, and references therein).

2.2 Methods

Magnetic hysteresis parameters and thermomagnetic curves were measured with a *Variable Field Translation Balance* (VFTB) with a maximum field $H_{\max} \approx 0.95$ T. Low-temperature measurements were conducted with a *MicroMag Vibrating Sample Magnetometer* (VSM, $H_{\max} = 1.7$ T) or a *Magnetic Properties Measurement System* (MPMS, $H_{\max} = 5$ T) at the *Institute for Rock Magnetism* in Minneapolis/USA. The VSM was used for determination of the temperature dependence of hysteresis parameters and the MPMS for measuring zero field cooling and warming curves of SIRM and for low-temperature magnetic hysteresis measurements.

For calculation of the hysteresis parameters saturation magnetisation M_S , saturation remanence M_{RS} and coercive force H_C , the paramagnetic susceptibility was determined between 0.8 T and maximum field in the case of VFTB measurements and between 1.2 and 1.7 T for VSM measurements. This slope was then

used for subtracting the paramagnetic signal from the hysteresis curves. The remanence coercivity H_{CR} was determined with the VFTB by measuring back-field curves. Thermomagnetic curves were measured in saturating fields or, where saturation was not possible in the available fields, curves were measured in the maximum field of the VFTB of 0.95 T. For estimating the Curie temperature T_C the paramagnetic component determined from the room temperature hysteresis curve was subtracted. All thermomagnetic curves were measured in air.

2.3 Measurements of magnetic hysteresis and thermomagnetic curves

2.3.1 Olby and Laschamp samples

Samples from Olby and Laschamp can be divided into two major groups: The first group exhibits more than one Curie temperature, the first between 137 °C and 283 °C and the second between 409 °C and 594 °C. The second group shows only one single Curie temperature between 553 °C and 591 °C. These two groups can also be distinguished in terms of magnetic stability. Figure 2.1 shows the ratio of saturation remanent magnetisation M_{RS} over saturation magnetisation M_S versus the coercive force H_C of the sample set. Samples with two Curie temperatures show a lower M_{RS}/M_S ratio and lower coercivity compared to the samples with one T_C .

Thermomagnetic curves can be grouped into four major curve types (see Figure 2.2). Samples with only one Curie temperature show almost fully reversible thermomagnetic curves with a slightly reduced magnetisation in the cooling run (Figure 2.2a). The measured Curie temperatures around 580 °C indicate magnetite as the dominating magnetic phase. Figure 2.2b shows a sample with two Curie temperatures where the curve is also almost reversible. Figures 2.2c and d display non-reversible thermomagnetic curves and two T_C . In Figure 2.2c a second T_C is only faintly visible during the heating run. The second magnetic phase evolves at higher temperatures and the respective Curie temperature becomes clearly visible on cooling. Saturation magnetisation increases after heating to the peak temperature. The fourth group of samples shows a two-phase ther-

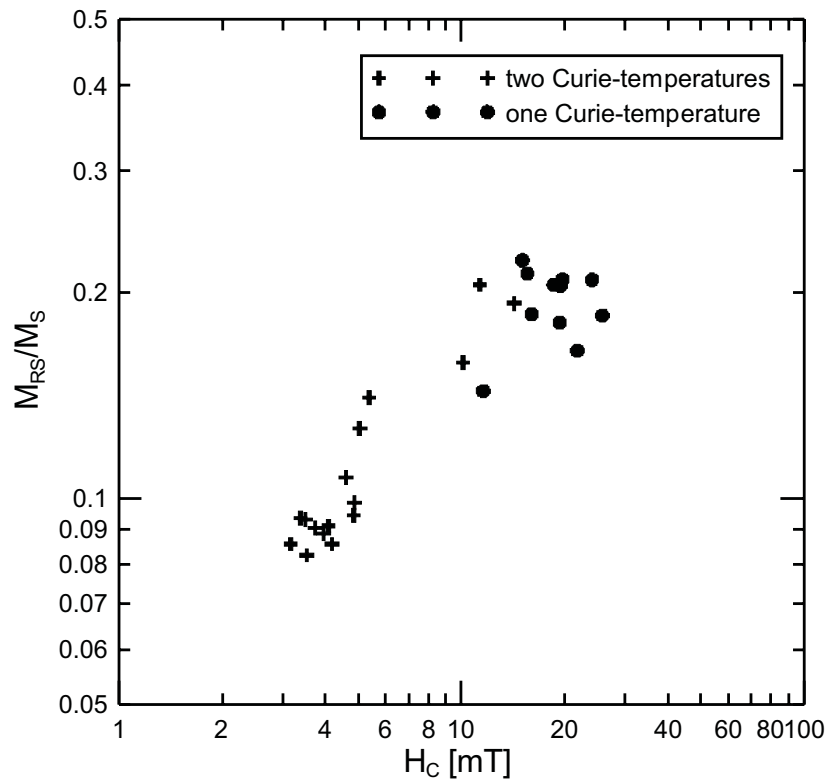


Figure 2.1: M_{RS}/M_S versus H_C of samples from Olby and Laschamp. The higher magnetic stability of samples with one Curie temperature in comparison to samples with two Curie temperatures can be seen from their position in the diagram.

momagnetic curve on heating already (Figure 2.2d). During the heat treatment the overall saturation magnetisation decreases in contrast to group (c), and the cooling curve thus lies below the heating curve. During cooling there are still two Curie temperatures observable, though. Note that after heat treatment, the cooling curves of groups (b), (c) and (d) look very similar having two Curie temperatures in the above mentioned temperature intervals. Rock magnetic parameters and the types of thermomagnetic curves for Olby/Laschamp samples are summarised in Table 2.1.

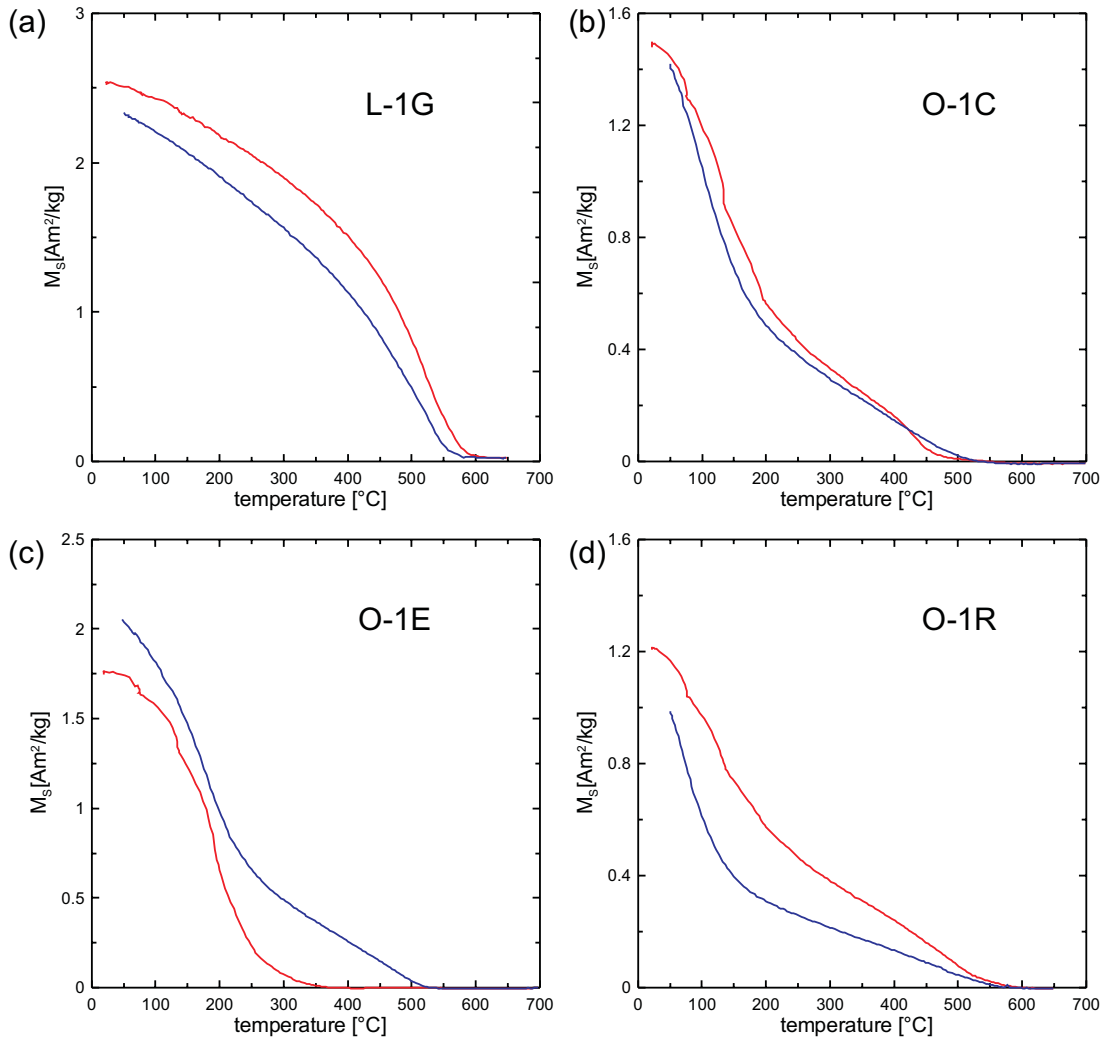


Figure 2.2: Different types of $M_S(T)$ curves measured on samples from Olby and Laschamp. The paramagnetic signal is subtracted. Measurement in air. (a) Typical reversible curve for samples with one T_C . (b) Reversible curve for samples with two Curie temperatures. (c) and (d): Irreversible curves for samples with two Curie temperatures.

Table 2.1: Rock magnetic parameters of Olby and Laschamp samples. For definition of $M_S(T)$ curve types see Figure 2.2.

sample	H_C [mT]	H_{CR} [mT]	M_{RS} [$\frac{Am^2}{kg}$]	M_S [$\frac{Am^2}{kg}$]	$T_C(1)$ [$^{\circ}C$]	$T_C(2)$ [$^{\circ}C$]	H_{CR}/H_C	M_{RS}/M_S	$M_S(T)$ type
O-1A	3.7	10.2	0.14	1.52	196	481	2.73	0.09	b
O-1C	4.1	10.5	0.14	1.50	207	460	2.57	0.09	b
O-1E	5.0	12.1	0.22	1.74	260	582	2.40	0.13	c
O-1G	5.4	12.5	0.26	1.85	270	594	2.32	0.14	c
O-1K	4.6	11.2	0.21	1.98	268	409	2.44	0.11	c
O-1M	3.2	8.9	0.10	1.13	194	464	2.81	0.09	b
O-1N	4.9	13.9	0.19	1.88	194	536	2.86	0.10	b
O-1P	3.4	7.0	0.11	1.21	211	444	2.06	0.09	c
O-1Q	4.8	14.4	0.13	1.39	205	523	2.97	0.09	d
O-1R	4.0	12.7	0.11	1.23	201	528	3.22	0.09	d
O-1S	10.1	28.9	0.35	2.20	160 [†]	520 [†]	2.86	0.16	d
O-2A	3.5	10.7	0.20	2.44	283 [†]	535 [†]	3.02	0.08	c
O-2C	21.8	45.0	0.41	2.49	589	–	2.07	0.16	a
O-2D	19.7	40.0	0.53	2.54	587	–	2.03	0.21	a
O-2F	18.6	38.5	0.54	2.65	589	–	2.07	0.20	a
O-2G	15.0	38.4	0.36	1.63	580	–	2.55	0.22	a
O-2H	19.4	39.2	0.49	2.39	584	–	2.02	0.20	a
O-2I	14.3	33.3	0.50	2.61	240	584	2.34	0.19	b
O-2K	11.3	28.6	0.51	2.50	261	576	2.53	0.20	b
O-2L	15.6	36.2	0.36	1.67	578	–	2.33	0.21	a
O-3C	3.5	9.4	0.10	1.09	137	454	2.68	0.09	b
O-3E	4.2	10.2	0.18	2.11	304	513	2.44	0.09	c
O-3F	11.6	31.2	0.10	0.70	553	–	2.70	0.14	a
L-1A	24.0	49.8	0.39	1.90	587	–	2.07	0.21	a
L-1E	19.4	44.0	0.18	0.98	591	–	2.28	0.18	a
L-1F	25.8	55.7	0.35	1.88	589	–	2.16	0.18	a
L-1G	16.0	36.1	0.45	2.45	582	–	2.25	0.19	a

[†]Curie temperature determined on cooling curve

2.3.2 Vogelsberg samples

The Vogelsberg samples were obtained from drill core B28/1 which penetrates an approximately 30 m thick tertiary basaltic lava flow whose magnetomineralogy has been described by PETERSEN (1976). The author showed that the magnetomineralogy in such thick lava flows does not only depend on the overall chemical composition of the magma and on the intrinsic oxygen fugacity f_{O_2} of the parent magma but also on factors like cooling history and potential differential diffusion of oxygen and hydrogen within the flow. Generally, the composition, grain size and oxidation state of the magnetominerals will vary inside such flows and will largely be dependent on the vertical position within the lava body.

Figure 2.3 and Table 2.2 show the depth dependence of rock magnetic parameters of samples from Vogelsberg drill core B28/1. The Curie temperature shows a peculiar behaviour. The upper two thirds of the drill core have Curie temperatures close to that of magnetite (between 550 °C and 598 °C) whereas samples below 23.0 m exhibit two Curie temperatures.

This lower part of the core can be further subdivided: Samples between 23.0 m and 28.5 m have a lower bulk specific saturation magnetisation M_S , a lower saturation remanent magnetisation M_{RS} and a reduced magnetic stability as reflected by the coercive force H_C compared to the rest. Furthermore, all samples of this depth range have two T_C . The appearance of partial self-reversal (discussed in chapter 4) which is represented by the grey band in Figure 2.3 coincides with this depth interval. For samples below this interval M_S , M_{RS} and H_C increase to values comparable to samples in the upper part above 23.0 m.

Noteworthy is the very high H_C for samples above 23.0 m which reaches values of up to 45 mT. If, according to the Curie temperature of the basalts, magnetite is the main remanence carrying mineral, these high values are typically reached by elongated SD magnetite (PARRY, 1982) and thus point to shape anisotropy as the dominant factor governing magnetic stability. Therefore, elongated or lamellar single-domain magnetite formed by high-temperature oxidation is likely to be the predominant magnetic mineral in this depth interval. This finding will be further discussed in chapter 3 dealing with the microscopic observations.

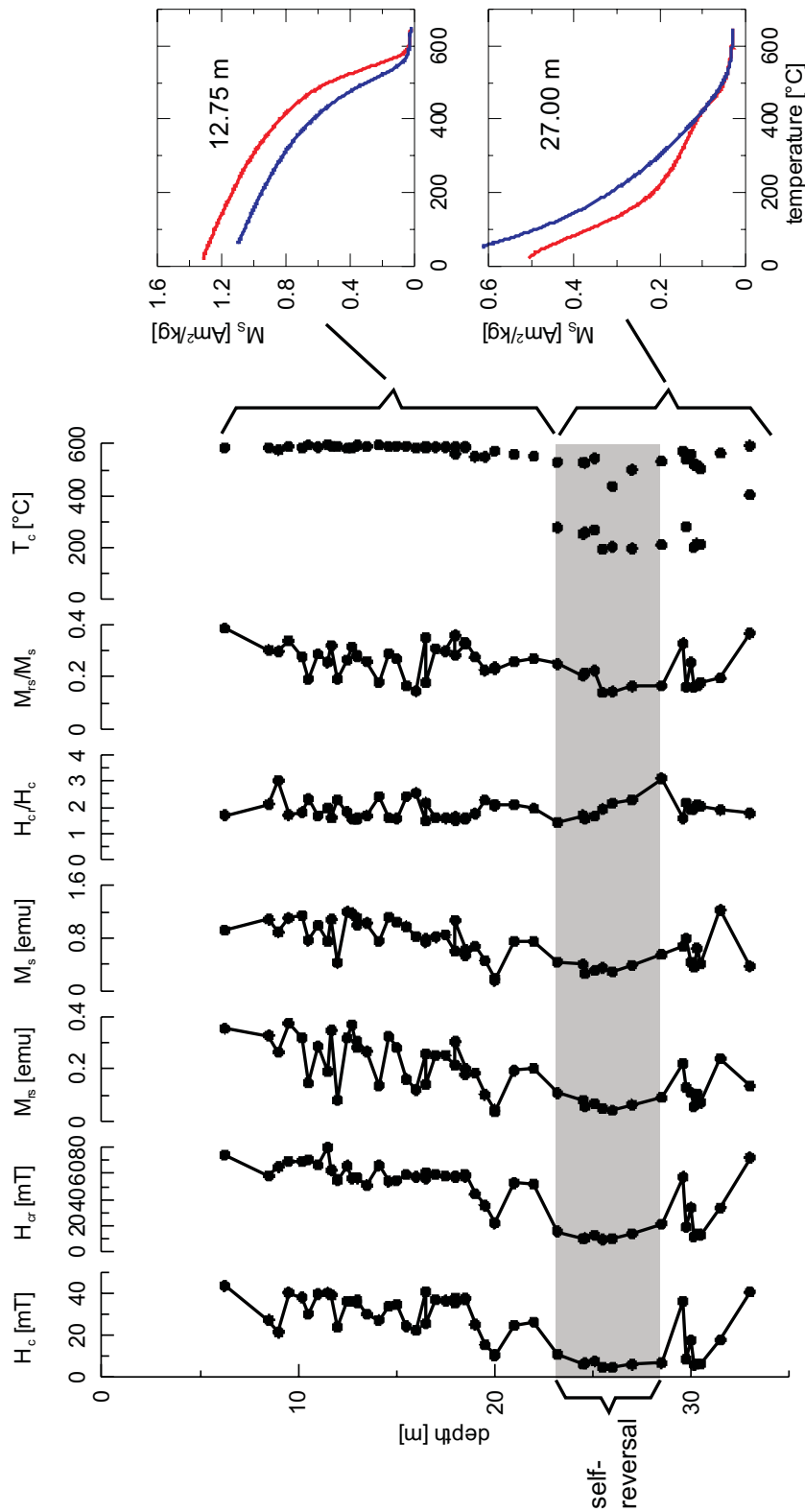


Figure 2.3: Rock magnetic properties of samples from Vogelsberg in dependence of their position in the drill core and typical example $M_S(T)$ curves. The depth interval where partial self-reversal occurs is shaded in grey.

Table 2.2: Rock magnetic parameters of Vogelsberg samples. For definition of $M_S(T)$ curve types see Figure 2.2.

depth	H_C	H_{CR}	M_{RS}	M_S	$T_C(1)$	$T_C(2)$	H_{CR}/H_C	M_{RS}/M_S	$M_S(T)$
[m]	[mT]	[mT]	$[\frac{Am^2}{kg}]$	$[\frac{Am^2}{kg}]$	[°C]	[°C]			type
6.25	43.7	74.2	0.35	0.92	585	–	1.70	0.38	a
8.5	27.4	58.2	0.33	1.09	585	–	2.12	0.30	a
9	21.5	65.0	0.26	0.89	576	–	3.02	0.30	a
9.5	40.6	69.3	0.37	1.11	590	–	1.71	0.34	a
10.2	38.3	69.2	0.32	1.15	586	–	1.81	0.28	a
10.5	30.4	70.4	0.15	0.77	595	–	2.32	0.19	a
11	39.8	66.6	0.29	1.00	588	–	1.67	0.29	a
11.5	40.5	79.7	0.19	0.75	598	–	1.97	0.25	a
11.7	39.2	62.4	0.35	1.09	591	–	1.59	0.32	a
12	24.0	54.9	0.08	0.42	592	–	2.28	0.19	a
12.5	36.3	65.9	0.32	1.20	583	–	1.81	0.26	a
12.75	36.1	56.3	0.37	1.18	584	–	1.56	0.31	a
13	35.8	56.4	0.28	1.00	594	–	1.58	0.28	a
13	37.0	57.0	0.31	1.11	n/d [†]	n/d	1.54	0.28	a
13.5	30.3	51.0	0.27	1.03	590	–	1.69	0.26	a
14.1	27.4	66.2	0.14	0.76	596	–	2.42	0.18	a
14.6	33.9	53.9	0.32	1.12	589	–	1.59	0.29	a
15	34.8	54.6	0.28	1.05	592	–	1.57	0.27	a
15.5	24.4	59.0	0.16	0.98	592	–	2.42	0.16	a
16	22.5	57.4	0.12	0.83	585	–	2.55	0.14	a
16.5	40.9	60.9	0.26	0.74	589	–	1.49	0.35	a
16.5	25.8	56.2	0.14	0.78	585	–	2.18	0.18	a
17	37.1	59.2	0.25	0.82	588	–	1.60	0.31	a
17.5	36.6	57.9	0.25	0.85	588	–	1.58	0.30	a
18	38.1	57.3	0.21	0.60	562	–	1.51	0.36	a
18	35.6	58.0	0.30	1.07	588	–	1.63	0.28	a
18.5	37.5	57.5	0.20	0.62	589	–	1.53	0.32	a
18.5	37.5	59.4	0.18	0.54	587	–	1.58	0.33	a
19	25.3	44.3	0.18	0.67	551	–	1.75	0.27	a
19.5	15.6	35.4	0.10	0.45	550	–	2.27	0.22	a
20	10.7	21.9	0.04	0.19	161	590	2.06	0.23	c
20	10.5	22.1	0.03	0.15	133	572	2.11	0.23	c

[†]not determined

Table 2.2: (continued)

depth	H_C	H_{CR}	M_{RS}	M_S	$T_C(1)$	$T_C(2)$	H_{CR}/H_C	M_{RS}/M_S	$M_S(T)$
[m]	[mT]	[mT]	$[\frac{Am^2}{kg}]$	$[\frac{Am^2}{kg}]$	[°C]	[°C]			type
21	25.0	52.6	0.19	0.75	560	–	2.11	0.26	a
22	26.5	51.8	0.20	0.75	552	–	1.96	0.27	a
23.2	11.0	15.6	0.11	0.43	275	529	1.42	0.25	c
24.5	6.2	10.5	0.08	0.39	250	529	1.69	0.20	c
24.6	6.8	10.6	0.06	0.26	256	526	1.56	0.21	c
25.1	7.7	12.7	0.07	0.30	266	544	1.65	0.22	c
25.5	4.9	9.4	0.05	0.34	191	–	1.94	0.14	b
26	4.7	10.1	0.04	0.29	200	435	2.15	0.14	b
27	6.1	13.9	0.06	0.38	194	500	2.28	0.16	c
28.5	6.9	21.5	0.09	0.55	208	533	3.11	0.17	d
29.6	36.3	57.3	0.22	0.67	572	–	1.58	0.33	a
29.75	8.8	19.1	0.13	0.79	279	542	2.17	0.16	d
30	17.7	33.9	0.11	0.43	559	–	1.92	0.25	a
30.15	6.0	11.7	0.06	0.35	199	520	1.94	0.16	d
30.3	6.6	13.8	0.11	0.64	212	518	2.10	0.16	d
30.5	6.4	13.0	0.07	0.40	208	503	2.04	0.18	c
31.5	17.8	33.8	0.24	1.23	564	–	1.89	0.19	a
33	40.8	72.2	0.13	0.37	402	593	1.77	0.37	d

Figure 2.4 shows the M_{RS}/M_S ratio versus H_C for the whole drill core. The data shows similarity to Figure 2.1 with the Olby/Laschamp samples. Again, samples with one Curie temperature show a higher M_{RS}/M_S ratio and higher H_C than the samples with two Curie temperatures. M_{RS}/M_S is generally higher for the Vogelsberg core compared to Olby/Laschamp samples and lies close to the theoretical value for uniaxial anisotropy (0.5) for some samples of the depth range 6.25 – 22.0 m. Neither Olby/Laschamp nor Vogelsberg hysteresis loops of samples with two Curie temperatures show signs of two ferrimagnetic phases like wasp-waisted loops at room-temperature.

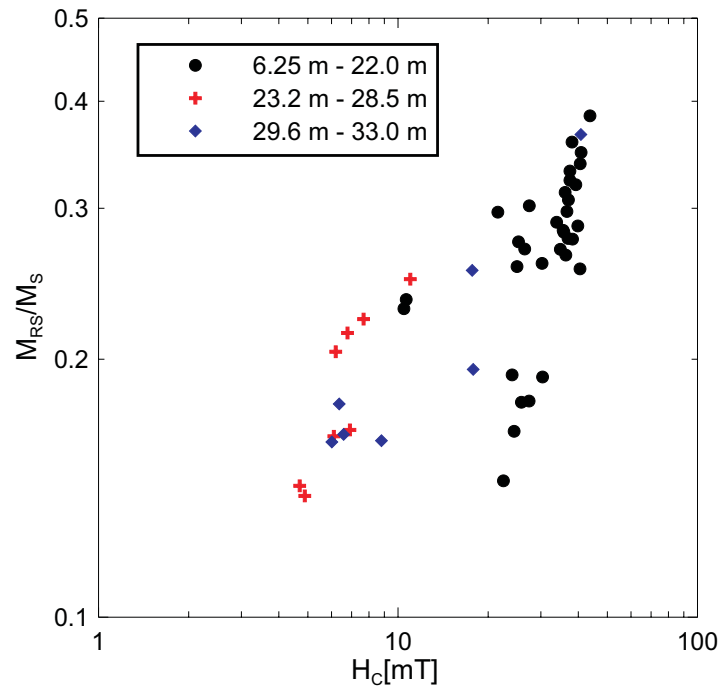


Figure 2.4: M_{RS}/M_S versus H_C of samples from Vogelsberg. Different symbols depict samples from different depth intervals in the drill core.

2.4 Low-temperature measurements

Low-temperature experiments are used to identify certain magnetic minerals in the following ways:

- Observation of characteristic low-temperature crystallographic phase transitions (e.g. VERWEY (1939) or MORIN (1950) transition) which affect magnetic properties.
- Detection of magnetic phases with Curie or Néel temperatures below room temperature.
- Observation of NÉEL (1948) $M_S(T)$ curve types below room temperature.

Hysteresis measurements between 10 K and room temperature (or, in some cases 450 K) were conducted for 17 samples from both sample locations to further characterise the remanence carriers (KRÁSA, 2002). The measurements were performed in 15 K steps with a maximum magnetic field of 1.7 T. A major

instrumental problem with this kind of measurements is the increase of magnetic stability towards low temperatures and thus the incomplete magnetic saturation of certain samples (MATZKA ET AL., 2003). This effect can cause artefacts in the analysis and thus misinterpretation of the data. In order to avoid this problem, some of the samples were also measured with a *Magnetic Properties Measurement System* (MPMS) with a maximum field of 5 T.

In certain cases, the hysteresis loops at temperatures below $\approx 80\text{K}$ exhibit a “goose-necked” or “wasp-waisted” (TAUXE, 1998) shape as shown in Figure 2.5a and b, respectively. These loop types give evidence for either a mixture of SP and SD particles of one and the same magnetic mineral phase or a mixture of different high and low coercivity magnetic mineral phases. To decide, which of these two causes is responsible for the peculiar shape of the hysteresis loops, TAUXE ET AL. (1996) proposed to determine the difference $\Delta M(H)$ between the two irreversible branches of the hysteresis loop and to calculate the derivative $d(\Delta M)/dH$. The authors state, that if plotted versus the field H this derivative yields a single peak representing a single coercivity in the case of SP/SD mixtures and two peaks if two phases with different coercivities are present. The reason for the presence of two peaks is already apparent in the hysteresis loop as a “hump” in the descending branches shortly after field reversal (Figure 2.5a).

In contrast to TAUXE ET AL. (1996) data of ROBERTS ET AL. (1995) show that the lack of such a hump is not necessarily evidence for the constriction of the loop being caused by a mixture of SD and SP particles of one and the same mineral but could also be caused by a mixture of two different mineral phases. Especially if the magnetically softer phase has a much lower coercivity than the harder phase and saturates very quickly (resembling an SP magnetisation curve) the composite data can be very similar to the data measured on SP/SD mixtures. In the absence of intergrain interactions, the hysteresis loop of the composite is obtained by simply superposing the two weighted single phase hysteresis loops (KNELLER, 1962) and the composite H_C will lie close to the value of the softer phase. This effect is very nicely seen in the MD magnetite – hematite mixture of ROBERTS ET AL. (1995). It is very likely that the basalt samples showing only one peak in $d(\Delta M)/dH$ contain a mixture of two different minerals rather than SP particles because the constricted shape disappears at temperatures above 80

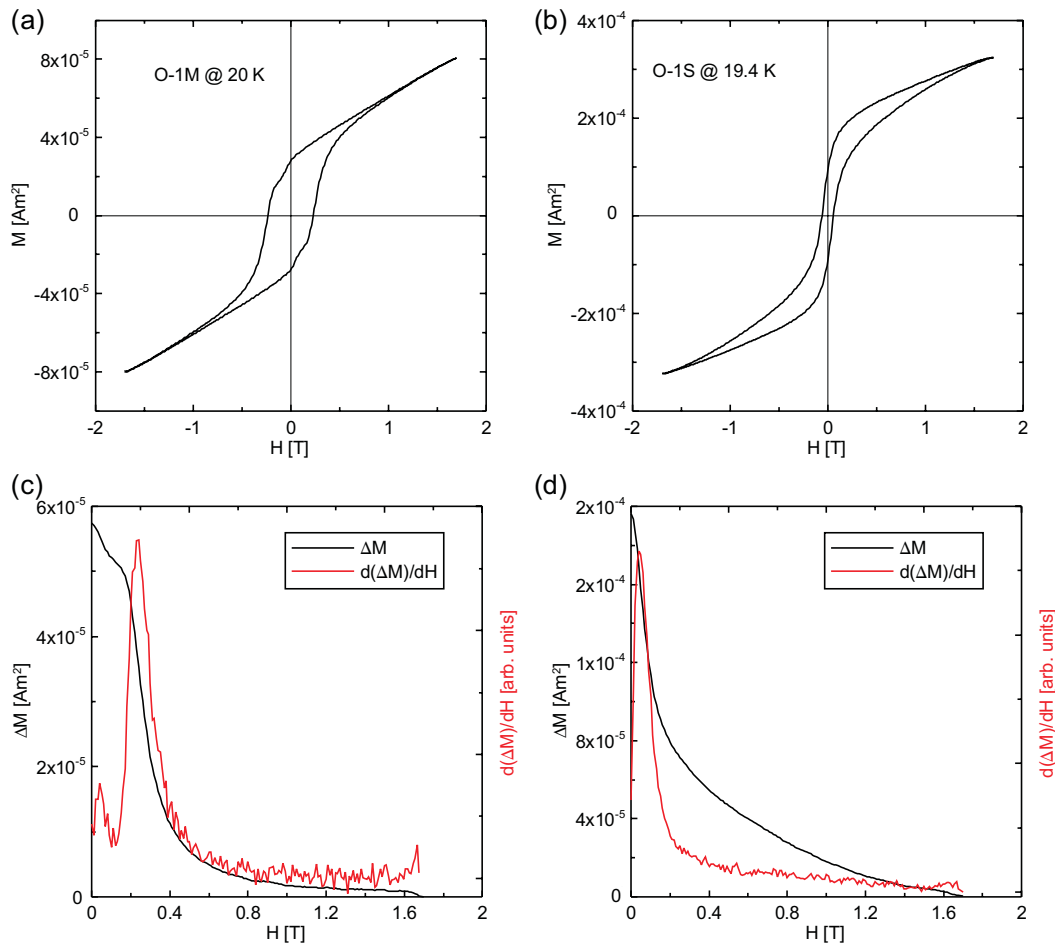


Figure 2.5: Typical low-temperature constricted hysteresis loops ((a) “goose-necked” and (b) “wasp-waisted”) and data analysis after TAUXE ET AL. (1996) ((c) and (d)). The $d(\Delta M)/dH$ plot of sample O-1M (c) shows two peaks typical for a mixture of high and low coercivity phases. Data for sample O-1S (d) shows only one peak.

to 100 K in all cases. If the reason for the constricted loops were SP particles, one would expect that this constriction is visible over the whole temperature range, whereas in the case of two different minerals the peculiar shape will disappear as soon as the Curie or Néel temperature of the low coercivity phase is exceeded.

It has to be noted, though, that analysis of hysteresis loops alone for the identification of magnetic phases in a sample remains highly ambiguous (DUNLOP AND ÖZDEMİR, 1997). Additional, and more significant information can be gathered from analysing the temperature dependence of magnetic hysteresis parameters H_C and M_S .

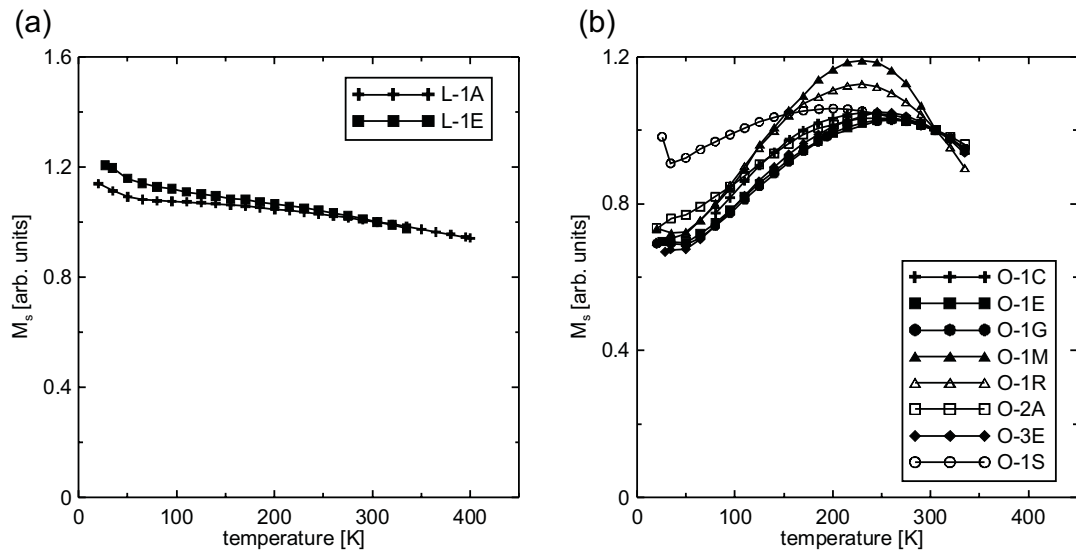


Figure 2.6: Temperature dependence of saturation magnetisation at low temperatures of Olby/Laschamp samples. M_S is normalised on 1 at 300 K. (a) Samples with one Curie temperature. (b) All samples with two Curie temperatures show Néel P-type behaviour.

Figure 2.6 shows the temperature dependence of saturation magnetisation M_S at low temperatures for samples with one Curie temperature (a) and samples with two Curie temperatures (b), respectively. The former show a monotonic decrease of M_S with temperature as expected for samples containing titanomagnetites with a composition close to magnetite. The latter exhibit a more complex behaviour with an increase of M_S up to ≈ 250 K and a subsequent decrease towards higher temperatures. This temperature dependence with a maximum in M_S corresponds to Néel's P-type (NÉEL, 1948) and appears only for titanomagnetites with $x > 0.5$ and titanomaghemites (SCHULT, 1968; KAKOL ET AL., 1991a; MATZKA ET AL., 2003). The same respective curve types are also shown by the Vogelsberg drill core samples, i.e. a monotonic curve shape for samples above 23.0 m and Néel's P-type below 23.0 m (Figure 2.7). P-type samples additionally display a strong increase in M_S towards lower temperatures below ≈ 50 K. MATZKA ET AL. (2003) who carried out similar experiments on the temperature dependence of hysteresis parameters of ocean basalt samples, assign this increase to the Curie temperature of a primary hemoilmenite phase formed coevally with the primary titanomagnetites.

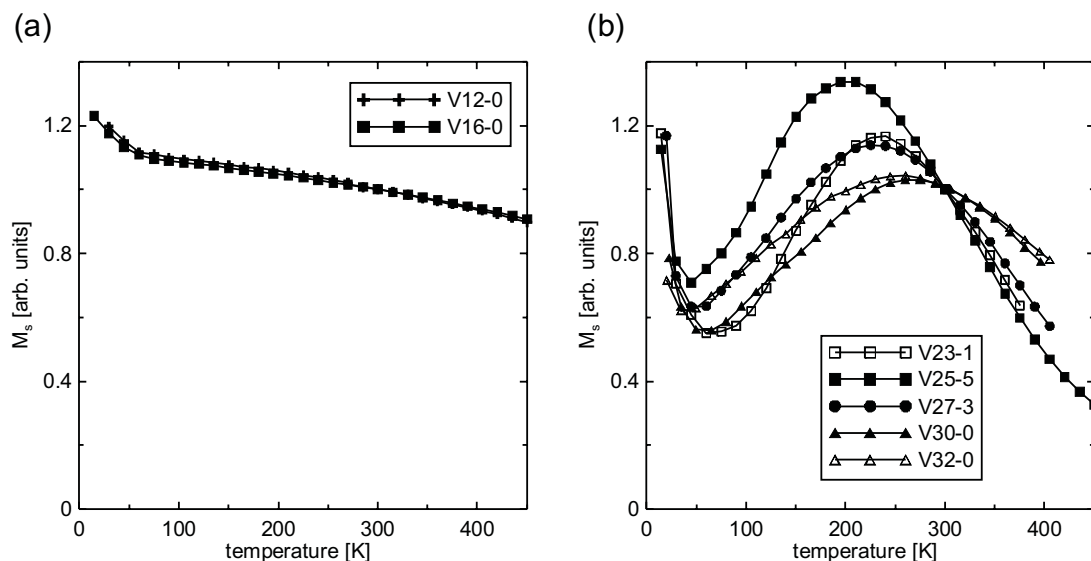


Figure 2.7: Temperature dependence of saturation magnetisation at low temperatures of Vogelsberg samples. M_S is normalised on 1 at 300 K. (a) Samples above 23.0 m (single T_C). (b) Samples below 23.0 m (two T_C). Again, Néel P-type is clearly visible. Additionally, a Curie temperature at ≈ 50 K is discernible which is presumably due to the presence of primary hemoilmenite.

Indeed, reflected light microscopy shows abundant primary hemoilmenite grains in the basalts from Vogelsberg (see section 3.1). The composition of this hemoilmenite phase (and of course also of the titanomagnetite phase) depends on the intrinsic oxygen fugacity of the basaltic melt. According to BUDDINGTON AND LINDSLEY (1964) and TAYLOR (1964) the ilmenite content of the hemoilmenite phase ($\text{Fe}_{2-y}\text{Ti}_y\text{O}_3$ with $0 < y < 1$) coexisting with a titanomagnetite with $x > 0.5$ will be above $y = 0.85$ and thus its Curie temperature will be below room temperature (NAGATA, 1961). For compositions $y > 0.95$ T_C will drop below 70 K. As the Curie temperatures observed in the low-temperature experiments on Vogelsberg samples lie around 50 K, the hemoilmenite composition will be slightly above $y > 0.95$. In any case, the hemoilmenite phase will not contribute to the remanent magnetisation above room temperature.

Sample V23-1 shows the most pronounced minimum shifted to a slightly higher temperature (65 K) compared to the other samples in M_S at low temperatures (Figure 2.7b). This sample was subjected to further MPMS experiments measuring zero field cooled (ZFC) and field cooled (FC) low-temperature satu-

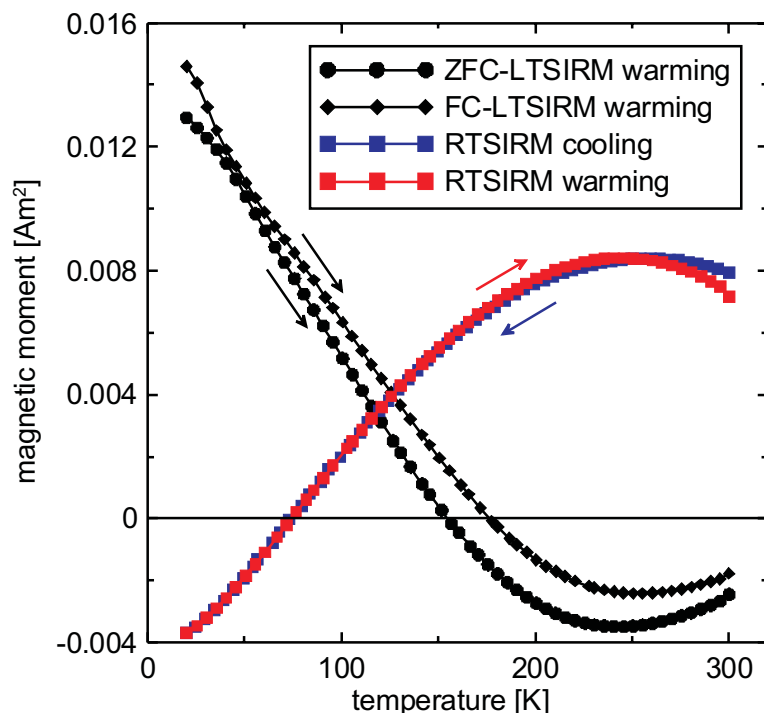


Figure 2.8: Zero field cooled and field cooled low-temperature SIRM warming curves and room temperature SIRM cooling and warming curves measured on sample V23-1.

ration IRM (LTSIRM) warming curves and room temperature saturation IRM (RTSIRM) cooling and warming curves (Figure 2.8). These measurements show that sample V23-1 actually displays Néel's N-type as the magnetisation changes sign in all four experiments. The compensation temperature at which magnetisation is zero in the RTSIRM cooling/warming cycle is 76 K. The difference between ZFC and FC LTSIRM warming curves at temperatures below 50 K is evidence for unblocking of thermoremanence carried by the hemoilmenite phase.

The temperature dependence of coercive force H_C is shown in Figures 2.9 and 2.10. Samples with one Curie temperature of both sample sets (Figures 2.9a and 2.10a) show a marked kink or even minimum in H_C between 110 and 125 K. This feature is typical for titanium poor titanomagnetites ($0 \leq x \leq 0.1$) as the magnetocrystalline anisotropy constant K_1 for TMs of this composition changes sign in this temperature range (SYONO, 1965) at the so-called magnetocrystalline anisotropy isotropic point T_k . As K_1 has a zero-crossing at this point

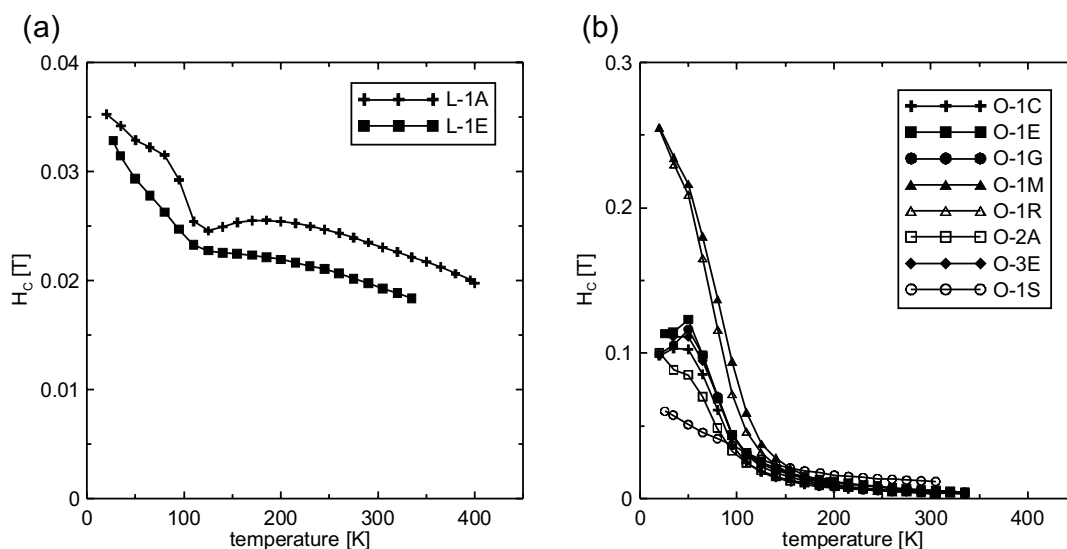


Figure 2.9: Temperature dependence of coercive force at low temperatures of Olby/Laschamp samples. (a) Samples with one Curie temperature. (b) Samples with two Curie temperatures. Note the different scales of the coercivity axes.

also the coercivity will be greatly reduced if the magnetic stability is governed by magnetocrystalline anisotropy. The result is further evidence for the presumed near magnetite composition (exsolved titanomagnetite) of the dominant magnetic phase in these samples.

Samples with two Curie temperatures (Figures 2.9b and 2.10b) show a step increase in H_C towards low temperatures. Similar to the peculiar shape of the M_S temperature dependence this finding can also be explained by titanomagnetite/titanomaghemite as the magnetic phases. Both K_1 (SYONO, 1965; KAKOL ET AL., 1991a,b) as well as λ_{100} (KLERK ET AL., 1977) increase much stronger towards low temperatures for titanomagnetites with $x > 0.5$ than for near magnetite compositions. Noteworthy is the maximum of H_C at temperatures around 50 K measured on two- T_C samples from Vogelsberg (Figure 2.10b). Coercivity is decreasing towards lower temperatures from that point and the magnitude of the phenomenon roughly increases with increasing maximum coercivity at 50 K, i.e. the effect is most pronounced for sample V23-1 with a maximum H_C above 0.3 T and is not detectable for sample V32-0 with a maximum H_C of only 0.064 T. The latter makes it likely that this effect is caused by the coercivity of the hemoil-

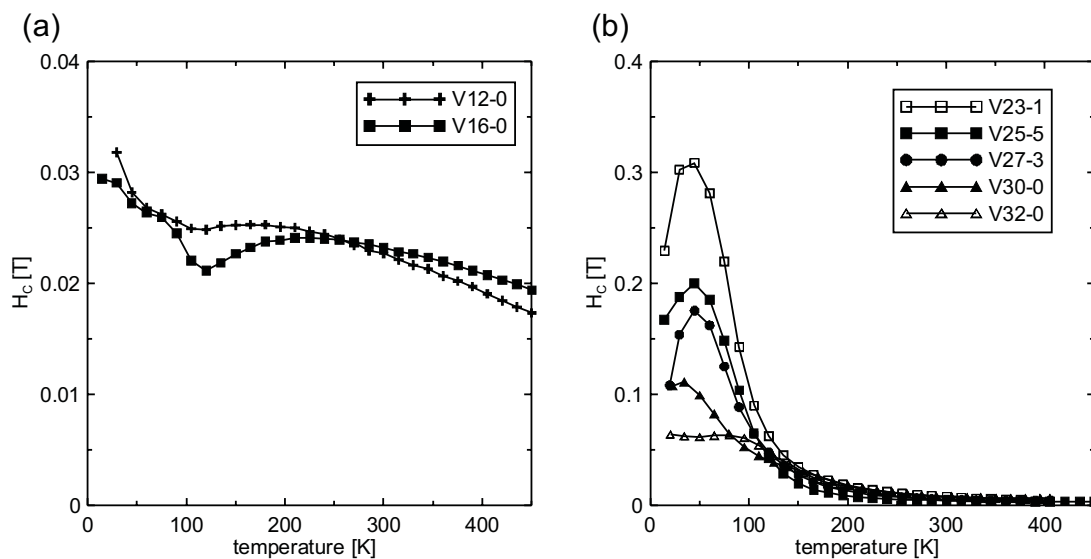


Figure 2.10: Temperature dependence of saturation magnetisation at low temperatures of Vogelsberg samples. M_S is normalised on 1 at 300 K. (a) Samples above 23.0 m (single T_C). (b) Samples below 23.0 m (two T_C). Note the different scales of the coercivity axes.

menite phase which gets ferrimagnetic below 50 K. As discussed earlier, the presence of two coercivities will lead to a constricted hysteresis loop shape and the composite coercivity will be reduced if the hemoilmenite phase has a lower coercivity than the titanomagnetite/titanomaghemite phase. This is quite plausible as this phase has an extremely high H_C of up to 0.3 T at 50 K. Lower titanomagnetite/titanomaghemite coercivities approach the H_C of the hemoilmenite phase and thus the effect will be less pronounced.

2.5 Conclusions

It could be shown that the studied set of samples can be divided into two distinct groups with markedly different magnetomineralogies. The first group consists of samples with only one Curie temperature lying in the range of Ti-poor titanomagnetite or magnetite. The relatively high magnetic stability of these samples makes it likely that the magnetic phase is the result of high-temperature oxidation forming magnetite/ilmenite intergrowths with magnetite being in or near

the single-domain (SD) range. The second group displays at least two Curie temperatures between 137 and 283 °C and between 409 and 594 °C. Keeping in mind the constrictions of magnetomineralogy imposed by basalt petrology (e.g. BUDDINGTON AND LINDSLEY, 1964; HARGRAVES AND PETERSEN, 1971) it is likely that these two Curie temperature ranges correspond to two distinct mineral phases: A non-oxidised or only slightly oxidised pristine titanomagnetite (mother phase) on the one hand and a much higher oxidised titanomaghemite or its inversion product caused by increasing crystallographic instability of titanomaghemite with high z -value on the other hand (daughter phase). One of the main questions regarding the latter group is, if the two spinel phases occur in different grain populations or if they coexist in single grains. This question will be answered by microscopic means in the next chapter.

Chapter 3

Microscopic observations

The aim of the microscopic observations is to identify the two magnetic phases with different Curie temperatures which were detected by rock magnetic measurements described in the previous chapter. As the majority of two- T_C samples exhibits partial or complete self-reversal (see chapter 4), the question arises if the phenomenon is caused by magnetic interactions between these two phases. Magnetostatic or exchange interaction can only occur if the two affected minerals are in close contact to each other. Thus, different microscopic techniques were employed to find possible evidence for such a configuration.

3.1 Reflected light microscopy

The specimens used for microscopic observations were embedded in *Struers Acryfix* synthetic two-component resin. They were then ground on abrasive paper with increasingly finer grain sizes (P220, P320, P500, P800, P1000) and afterwards polished with diamond polishing paste. Here, in a first step the samples were treated for two hours with a diamond grain size of $3\mu\text{m}$ and in a second step for two hours with $0.25\mu\text{m}$ grain size. The light microscopic observations were performed with a *Leitz Ortholux Plan* microscope under reflected light. Specimens from both Vogelsberg and Olby sampling locations show euhedral to subhedral titanomagnetite grains. As already described by HELLER AND PETERSEN (1982b), the magnetic phase has a bimodal size distribution: Grains with a diameter of less than $10\mu\text{m}$ and a smaller number of grains with a size above $30\mu\text{m}$.

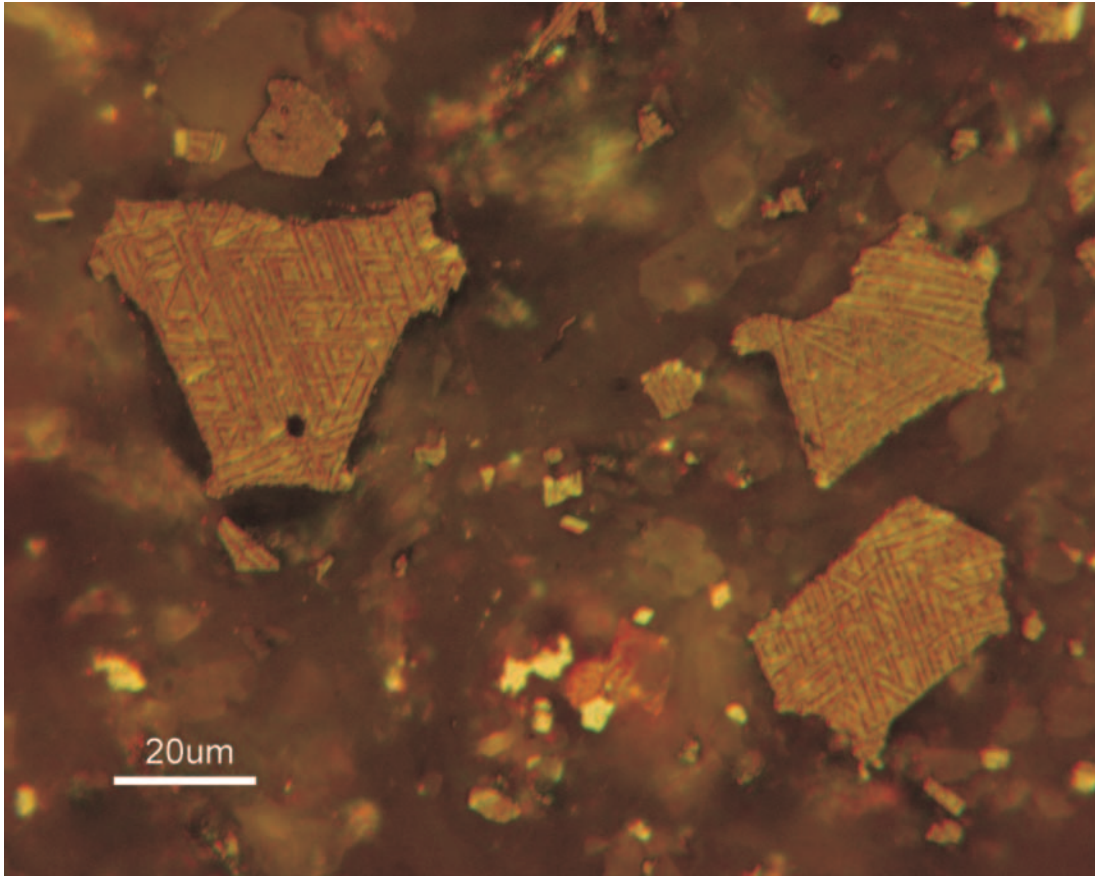


Figure 3.1: Polished section of sample L-1A covered with magnetic colloid in order to distinguish between magnetic (colloid-covered, brownish) and non-magnetic (not colloid-covered, brighter) grains ($50\times$ oil lens). Grains from this sample show exsolved ilmenite lamellae formed by high-temperature oxidation. The ilmenite is not covered by the magnetic colloid.

Samples with a single Curie temperature corresponding to a composition near magnetite (chapter 2) show oxy-exsolution lamellae of alternating titanomagnetite and hemoilmenite (Figure 3.1). The hemoilmenite can be distinguished either by its strong optical anisotropy (RAMDOHR, 1955) absent in titanomagnetite or by covering the polished section with magnetic colloid. As hemoilmenite is paramagnetic at room temperature, it does not attract the colloid. The lamellar structure of the grains is formed by high-temperature oxidation, a process which is caused by the fact that the oxygen fugacity f_{O_2} of the basalt does not change in the same manner as the equilibrium f_{O_2} of the primary ore minerals with

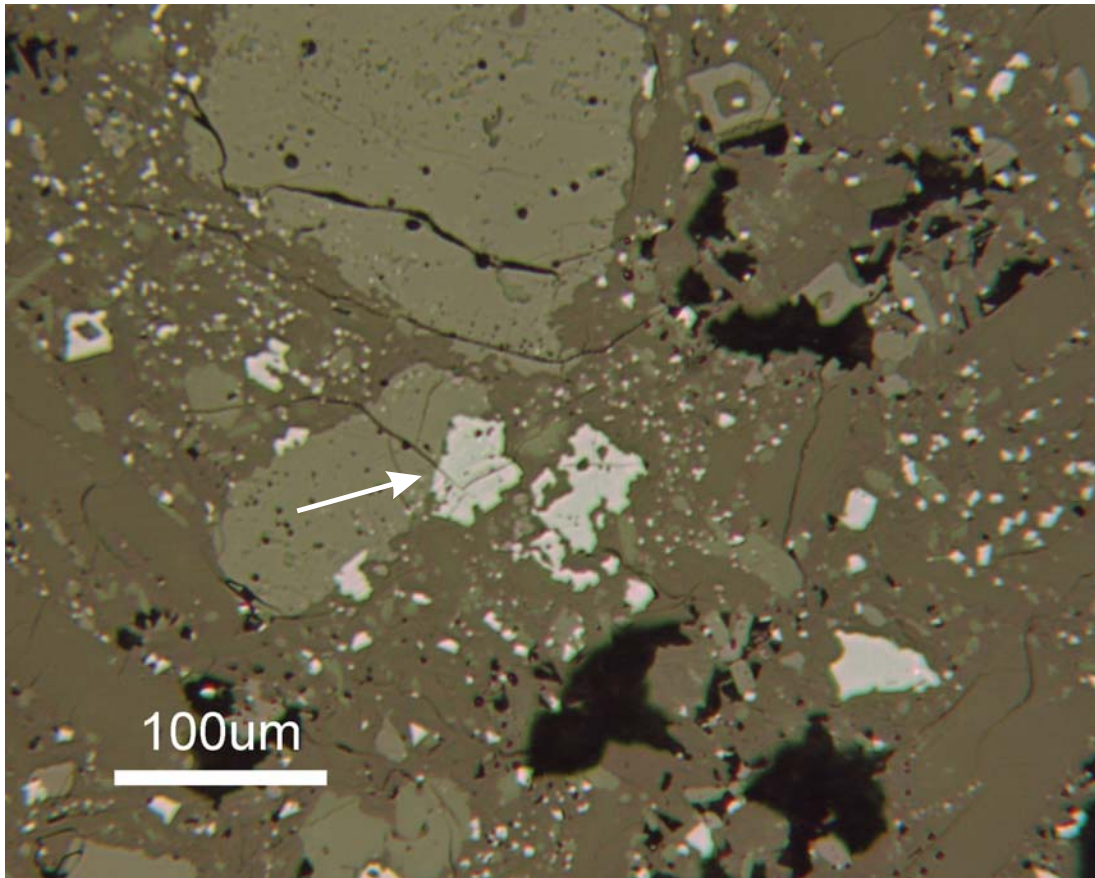


Figure 3.2: Polished section of sample O-1E viewed with low magnification ($10\times$ air lens). A large number of cracks pervading both matrix and ore grains is visible. The arrow marks a crack over the matrix-ore boundary.

decreasing temperature (see section 1.1). The fine exsolution structures explain the high coercivity of single phase samples identified in chapter 2. Due to the subdivision of the grains into fine platelets or needles of magnetite, coercivity is dominated by shape anisotropy and the magnetite shows magnetic single-domain behaviour.

Samples with more than one Curie temperature from Vogelsberg and Olby exhibiting the phenomenon of partial self-reversal do not show any signs of high-temperature oxidation. When these samples are observed with an air lens, a large number of cracks with a width $< 5 \mu\text{m}$ can be found (Figure 3.2). These cracks are not confined to grain boundaries but rather pervade both the matrix minerals and the ore grains. For ease of reference they will be labelled *matrix cracks* in the

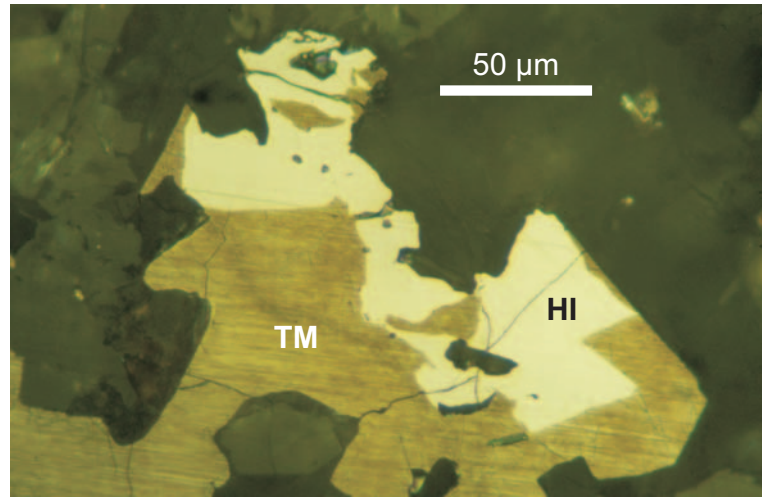


Figure 3.3: Microscopic detail of sample V25-5 ($50\times$ oil lens). The polished section is covered with magnetic colloid. The picture shows a titanomagnetite grain intergrown with hemoilmenite. Titanomagnetite (TM) is covered with colloid whereas hemoilmenite (HI) is not covered as it is paramagnetic at room temperature.

following. These are not to be mistaken for so-called shrinkage cracks which were studied by PETERSEN AND VALI (1987). The latter form by low-temperature oxidation and the related reduction of the titanomagnetite lattice parameter. Shrinkage cracks are therefore confined to the ore grains. Furthermore, they are much narrower ($< 1 \mu\text{m}$) and in most cases only clearly visible after etching the grains with hydrofluoric acid.

Samples from Vogelsberg also contain abundant hemoilmenite in addition to the titanomagnetite phase. The two phases are often intergrown (Figure 3.3). Again, the hemoilmenite can be recognised by not attracting the magnetic colloid. This indicates that this phase is paramagnetic at room temperature and thus will not contribute to the remanent magnetisation at or above room temperature (see also section 2.4).

The larger titanomagnetite grains frequently have an inhomogeneous appearance. The matrix cracks are often filled by a secondary mineral which is much brighter than the titanomagnetite (Figure 3.4). The filling is more resistant to polishing and is thus elevated above the surface of the titanomagnetite. The colour and the polishing properties give rise to the assumption that this sec-

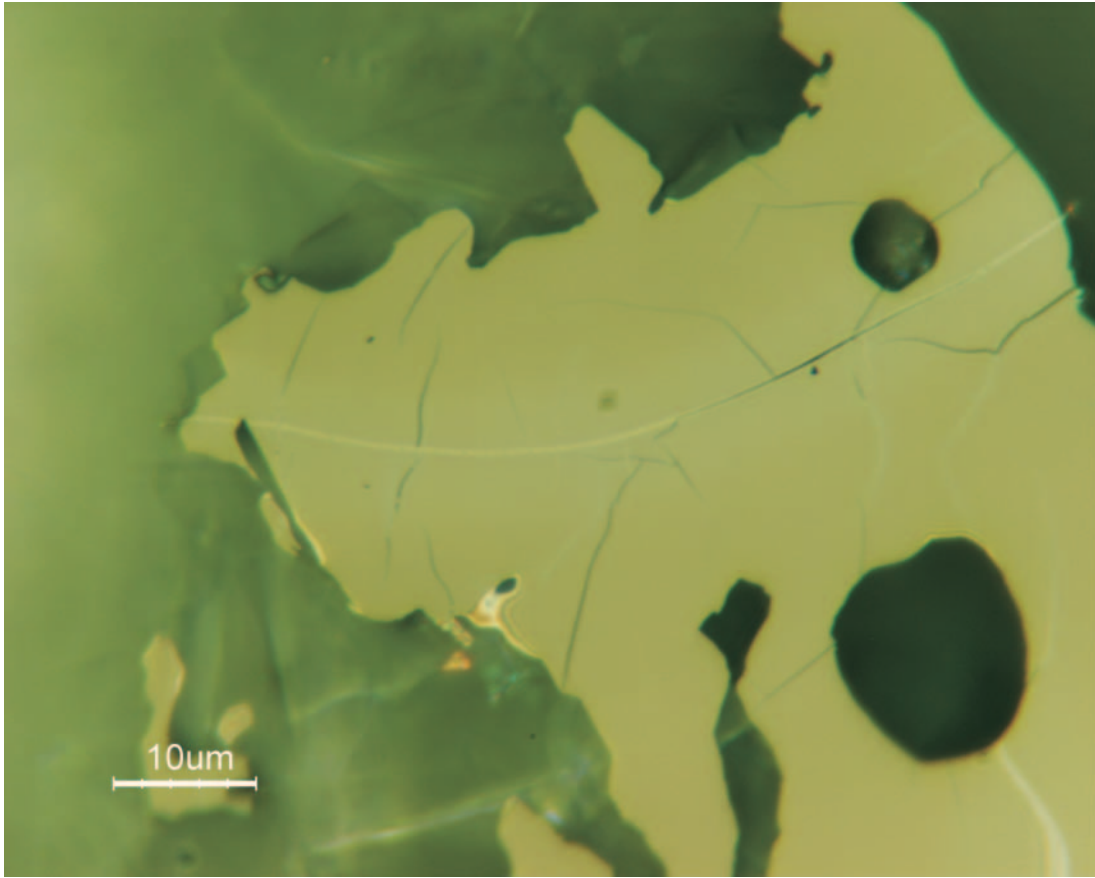


Figure 3.4: Titanomagnetite grain from sample O-1C (125 \times oil lens). The broad crack in the middle of the picture is cutting through both the matrix and the ore grain and is filled by a secondary bright mineral (The crack is not visible in the surrounding matrix as the section is covered with immersion oil). Starting from this broad crack a number of narrower unfilled cracks is penetrating the crystal. The adjacent areas of the grain have slightly brighter colour than the bulk of the titanomagnetite.

secondary mineral is hematite. However, due to the small width of the cracks, optical anisotropy typical for hematite (RAMDOHR, 1955) could not be observed unequivocally. The surrounding titanomagnetite grain shows barely visible colour variations. A narrow band adjacent to the crack is slightly brighter than the rest of the grain. A number of finer and only faintly visible fissures are emanating from the central crack which are penetrating mainly the brighter areas. The colour variations along cracks are visible in all samples exhibiting self-reversal (see chapter 4).

The inhomogeneity of titanomagnetites in Olby samples was also discussed by HELLER AND PETERSEN (1982b) who argued that the brighter colour of some areas in titanomagnetite grains is caused by low-temperature oxidation. This is in accordance with colour descriptions of titanomagnetite and maghemite by RAMDOHR (1955). RAMDOHR describes magnetite as being brownish changing towards a slightly more pink-brownish tone with increasing Ti content. Maghemite is characterised by a brighter greyish appearance¹. Additional evidence for maghemitisation as the reason for the colour change comes from the tiny fissures described above: These can be interpreted as shrinkage cracks which, according to PETERSEN AND VALI (1987), are developing at the surface of a particle. They proceed to the interior of the grain with increasing depth of the maghemitisation front. In the present case, maghemitisation and consequently also the shrinkage cracks are likely to start preferentially at the surface adjoining the larger matrix cracks as this is the only free surface of the grain (see Figure 3.4).

Under natural conditions, titanomagnetite oxidises by removal of iron from the crystal lattice (iron migration model, see section 1.1). In ocean basalts, the removed iron can often be found as a red hematite halo around the ore grains in the silicate matrix. In the samples of this study, hematite is occupying the matrix cracks. This hematite is presumably also a product of the excess iron diffusing out of the titanomagnetite crystal lattice. Evidence comes from the fact that the cracks in the surrounding silicate minerals are void. The presence of hematite in cracks pervading titanomagnetites is thus unlikely to be caused by precipitation from any hypothetical fluids migrating through the cracks. Moreover, occasionally occurring titanomagnetite grains with unfilled cracks do not show any colour variations in the vicinity of these cracks (Figure 3.5). It can be concluded that in this case maghemitisation did not take place. Further evidence for low-temperature oxidation in the vicinity of cracks and for hematite as the secondary mineral will be discussed in section 3.2.

¹Note however, that the colour of minerals can only be judged properly during the actual microscopical observations and in direct comparison to other minerals. The micrographs presented here certainly exhibit significant colour deviations due to the limitations of colour printers. A further potential source of colour deviation might be imperfect calibration of the digital camera regarding the colour temperature of the light source.

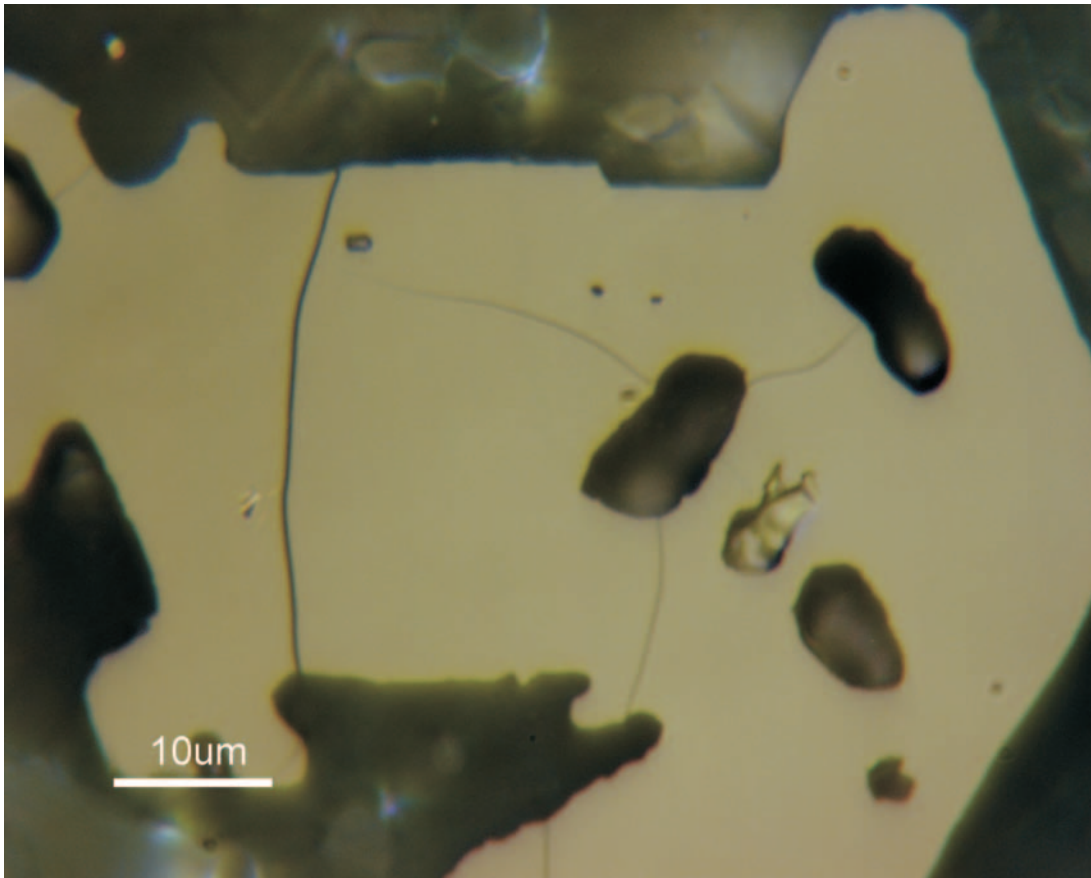


Figure 3.5: Titanomagnetite grain from sample O-1G (125 \times oil lens). The broad matrix crack is not filled by any secondary mineral and the adjacent titanomagnetite does not show any colour variations.

HELLER AND PETERSEN (1982b) found for the samples from Olby that the brighter and darker parts in the inhomogeneously oxidised titanomagnetite grains also show differences in terms of coverage by magnetic colloid. The authors report that the oxidised (brighter) parts along cracks attract less colloid compared to the rest of the grain in the case of a low degree of oxidation and are covered more intensely if the degree of low-temperature oxidation is high. HELLER AND PETERSEN conclude that the amount of colloid covering a certain part of the grain directly reflects the spontaneous magnetisation of the underlying material. This is taken as evidence for the initial decrease and later increase of spontaneous magnetisation during low-temperature oxidation as described by PETERSEN ET AL. (1979). In the present study, a higher colloid density on oxidised parts of grains

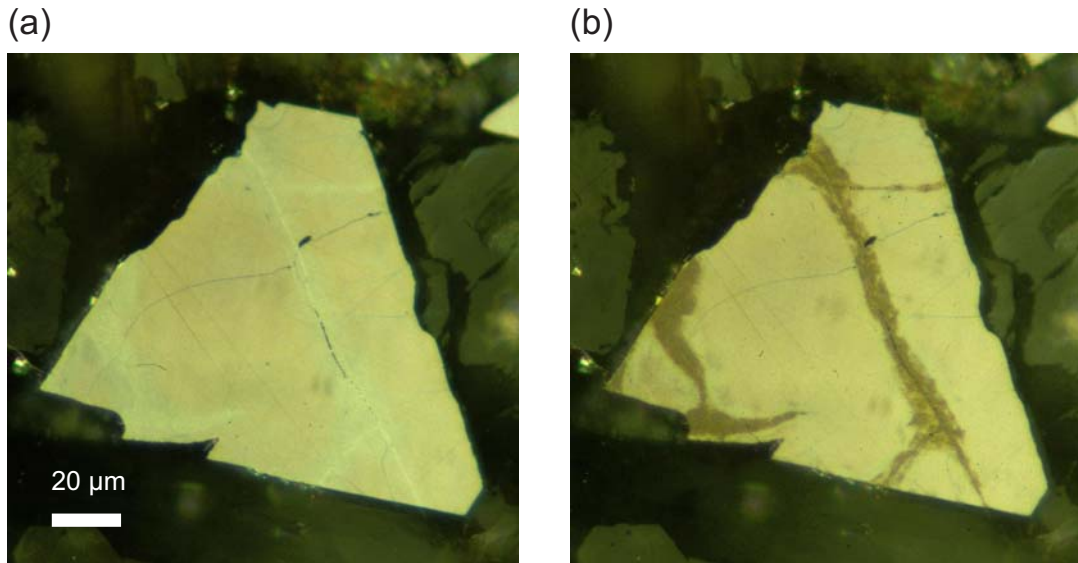


Figure 3.6: Titanomagnetite grain from sample V28-5 ($50\times$ oil lens). (a) The titanomagnetite shows the colour variations due to low-temperature oxidation discussed in the text. (b) The same grain covered by highly diluted magnetic colloid. Only the oxidised parts adjacent to cracks are covered whereas the non-oxidised parts attract practically no colloid at all.

was also found for samples from Vogelsberg (Figure 3.6). It has to be noted though, that the colloid density is not only a function of spontaneous magnetisation but is rather dominated by the gradient of the magnetic stray field and thus also by surface pole density. As will be discussed in section 3.3 in more detail, conventionally polished titanomagnetites have a superficial domain structure which is entirely controlled by surface stress imparted by the polishing process. This causes so-called maze domains (SOFFEL, 1966) which obscure the actual volume domain structure and are characterised by very narrow and kinked magnetic domains. The surface pole density on such a domain structure is unusually high as the magnetisation direction flips on very short length scales. Thus, homogeneous, diamond polished titanomagnetites show a uniform colloid distribution (see Figure 3.3). In partially oxidised titanomagnetites another source of high stress is the variation of the lattice parameter due to maghemitisation. Therefore, the oxidised parts or the border regions between oxidised and non-oxidised areas will presumably be covered more intensely by the colloid independently of spontaneous magnetisation variations.

Based on microscopic observations, there is much debate in the literature if the remanence of igneous rocks in general is carried by large microscopically visible ore grains or rather by the very fine fraction not accessible to classical microscopy. Coarser grains generally dominate strong field magnetic measurements like $M_S(T)$ curves due to their large volume fraction. In contrast, the properties of magnetic remanence can be controlled by the fine grains despite their lower volume proportion, if these are in the SD or PSD range. However, it will be demonstrated in chapter 4 that the temperature dependence of saturation magnetisation on the one hand and thermoremanent magnetisation on the other hand behave in the same manner. This suggests that the inhomogeneous large grains are the dominant remanence carriers of two- T_C samples described in this study and justifies further microscopical investigations on these particles.

3.2 Electron microprobe analysis

To evaluate the cause of colour variations in the titanomagnetite grains, polished sections of three samples were studied with a *Cameca SX50* electron microprobe at the *Section of Mineralogy, Petrology and Geochemistry* of the *Department of Earth and Environmental Sciences* in Munich. Microprobe analysis allows to determine the chemical composition of samples in volumes as small as $\approx 5 \mu\text{m}^3$. An electron beam directed on the surface of a polished section excites the emission of the characteristic X-ray radiation of the contained chemical elements. The X-ray spectrum is then measured by using wavelength dispersive spectrometers to determine the relative content of different elements. If the absolute content of elements has to be determined, the relative values are compared to calibration standards with a known composition. The *Cameca SX50* is equipped with five spectrometers which can be fitted with specific analysis crystals for different elements. The elements determined in this study and the respective analysis crystals are given in Table 3.1. The analysis crystals are diffracting a characteristic line of the x-ray spectrum (in the present case the K_α line of the respective elements) and the intensity of this line is then determined.

In order to study the element distribution over single titanomagnetite grains, analyses were performed on a 256×256 grid covering the particles. Each point in

Table 3.1: Microprobe analysis: Elements, spectrometers, and analysis crystals.

element	Fe	Ti	O	Mg	Si
spectrometer	2	3	4	5	1
analysis crystal	LIF	PET	PC1	TAP	TAP

composition of crystals: LIF: LiF, PET: $C_5H_{12}O_4$, PC1: W/Si Multilayer, TAP: $C_8H_5O_4Tl$

this grid was analysed for 250 to 1000 ms and the results were plotted as micrographs of element abundance. As the main goal was to study inhomogeneities of element distribution, the analyses were not calibrated with standards and thus only relative element distributions were obtained. The electron beam was operated at an energy of 15 keV and a beam current of 40 nA.

Figure 3.7 shows micrographs of a grain from sample O-1G. In order to define the boundary between brighter and darker parts of the grain (red line in the reflected light micrograph, top left), the 24-bit RGB coded picture was transformed into an 8-bit grey scale representation by using the image processing software *LU-CIA 4.6*. Then, a grey scale threshold value of 131 was chosen to transform the picture into a binary image (darker parts 0, brighter parts 1). This representation was then cleaned from noise and flattened and the contour of the thus determined brighter parts of the grain was overlaid on the original light microscopic picture. Therefore, the indicated outline is an objective measure for the colour variations of the grain.

The iron distribution image (top right) shows a high concentration at the filled centre line of the matrix cracks. The crack filling is also characterised by a low content of titanium (middle left) and a high concentration of oxygen (middle right). This element distribution inside the crack is clear indication for the presumed presence of hematite. The light optically darker parts of the primary titanomagnetite grain show a relatively homogeneous Fe content. Approaching the brighter areas, the Fe concentration is decreasing and is lowest at the rim of the cracks. The decrease in Fe corresponds to a slight increase in Ti content. Oxygen is distributed more or less homogeneously over the whole titanomagnetite. The

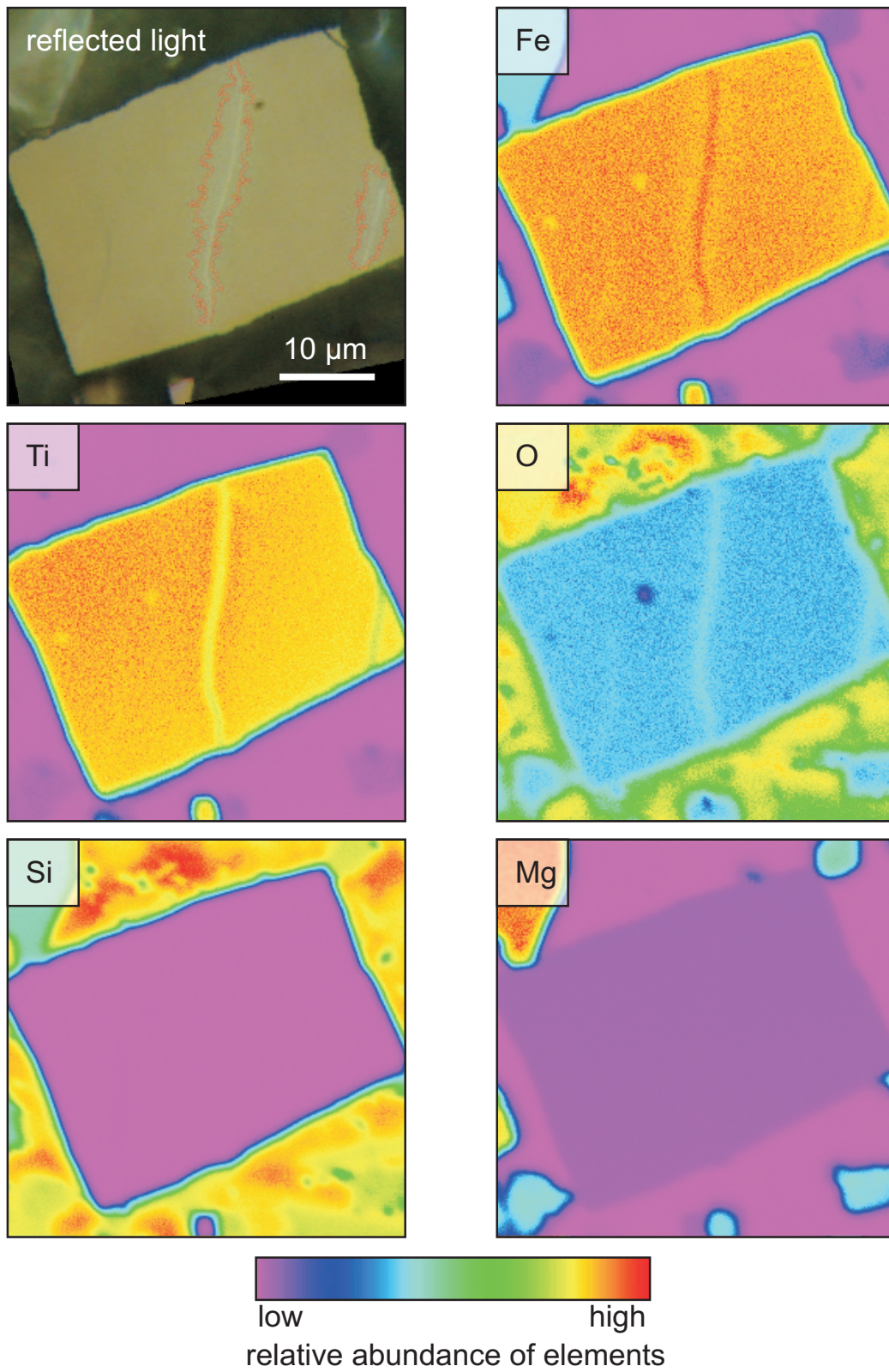


Figure 3.7: Reflected light micrograph and relative element distribution of a grain from sample O-1G.

silicon content (bottom left) is zero in the complete ore grain which indicates that the measured element distribution is not contaminated by the surrounding silicate matrix. This would be the case if certain parts of the polished grain are thin enough for the volume excited by the electron beam to extend into the matrix minerals. A small amount of magnesium is present in the titanomagnetite.

The decrease in Fe towards the crack is evidence for the assumption made in the previous section, that the brighter colour of areas adjacent to cracks is caused by low-temperature oxidation. As discussed before, oxidation proceeds by Fe migrating out of the crystal lattice. The Ti content should in principle remain constant irrespective of the degree of oxidation as Ti is not diffusing out of the crystal during maghemitisation. The higher abundance of Ti in the vicinity of cracks is presumably due to the decreasing lattice parameter in the course of oxidation. Thus, although the number of Ti cations per unit cell remains constant, effectively more Ti cations are inside the volume excited by the electron beam. In any case, the areas affected by low-temperature oxidation as seen from microprobe analysis are in good agreement with the brighter regions in the light microscopic image.

Light microscopic observations from the previous section show that the transition between oxidised and non-oxidised parts of the titanomagnetite grains is remarkably sharp. As low-temperature oxidation is a diffusion phenomenon proceeding gradually, the question arises why oxidation stops some 3 – 5 μm away from the crack. A possible explanation is that the hematite formed by precipitation of Fe migrating out of the titanomagnetite is clogging the crack. In such case the Fe concentration gradient at the border between titanomagnetite and crack vanishes and no oxygen necessary for oxidation is available any more. Consequently, Fe diffusion is suppressed and low-temperature oxidation effectively stops. A scheme of the proposed process is shown in Figure 3.8a. As Fe cations are migrating out of the crystal lattice during oxidation, the charge balance is maintained through the transformation of Fe^{2+} to Fe^{3+} ions by releasing an electron (PETERSEN ET AL., 1979). Inside the crack oxygen is ionised by the free electrons emanating from the titanomagnetite. The ionised oxygen combines with the Fe cations to form hematite. Figure 3.8b shows the presumed Fe concentration gradient along a profile across the titanomagnetite at the beginning of the

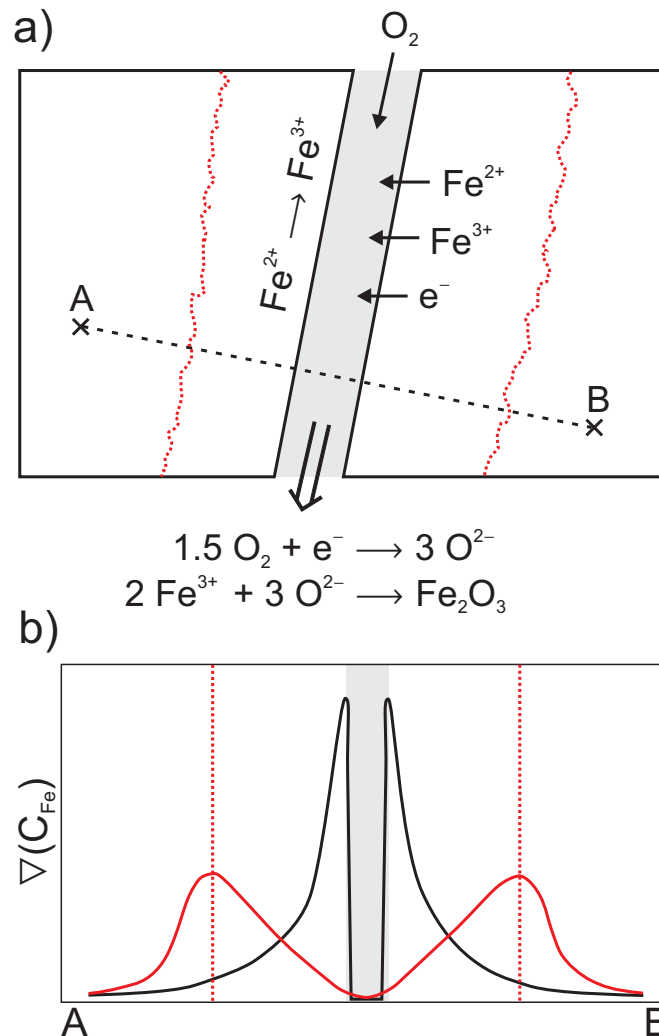


Figure 3.8: (a) Schematic model of a titanomagnetite grain which is subject to partial oxidation. The red dotted line marks the boundary between oxidised and non-oxidised parts. (b) Presumed Fe concentration gradient along the profile marked in (a). Black line: Initial state of the non-oxidised grain. Red line: Concentration gradient after partial oxidation has occurred

process (black line) and after oxidation has proceeded (red line). In the course of oxidation, the maximum of the gradient is shifted from the crack towards the interior of the grain. The sharp border between oxidised and non-oxidised parts might also indicate that oxidation takes place at elevated temperatures (however below the lower temperature limit for pure high-temperature oxidation of approximately 500°C , PETERSEN ET AL., 1979) during the initial cooling of the

basalt. At higher temperatures the diffusion coefficient for Fe is substantially higher compared to room temperature values and oxidation proceeds at higher rates. After cooling to ambient temperatures, the diffusion velocity is reduced and the Fe concentration gradient which is now highest between oxidised and non-oxidised volumes of the grains will persist over long time periods.

Microprobe analyses were also performed on the grain depicted in Figure 3.5 which is penetrated by an unfilled crack. The element distribution images (Figure 3.9) show no indication for Fe migration, implying that no low-temperature oxidation has occurred. The unfilled crack is reflected by a minimum in Fe, Ti, and O. The microprobe analyses on this grain give additional evidence that the hematite present in other cracks is the product of excess Fe migrating out of the spinel crystal lattice.

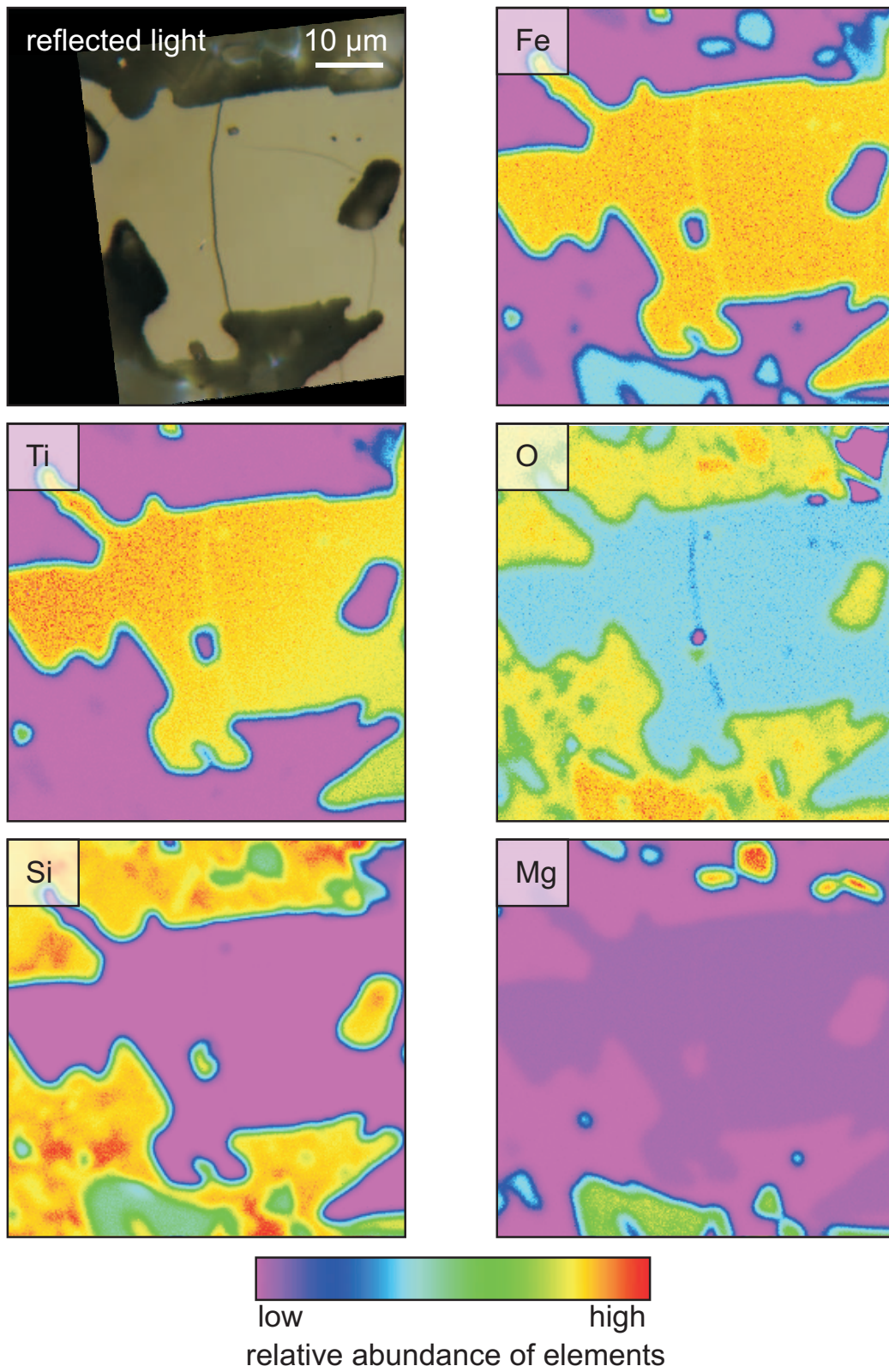


Figure 3.9: Reflected light micrograph and relative element distribution of a grain from sample O-1G with unfilled crack.

3.3 Magnetic force microscopy

3.3.1 Imaging technique

Low-temperature oxidation has a significant effect on the intrinsic magnetic properties of titanomagnetites. Thus, also the magnetic domain configuration is influenced by maghemitisation as shown theoretically by MOSKOWITZ (1980). In order to study the influence of partial oxidation on the domain structure of inhomogeneous ore grains from Vogelsberg and Olby, the samples were imaged by using a *Digital Instruments NANOSCOPE III* Magnetic Force Microscope (MFM) at the *Institute for Rock Magnetism (IRM), University of Minnesota* (Figure 3.10) and a *Digital Instruments NANOSCOPE IV* at the *University of Saarbrücken*. In principle, the MFM technique is sensitive to the interaction between a sample and a magnetised tip which is scanned over the sample's surface. The tip is mounted at the end of an elastic cantilever; the deflection of

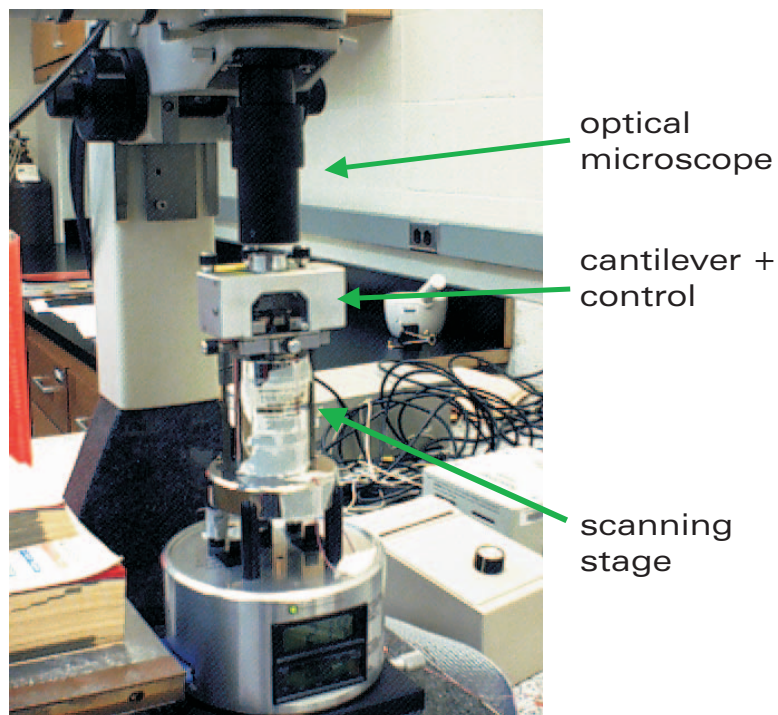


Figure 3.10: Magnetic force microscope at the Institute for Rock Magnetism (IRM) in Minneapolis.

this cantilever is proportional to the force exerted by the magnetic stray field \vec{B} of the sample on the magnetic moment \vec{m} of the tip (SCHÖNENBERGER AND ALVARADO, 1990). Assuming, that the magnetisation of the tip is that of a point dipole, this force is defined by

$$\vec{F} = (\vec{m} \cdot \nabla) \vec{B}. \quad (3.1)$$

The instrument was operated in tapping/lift mode, i.e. the tip is excited at its resonance frequency ω_0 without external forces. The tip passes each scanning line twice. First the topography is mapped, then the tip is lifted a certain distance (50 nm in this study) and the magnetic signal is recorded. Regarding the magnetic force, the tapping mode allows to measure either the amplitude variations ΔA of the oscillation or the phase shift of the output signal due to the change of the resonance frequency of the cantilever in the presence of an external force. The amplitude and frequency variations are proportional to the force gradient (RUGAR ET AL., 1990) and are defined by

$$\Delta A = \left(\frac{2A_0Q}{3\sqrt{3}k} \right) F' \quad (3.2)$$

$$\Delta\omega = \frac{\omega_0}{2k} F', \quad (3.3)$$

where A_0 : oscillation amplitude without external force, Q : quality factor of the resonance, k : spring constant of the cantilever, F' : force gradient.

As the phase difference between input and output signal changes very rapidly (depending on the damping) between 0 and $-\pi$ at the resonance frequency ω_0 of the oscillating system, the phase shift is very sensitive to changes in ω_0 . Thus, for achieving a higher sensitivity, the magnetic force gradient is measured by the phase shift.

In addition, magnetic domains were also observed with the Bitter technique using magnetic colloid to compare this classical technique to magnetic force microscopy.

3.3.2 Sample preparation

Magnetic domain observations require a special polishing procedure as the sample surface has to be free of any mechanical stresses. These surface stresses cause

so-called maze domain patterns (SOFFEL, 1966) which obscure the actual pattern of volume domains present below the surface. This phenomenon appears pronouncedly on titanomagnetites as these have a much higher magnetostriction constant λ_s than pure magnetite. To avoid this effect, the upper surface layer which is stressed by the mechanical diamond polishing procedure (see 3.1) has to be removed.

SOFFEL AND PETERSEN (1971) accomplished this by ionic etching of the polished sections. However, the degree of etching is sensitive to the chemical composition of the minerals, leading to a relief on the surface. This can yield valuable additional information about the minerals, though in the case of force microscopy the surface has to be as smooth as possible to avoid contamination of the magnetic signal by the topographic signal. This problem applies especially to this study as the ore grains of interest are inhomogeneous titanomagnetites.

Thus, another technique described by HOFFMANN ET AL. (1987) was used in this study. After the last diamond polishing step, additional oxide polishing (*Struers OP-S* suspension) was performed. The polishing liquid consists of colloidal SiO_2 with a grain size of $\approx 0.04\mu\text{m}$ and a slightly basic (pH 9.8) fluid (BJERREGAARD ET AL., 1992). This yields a surface with relatively low mechanical stresses as the polishing process is a combination of chemical and mechanical abrasion.

The main problem of domain observations in natural samples is the generally unknown crystallographic orientation of the grains. If the viewing surface is not aligned with regard to crystallographic axes, intrinsic domain patterns are frequently obscured by features like spike domains. However, this problem arises mainly in magnetic minerals which have a high saturation magnetisation M_S , and whose stability is entirely controlled by magnetocrystalline anisotropy as in the case of magnetite (DUNLOP AND ÖZDEMİR, 1997). AMBATIELLO AND SOFFEL (1996) showed that in titanomagnetites the magnetoelastic anisotropy outweighs magnetocrystalline anisotropy leading to uniaxial anisotropy. Moreover, M_S of titanomagnetite is much lower than of pure magnetite.

AMBATIELLO AND SOFFEL (1996) also demonstrated that the domain patterns in titanomagnetite are strongly dependent on the viewing plane with regard to the magnetisation direction, i.e. domain patterns differ if viewed perpendic-

ular or parallel to \vec{M} , respectively. Thus, before the samples were polished, the NRM direction was measured and each specimen was cut in order to yield two observation surfaces parallel and perpendicular to the bulk NRM direction. Although this procedure does not ensure that the magnetisation of individual grains is oriented in the same direction, a certain directional preference can be expected. MFM observations were performed on 7 samples exhibiting partial self-reversal from both Olby and Vogelsberg sites.

3.3.3 Results and comparison to microprobe and light microscopic observations

The MFM response depends on the gradient of forces between sample and magnetised tip. Therefore, MFM images of domains and domain walls differ from those obtained by the Bitter technique (depending on magnetic field gradient) or the magneto-optical Kerr effect (MOKE) registering rotation of the light polarisation plane. Figures 3.11 and 3.12 show two representative grains with a magnetisation direction predominantly parallel or perpendicular to the viewing plane, respectively. Lamellar domains can be found if the grain is magnetised predominantly parallel to the surface (see area (2) of the grain in Figure 3.11). MFM yields highest contrasts above domain walls as the sample's stray field, and thus the force gradient, is highest there. If the magnetisation direction is oriented perpendicular to the viewing plane (Figure 3.12, upper left corner), neighbouring domains appear alternately black and white as their magnetisation is directed antiparallel and the field leakage is highest above the interior of the domains. When the magnetisation direction of the domains is tilted with regard to the sample surface, MFM yields a pattern which is harder to interpret. This results from the fact that the field emerging from these domains has a relatively complex configuration.

Different domain patterns can often be found in one and the same grain (see Figure 3.11), indicating that the easy axis of the uniaxial titanomagnetites can have varying directions across the grain (APPEL AND SOFFEL, 1984; AMBATELLO AND SOFFEL, 1996). Frequently, very narrow "batch-like" domain configurations can be observed in certain parts of grains (area (1) in Figure 3.11).

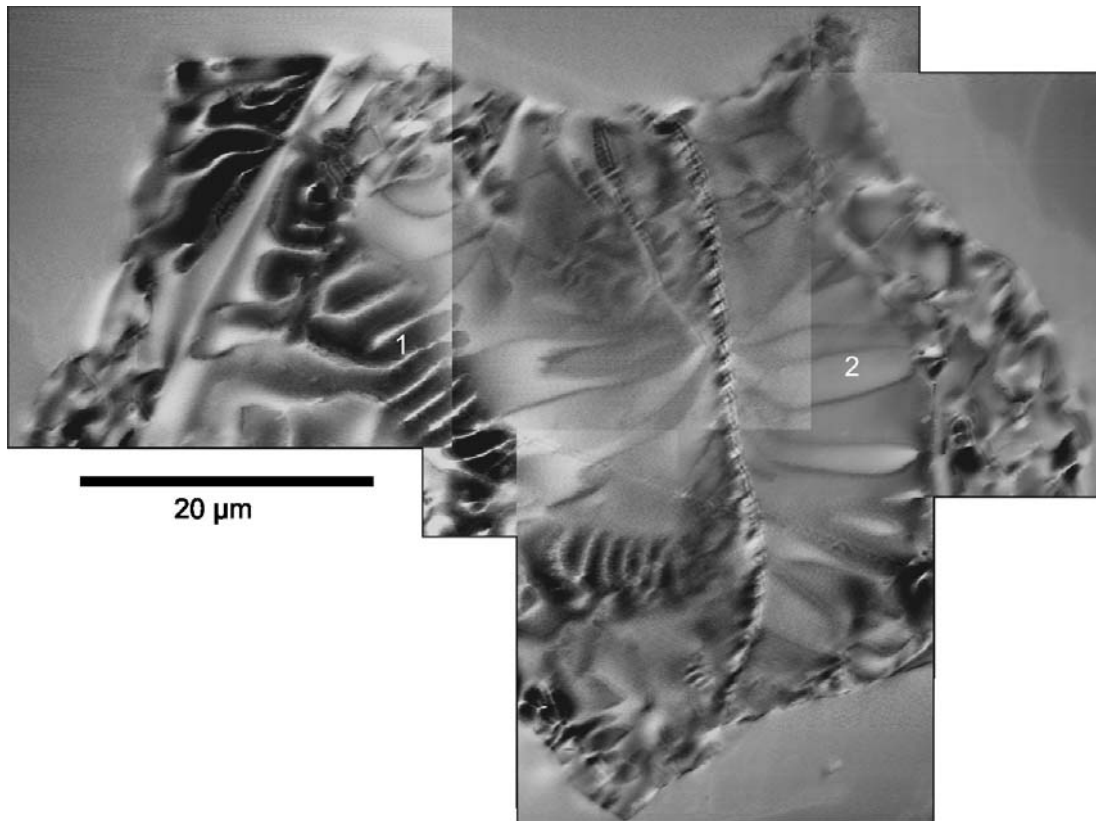


Figure 3.11: Composite MFM micrograph of grain 2 of sample V27. The bulk NRM of the sample is oriented approximately in the viewing plane. (1) Batch-like domains. (2) Lamellar domains.

It is still in debate if the latter are representing the underlying volume domains (APPEL AND SOFFEL, 1984, 1985; APPEL, 1987) or merely the stress controlled surface structure obscuring underlying lamellar domains (HALGEDAHL, 1987; METCALF AND FULLER, 1987a,b). Important for this problem is the distinction between surface stress, e.g. caused by the polishing procedure, and internal stress, caused by chemical, crystallographical or physical inhomogeneities. APPEL AND SOFFEL (1984) argue that batch-like domain patterns originate from an inhomogeneous anisotropy field due to high internal stresses and are different from maze domains. Evidence for this hypothesis comes from MFM observations on the inhomogeneously oxidised particles from the present study (Figure 3.13). Obviously, the magnetic domain configuration (panel a) is influenced by the variations in chemical composition across the grain (panel b). The oxidised part of

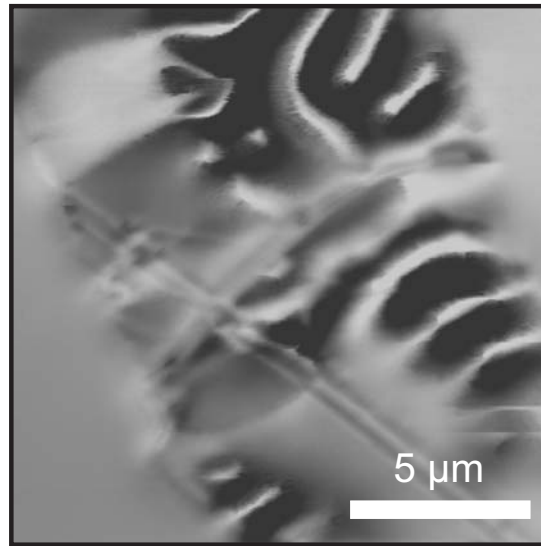


Figure 3.12: Micrograph of sample O-1C. Direction of bulk magnetisation is approximately perpendicular to viewing plane.

the grain along the central crack shows a comparatively simple domain structure comprising a single domain at each side of the crack. At the border between oxidised and non-oxidised areas, where the internal stresses caused by the change of lattice parameter are presumably highest, the above mentioned batch-like pattern (darker in colour) appears. This indicates that these domains are indeed stress induced and represent the volume domain structure. In the non-oxidised part above the batch-domain area, a magnetic structure is visible which presumably results from multiple domains with a magnetisation direction tilted with respect to the sample surface.

The grains in Figure 3.14 and 3.15 from sample O-1E and V27, respectively, qualitatively show the same overall magnetic domain structure (panels b). Again, the domain configuration is aligned with the low-temperature oxidised parts of the grain. This indicates that the primary domain structure is significantly biased by the partial oxidation of the grain. The spontaneous magnetisation of the oxidised part decreases and simultaneously the anisotropy field changes. The domains are thus forced to configure in accordance with these changes.

Regarding thermal demagnetisation and acquisition of thermoremanent magnetisation, an interesting implication arises from the compositional and magnetic

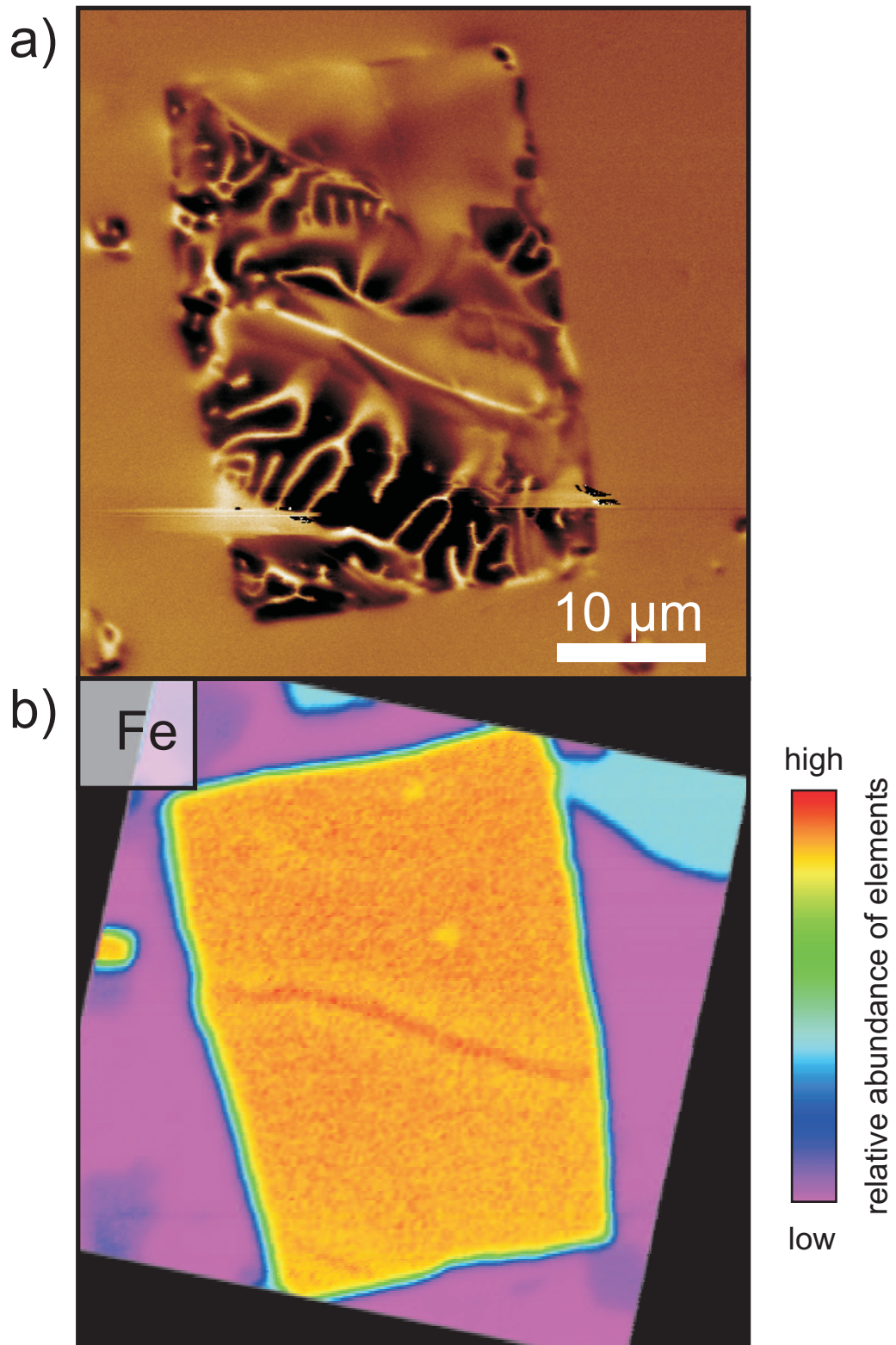


Figure 3.13: Grain from sample O-1G represented by (a) MFM and (b) iron distribution. The domain configuration is clearly influenced by the compositional variations along the crack.

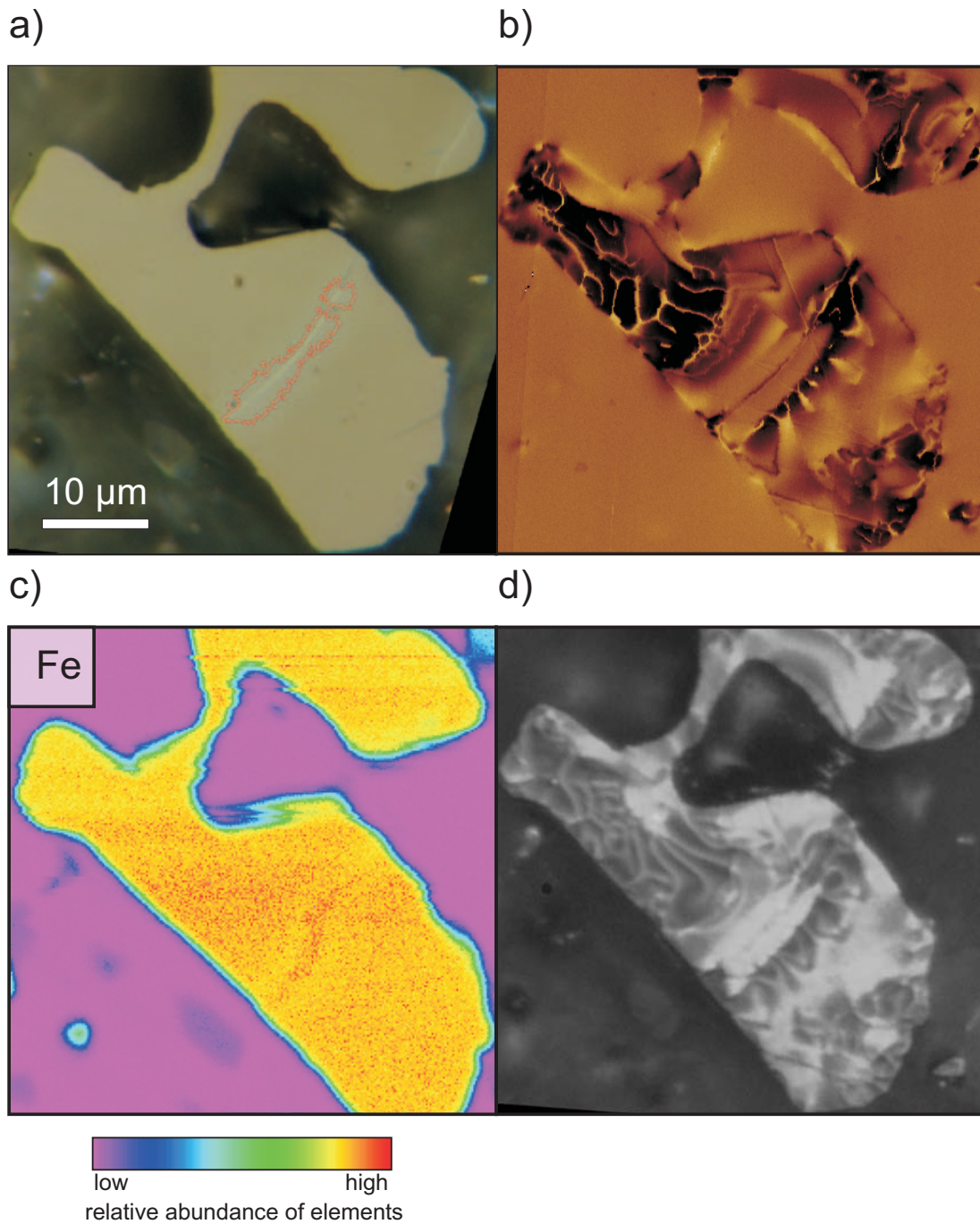


Figure 3.14: Detail of sample O-1E viewed with different microscopic and micro-analytical techniques. a) Reflected light micrograph. The oxidised brighter areas are indicated by a red line. b) MFM image. c) Electron microprobe image displaying the abundance of iron. d) Light microscopic domain image using the Bitter technique.

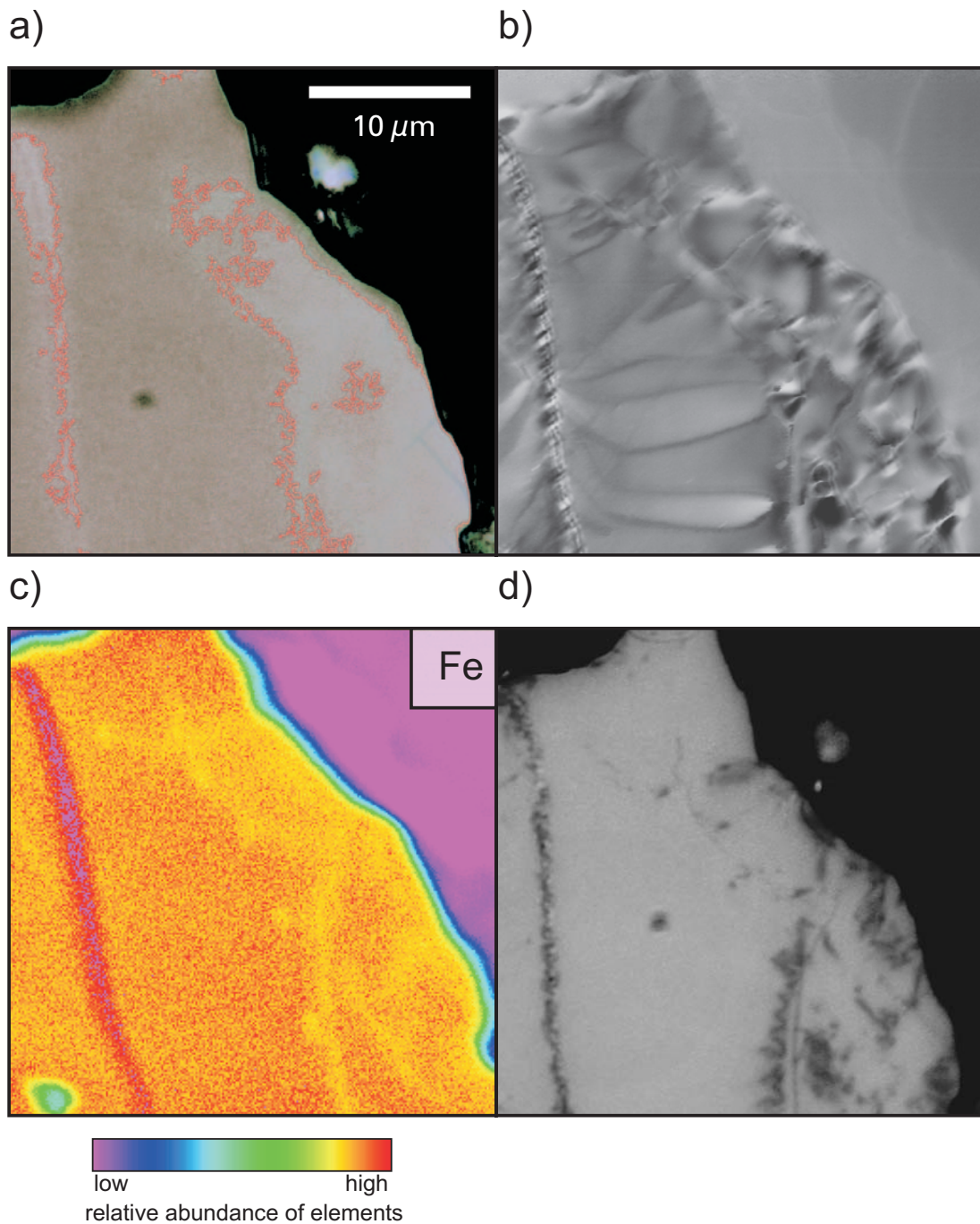


Figure 3.15: Detail of sample V27 (see Figure 3.11) viewed with different microscopic and microanalytical techniques. a) Reflected light micrograph (contrast enhanced by image processing techniques). The oxidised brighter areas are indicated by a red line. b) MFM image. c) Electron microprobe image displaying the abundance of iron. d) Light microscopic domain image using the Bitter technique.

changes: As the Curie temperature is increased in the oxidised parts of the grain, these are likely to have higher blocking and unblocking temperatures than the rest of the grain. Thus, magnetic interactions between the oxidised and non-oxidised parts presumably influence the domain configuration during thermal treatments. If this is the case, these inhomogeneously oxidised titanomagnetite particles are possibly the cause for self-reversal of the thermoremanent magnetisation occurring in these samples (see chapter 4).

Comparison with the Bitter technique shows some of the principal advantages of magnetic force microscopy: The Bitter pattern image of sample O-1E (Figure 3.14d) shows qualitatively the same domain structure as the MFM image. However, only domain walls can be viewed. Information about the magnetisation direction of the domains can not be retrieved from Bitter pattern observations. Moreover, the image suffers from low resolution as the size range of the domain structures is at the physical limits of light microscopy. The critical length scale is defined by the wavelength of light in the visible spectrum of ≈ 400 nm whereas MFM can yield a spatial resolution below 20 nm. Another advantage shown in Figure 3.15 is the much higher sensitivity of MFM (panel b) compared to the Bitter technique (panel d). The latter shows only a few structures in the oxidised part of the grain but fails completely to resolve the broad lamellar domains seen with MFM in the left part of the image.

3.4 Conclusions

It could be demonstrated that the basalts containing titanomagnetite grains with two magnetic phases show a large number of cracks pervading both silicate matrix and titanomagnetite grains. These open cracks are the locus of onset of low-temperature oxidation which removes iron from the titanomagnetite crystal lattice. This process of low-temperature oxidation by iron migration was made visible by different microanalytical techniques. The excess iron precipitates as hematite inside the cracks, thus clogging them and preventing further oxidation. The result are partially oxidised titanomagnetites with an inhomogeneous chemical composition and inhomogeneous magnetic properties. These variations also affect the magnetic domain configuration. Keeping in mind that low-temperature

oxidation increases the Curie temperature in certain parts of the ore grains, these particles are presumably responsible for the two Curie temperatures identified by thermomagnetic measurements. As the two phases are directly adjacent to each other, they are potential candidates for causing self-reversal of remanent magnetisation. The question if such a spatial arrangement of two magnetically different magnetic phases is in principle capable of acquiring a self-reversed magnetisation will be answered by numerical calculations in chapter 5.

Chapter 4

Self-reversal of thermal remanent magnetisation

The term self-reversal describes the phenomenon that a sample is able to acquire remanence which is directed opposite to an external magnetic field \vec{H}_{ext} . If the total remanence at room temperature $\vec{M}_{\text{R}}(T_0)$ is antiparallel to \vec{H}_{ext} , complete self-reversal has occurred, if only part of the remanence is directed opposite and $\vec{M}_{\text{R}}(T_0)$ is parallel to \vec{H}_{ext} , the term partial self-reversal is used. In standard palaeomagnetic practice these phenomena are seldom recognised, as step-wise thermal demagnetisation with measurements at room temperature is used to isolate the characteristic remanence. Either, demagnetisation plots show no deviation from single directional component behaviour or, if an antiparallel remanence component is isolated, it cannot be distinguished from an overprinted remanence acquired in opposite \vec{H}_{ext} . Self-reversal can only be identified unequivocally by continuous thermal demagnetisation. With this technique, the sample is heated in zero field and the magnetisation is measured continuously during heating and cooling. Thus, by measuring the remanence at elevated temperatures, demagnetisation of different remanence components and their possible interaction can be monitored. In the following sections, samples described in chapter 2 will be studied regarding their ability to acquire self-reversed magnetisation.

4.1 Continuous thermal demagnetisation

An overview of the differences between stepwise and continuous thermal demagnetisation can be found in SCHMIDT AND CLARK (1985). The instrument used in this work is a high-temperature spinner magnetometer (HOTSPIN) which was set up at the Munich laboratory. It is described in detail by MATZKA (2001). The maximum attainable temperature is 600 °C. The magnetometer simultaneously measures two orthogonal components of magnetisation with a ringcore fluxgate sensor.

Two examples for continuous thermal demagnetisation are shown in Figure 4.1. Sample V22-0 (Figure 4.1a) displays the temperature dependence of NRM for samples with a single ferromagnetic phase. On heating the sample in zero field to a certain temperature $T < T_C$, the remanence is decreasing and does not reach the initial value after subsequent cooling. The difference between cooling and heating shows, that part of the remanence is unblocked and thus lost during heating. According to Néel's classical single-domain TRM theory (NÉEL, 1949, 1951), NRM is proportional to the spontaneous magnetisation during cooling or heating in zero field as long as the temperature is below the minimum unblocking temperature. This relation holds for sample V22-0. In Figure 4.1b the NRM data of Figure 4.1a are fitted by an 8th order polynomial to smooth the data and interpolate missing data points. This curve is then normalised to the saturation magnetisation $M_S(T)$ which is a good approximation for spontaneous magnetisation at least at temperatures $T \ll T_C$ (SCHMIDT AND CLARK, 1985). The heating curve is linear and roughly horizontal up to a temperature of ≈ 300 °C where unblocking starts, marked by a decrease of magnetisation. The cooling curve shows the anticipated nearly horizontal line. Deviation from ideal behaviour is probably caused by the fact that $M_S(T)$ was measured on a sister specimen. An important conclusion which can be drawn from this kind of data is that the strong field parameter M_S derives from the same grain population as the weak field parameter thermoremanence.

Figure 4.1c shows sample V27-0 displaying a very different behaviour which is typical for partial self-reversal of NRM. NRM intensity is decreasing on the first heating run like in the case of sample V22-0. During subsequent cooling, however,

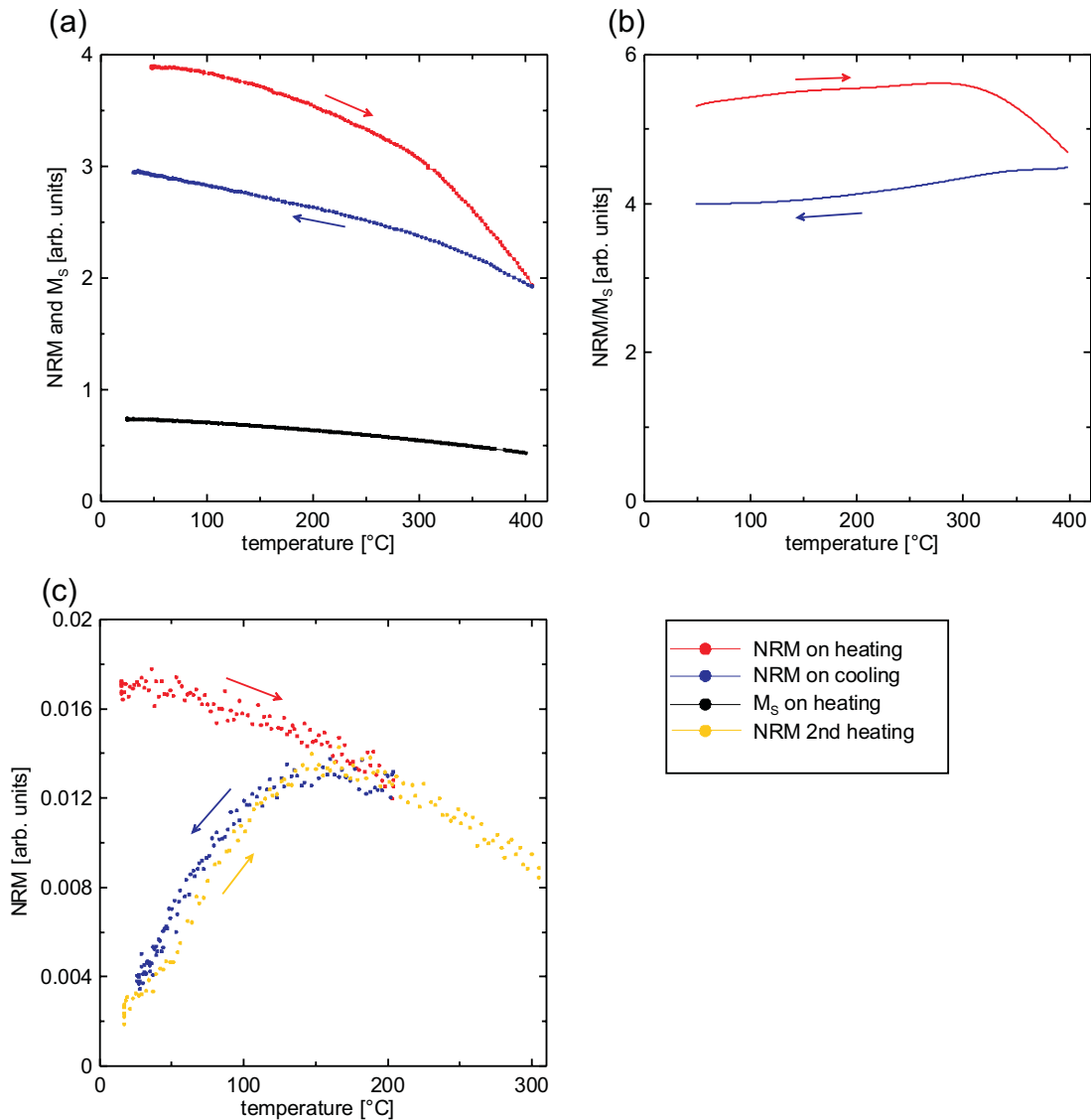


Figure 4.1: Two examples for continuous thermal demagnetisation. (a) Sample V22-0 with only one magnetic phase. (b) Data of (a) normalised to saturation magnetisation $M_S(T)$. The decrease of $\text{NRM}(T)$ in the heating run above $\approx 300^{\circ}\text{C}$ marks the onset of unblocking of remanence. The nearly horizontal progression of the cooling curve shows that $\text{NRM}(T)$ follows roughly the temperature dependence of saturation magnetisation M_S . (c) Sample V27-0 consisting of two magnetic phases with different Curie temperatures is exhibiting partial self-reversal. Part of the remanence is unblocked during the first heating run up to 300°C . On cooling the magnetisation is decreasing. This decrease is fully reversible in the subsequent heating run.

magnetisation is further decreasing. This indicates that during heating some remanence is unblocked and the particles belonging to the respective unblocking range are by some mechanism acquiring remanence in the opposite direction during cooling although the whole procedure is carried out in zero external field. The decrease on cooling is fully reversible during the following second heating run.

This observation is not to be mistaken for the multidomain effect of decreasing partial thermoremanence during cooling in zero field described by e.g. PETROVA AND TRUKHIN (1961), MARKOV ET AL. (1983) and MCCLELLAND AND SUGIURA (1987). The decisive difference is, that the MD phenomenon is not reversible in a subsequent heating run. The authors explain the decrease by so-called *trans-domain* processes. This term essentially describes the possible change of remanence below the blocking temperature of individual domain walls by nucleation of new or denucleation of existing domains. These new domains force already pinned domain walls to reconfigure. MOSKOWITZ AND HALGEDAHL (1987) argue that thermoremanence is blocked only after the change in domain number has finished. As this effect can be excluded here, it will not be discussed further in this chapter.

As mentioned above, the shape of the NRM(T) curve is controlled by two factors: The temperature dependence of saturation magnetisation M_S and the unblocking or blocking of remanences during heating and cooling, respectively. The effect of $M_S(T)$ on NRM(T) was studied by MATZKA (2001) and MATZKA ET AL. (2003) who showed that low-temperature oxidation controls the variation of NRM intensity with age in ocean floor basalts.

The work presented in this chapter will focus on the demagnetisation and remanence acquisition behaviour of samples with more than one magnetic phase. As the measurement of remanences is performed in zero external magnetic field, blocking of remanences during cooling can only take place either in the presence of a magnetostatic field of remanence carrying particles with an unblocking temperature above the maximum temperature reached in the experiment, or by exchange interaction across crystallographic phase boundaries of ferromagnetic (*sensu lato*) minerals. Which of these two mechanisms is acting in the samples of this study will be discussed later in this chapter and in chapter 5.

4.2 NRM demagnetisation results

The samples were not demagnetised in a single heating/cooling run up to the Curie temperature but in up to nine subsequent continuous measurement steps with increasing maximum temperature (e.g. 150, 200, 240, 300, 350, 400, 480, 525, 600 °C maximum temperature). This procedure allows to monitor the reversibility of heating/cooling cycles, to observe possible blocking of remanences during cooling and to compare the continuous measurement technique using the HOTSPIN to the conventional stepwise technique.

Data of samples L-1A and O-2C containing a single magnetic phase with $T_C = 587$ °C and 589 °C, respectively (see Table 2.1) are shown in Figure 4.2. NRM intensity is plotted in the panels labelled (a), panels (b) show the direction of magnetisation in the plane of the ringcore sensor (NRM phase plots). The phase angle 0° marks the z axis in sample coordinates, 90° the x or y axis depending on the measurement position. The phase data are also shown in a polar plot (Figure 4.2c) resembling the representation of ZIJDERVELD (1967). Due to the measurement technique, the present plot contains only information on two components of magnetisation. These plots are thus termed *Pseudo-Zijderveld plot* in the following.

Data of the final cooling in the phase plot allows to determine whether the sample was demagnetised completely by heating to the maximum temperature, as the directional data should be statistically distributed in that case. This is true for sample O-2C, but does not hold for sample L-1A. Although scattered, a preferred direction of magnetisation can still be identified. However, the intensity of the remaining $M_R(T_0)$ is below 0.5% of the initial value. The NRM intensity plots indicate unblocking of a single magnetic phase with a curve shape analogous to the data discussed in Figure 4.1a. A slight overprint is visible in the NRM phase plot and Pseudo-Zijderveld plot of sample O-2C. This remanence component is marked by a different direction ($\approx 180^\circ$) which is removed after heating the sample to 400 °C. All other measured samples with a single Curie temperature (chapter 2, Tables 2.1 and 2.2) show close resemblance to these two examples.

Figures 4.3, 4.4, 4.5 and 4.6 display NRM demagnetisation results of basalt samples from Olby and Vogelsberg showing partial self-reversal of magnetisation.

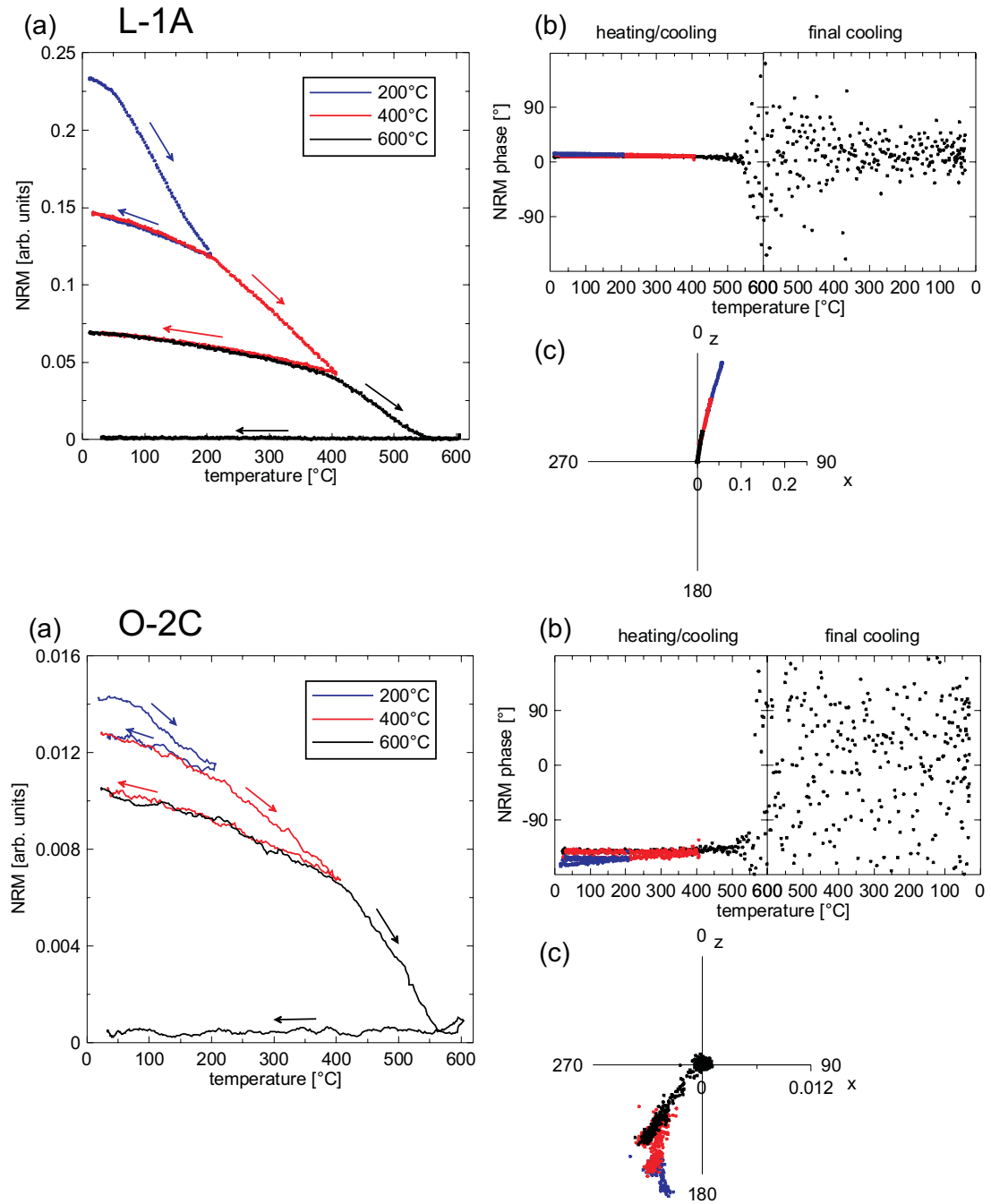


Figure 4.2: Results of samples L-1A (top) and O-2C (bottom) with a single magnetic phase. (a) NRM(T) intensity plot. (b) NRM direction versus temperature plot. (c) Pseudo-Zijderveld (two orthogonal components) representation of the NRM direction. Intensity data of sample O-2C is smoothed by a running average over nine data points in order to reduce scatter.

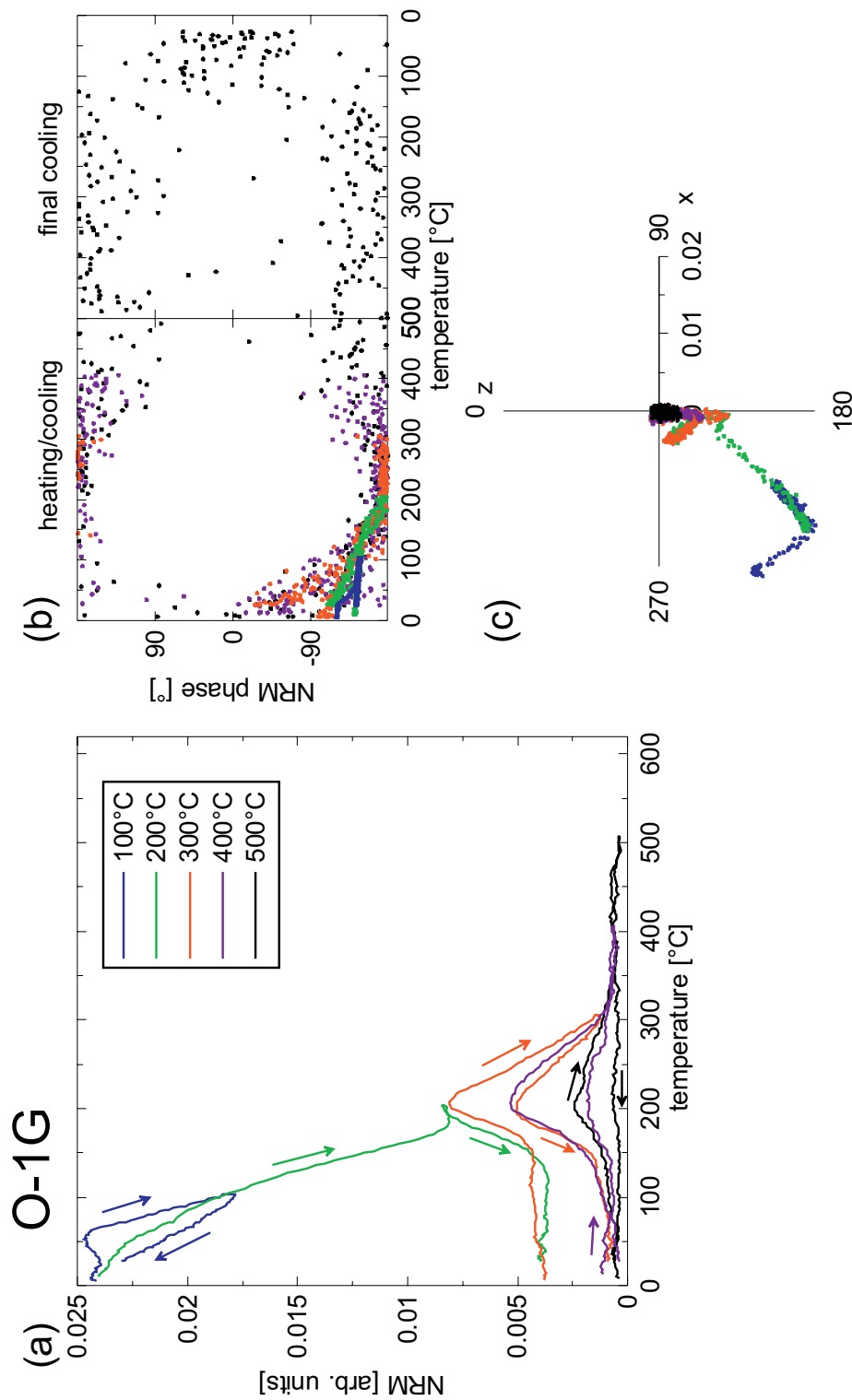


Figure 4.3: Results of the partially self-reversing sample O-1G. (a) NRM(T) intensity plot. (b) NRM direction versus temperature plot. (c) Pseudo-Zijderveld representation of the NRM direction.

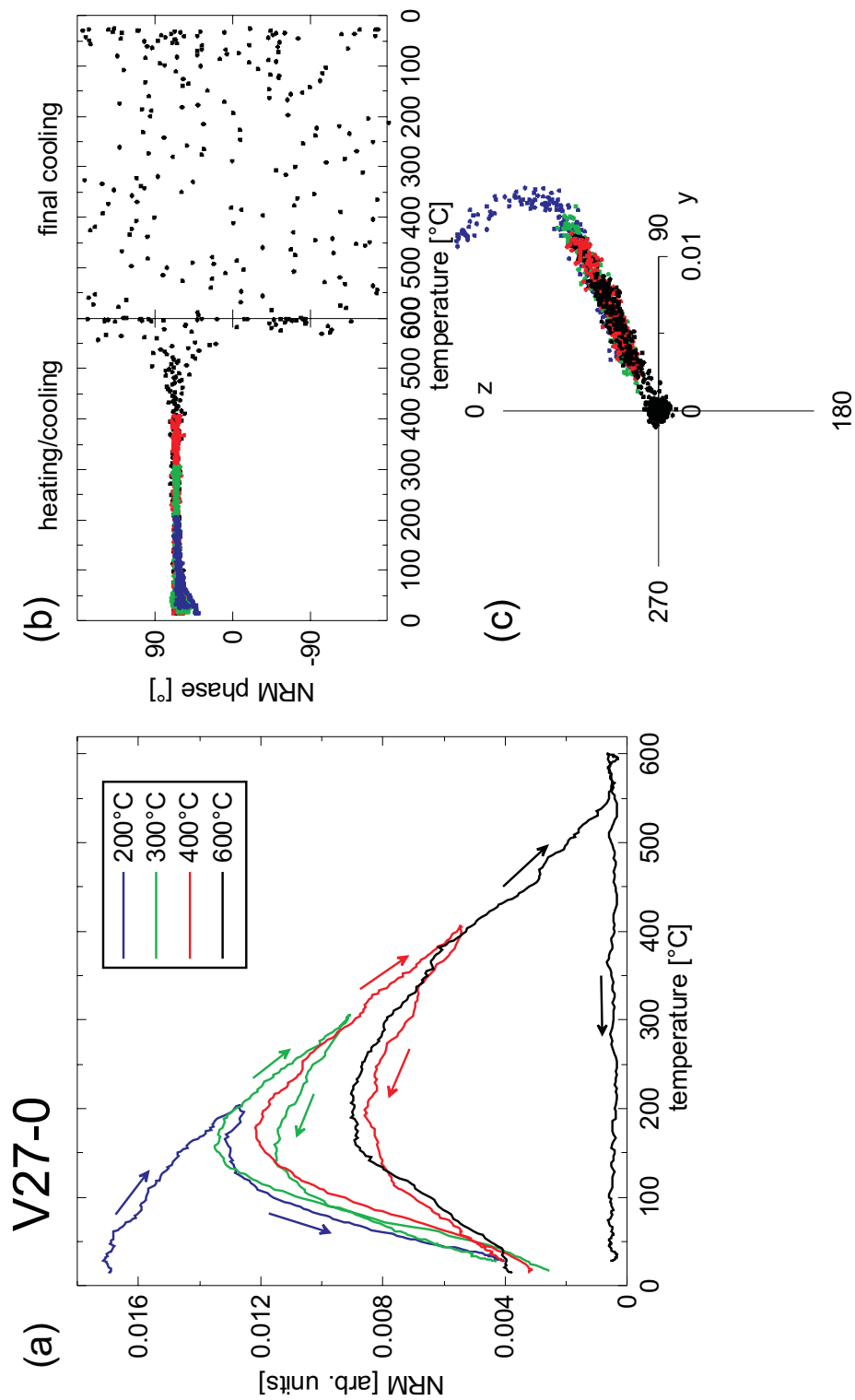


Figure 4.4: Results of the partially self-reversing sample V27-0. (a) NRM(T) intensity plot. (b) NRM direction versus temperature plot. (c) Pseudo-Zijderveld representation of the NRM direction.

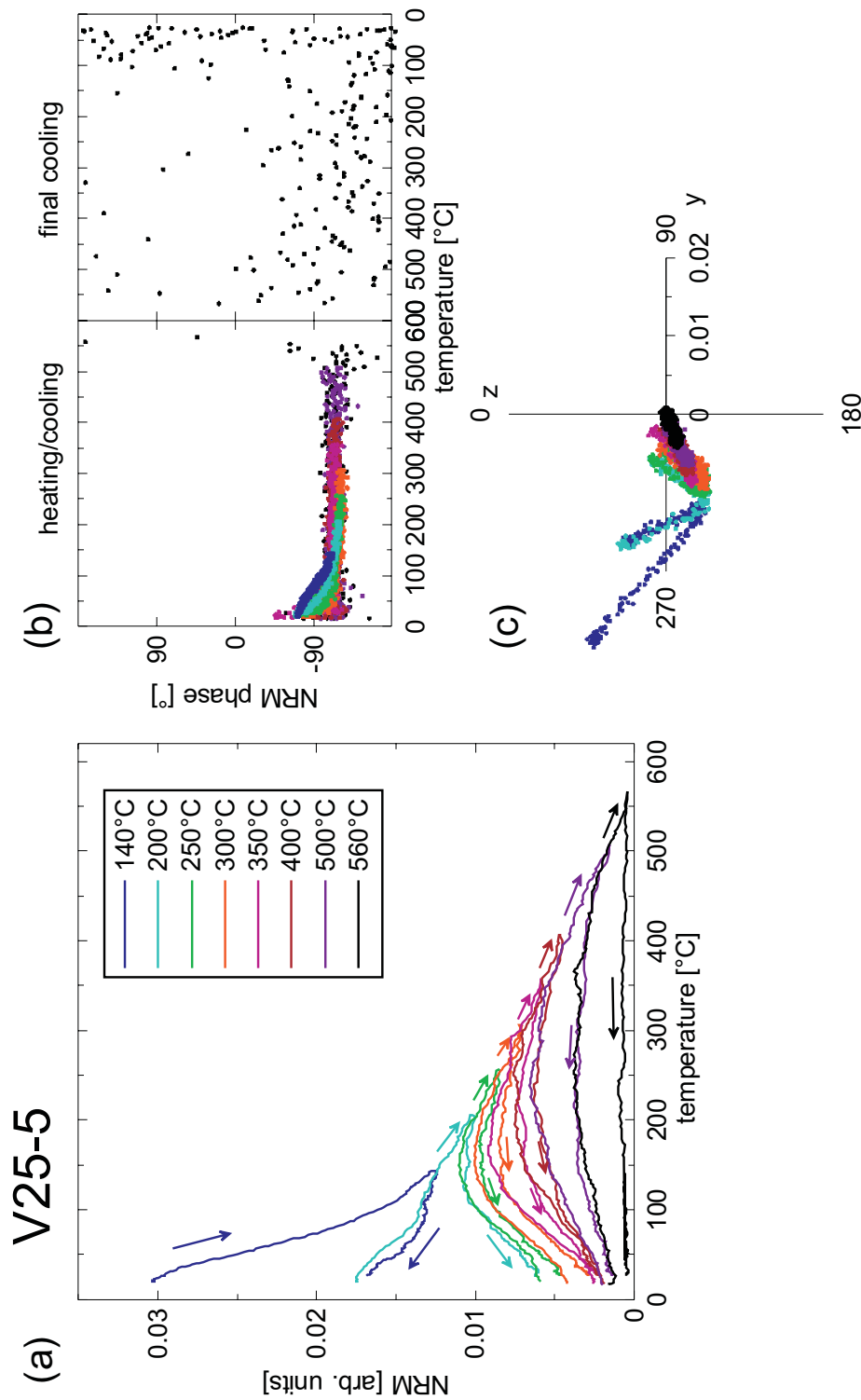


Figure 4.5: Results of the partially self-reversing sample V25-5. (a) NRM(T) intensity plot. (b) NRM direction versus temperature plot. (c) Pseudo-Zijderveld representation of the NRM direction.

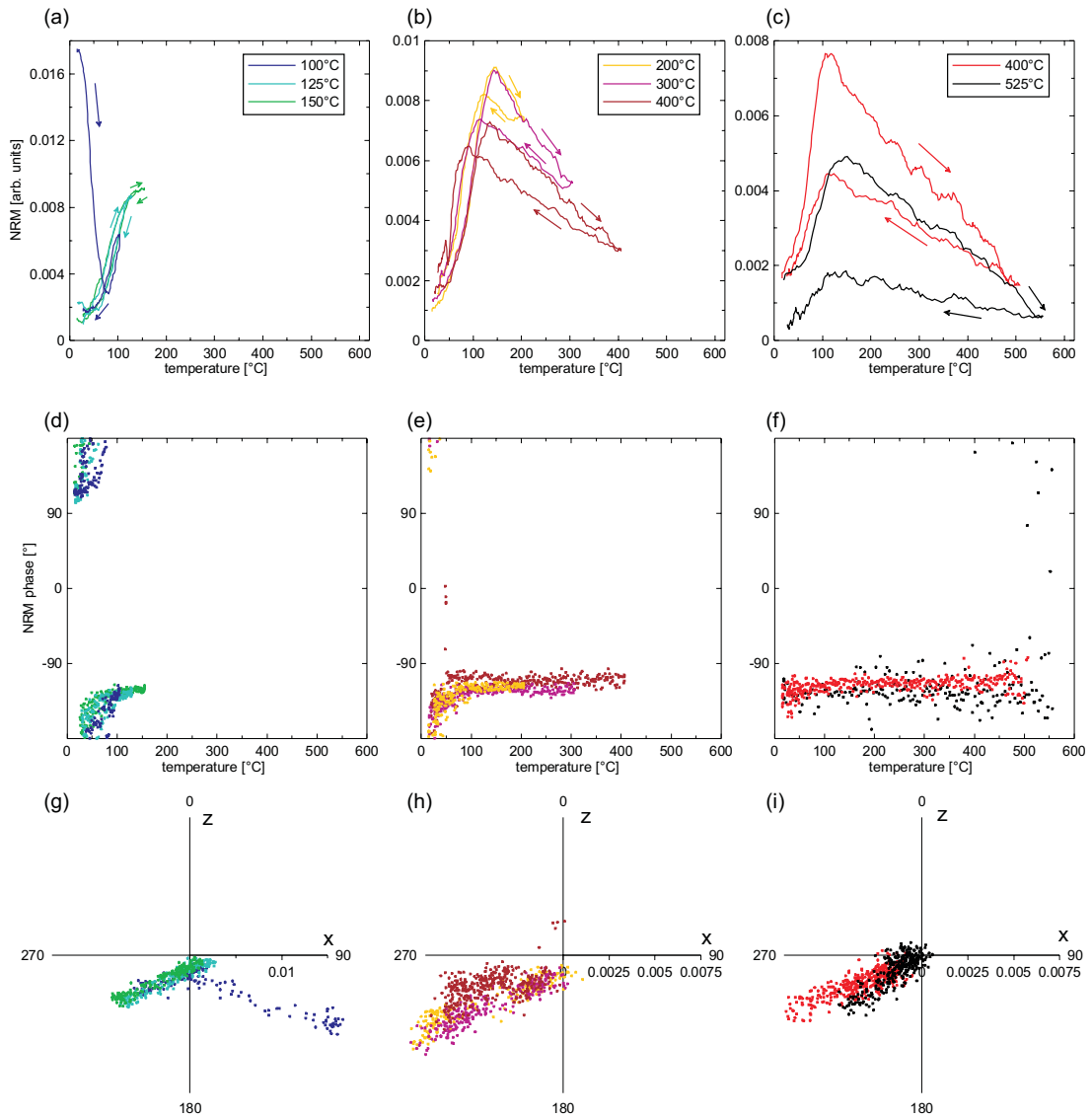


Figure 4.6: Results of sample O-1R. (a)-(c) $NRM(T)$ intensity plots with progressively increasing maximum temperature. The data is smoothed by a running average over nine data points to reduce scatter. Note the difference in scale of magnetisation axes. (d)-(f) NRM direction versus temperature plot. (g)-(i) Pseudo-Zijderveld representation of the NRM direction.

All of these samples contain two magnetic phases with different Curie temperatures (see chapter 2). During the first one or two heating cycles up to a temperature of ≈ 200 °C a soft overprint is removed. This remanence component can be identified by the deviating remanence direction (Figures 4.3, 4.4 and 4.5, respective panels b and c, Figure 4.6d and g). When studying basalts from the Rauher Kulm (Germany), CREER ET AL. (1970) found that partial self-reversal may be generally associated with high magnetic viscosity. Therefore, it is likely that the soft overprint is of viscous origin. Later, PETHERBRIDGE (1977) assigned this viscosity to multidomain grains of the mother phase (i.e. the primary titanomagnetite). After removal of the viscous component the cooling curve shows the decrease of $M_R(T)$ characteristic for partial self-reversal as already depicted in Figure 4.1c. As this decrease is neither observed in the respective $M_S(T)$ curves nor in the first heating runs, it is not controlled by the temperature dependence of saturation magnetisation but by the blocking of thermoremanence. Data of sample O-1R show that this remanence is antiparallel to the direction of remanence carried by particles with higher unblocking temperatures, i.e. the angular difference between the two remanence components is 180° (Figure 4.6h and i). This indicates that the blocking of the low-temperature component is in some way influenced by the high-temperature component.

The upper limit of the blocking temperature range of the low-temperature component can be approximated by the temperature at which M_R reaches a maximum, $T(M_{R,\max})$. This temperature lies in all cases below the lower Curie temperature $T_C(1)$ (see Table 2.1 and 2.2). As T_C defines the maximum blocking/unblocking temperature for thermoremanences carried by the respective magnetic phase, this indicates that the low-temperature reversed remanence is carried by the magnetic phase with $T_C(1)$.

Sample V25-5 (Figure 4.5) shows peculiar behaviour in the Pseudo-Zijderveld plot regarding the direction of NRM in the course of demagnetisation. In contrast to the other samples, the existing overprint is not removed during the first heating. It vanishes completely only above 400 °C. In this case, the unblocking spectrum of the overprint partly overlaps with the unblocking spectrum of the two antiparallel coupled remanence components (phase 250°). The measured direction is the vectorial sum of all components. Thus, heating-cooling cycles below

400 °C yield intermediate directions as the overprint is progressively demagnetised. The direction of the overprint is approximated by the room temperature end points of the Pseudo-Zijderveld curves (phase $\approx 290^\circ$). Note, that by conventional stepwise thermal demagnetisation only these room temperature data points would be obtained leading to the erroneous result of a single component remanence.

Complete self-reversal is observed for sample O-1C (Figure 4.7). The NRM(T) plots display a minimum in NRM intensity at which the remanence direction reversibly shifts by 180° . This minimum in intensity thus marks the compensation temperature T_K where the total remanence reverses sign. An overprinted antiparallel remanence as the cause of the reversal can be excluded, as the compensation of the two remanence components ($M_R = 0$) takes place at all heating-cooling runs between 200 °C and 600 °C peak temperature. After reaching the maximum temperature of 600 °C, the sample is completely demagnetised as seen in the phase plot (Figure 4.7b). Thus, the acquisition of a spurious thermoremanence due to a residual field in the instrument can also be excluded.

The compensation temperature T_K is shifted from $\approx 180^\circ\text{C}$ in the 200 °C run to below 100 °C in the 400 °C and subsequent runs. Associated with this is an increase of the maximum NRM(T) value (at $\approx 150^\circ\text{C}$) of the high-temperature phase (Figure 4.7b). A possible cause of this phenomenon is thermal alteration of the magnetominerals during measurement. Assuming that the low-temperature phase is non-oxidised titanomagnetite (see chapter 2) one can speculate that a fraction of this phase is oxidised during the heat treatment thus forming part of the high-temperature phase. Due to the increased remanence carried by this oxidised phase and the gradual blocking of the low-temperature phase, T_K will be shifted to lower temperatures as described above.

Less obvious is the case of sample O-1E (Figure 4.8) where a relatively strong overprint is present. However, after its removal at 200 °C the sample also exhibits the 180° phase shift with a minimum of $|\text{NRM}(T)|$ at $\approx 100^\circ\text{C}$.

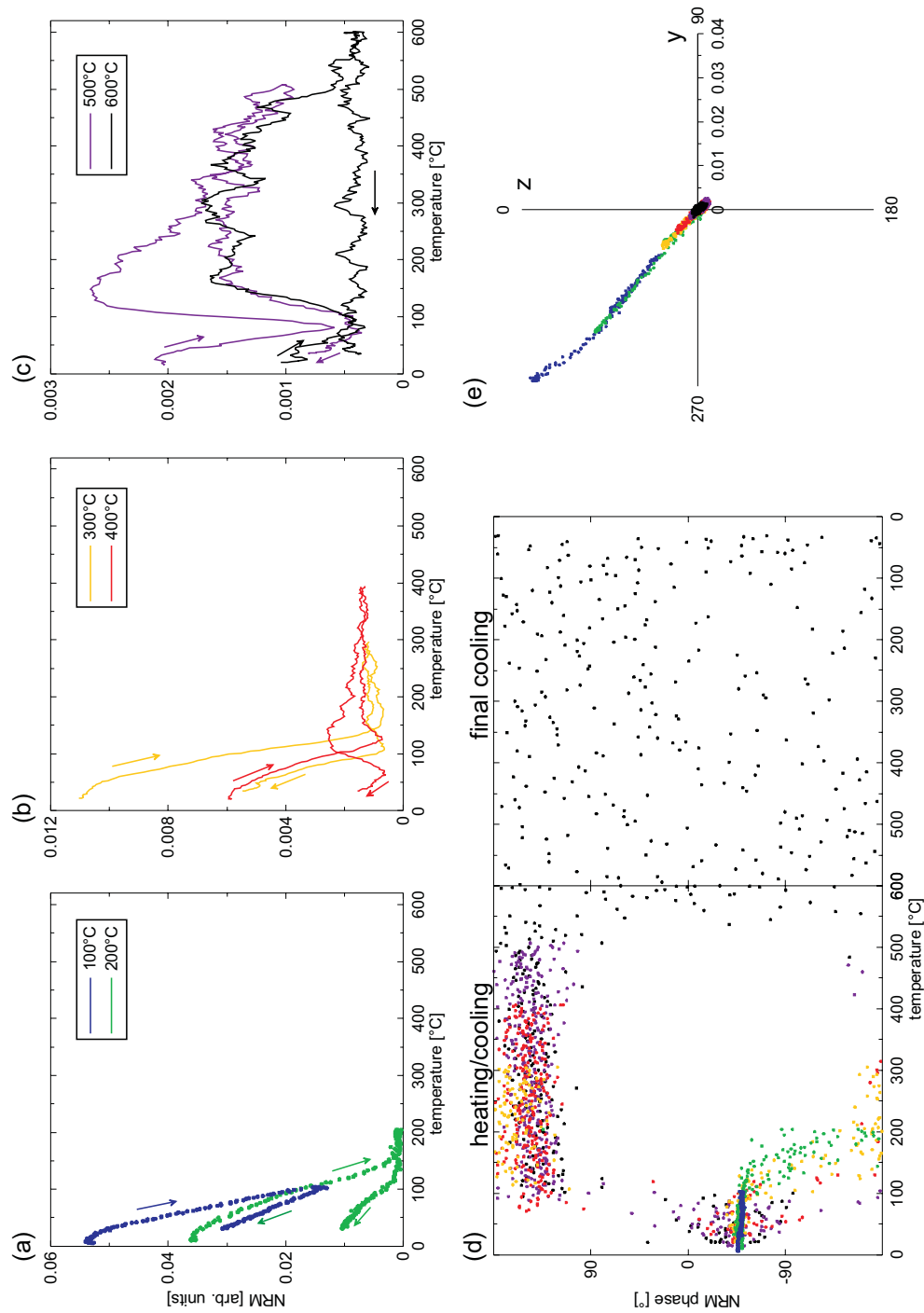


Figure 4.7: Results of sample O-1C displaying total self-reversal. (a)-(c) $NRM(T)$ intensity plots with progressively increasing maximum temperature. The data in panels (b) and (c) is smoothed by a running average over nine data points to reduce scatter. Note the difference in scale of magnetisation axes. (d) NRM direction versus temperature plot. Total self reversal is marked by a reversible 180° shift in NRM direction at higher temperatures. (e) Pseudo-Zijderveld representation of the NRM direction.

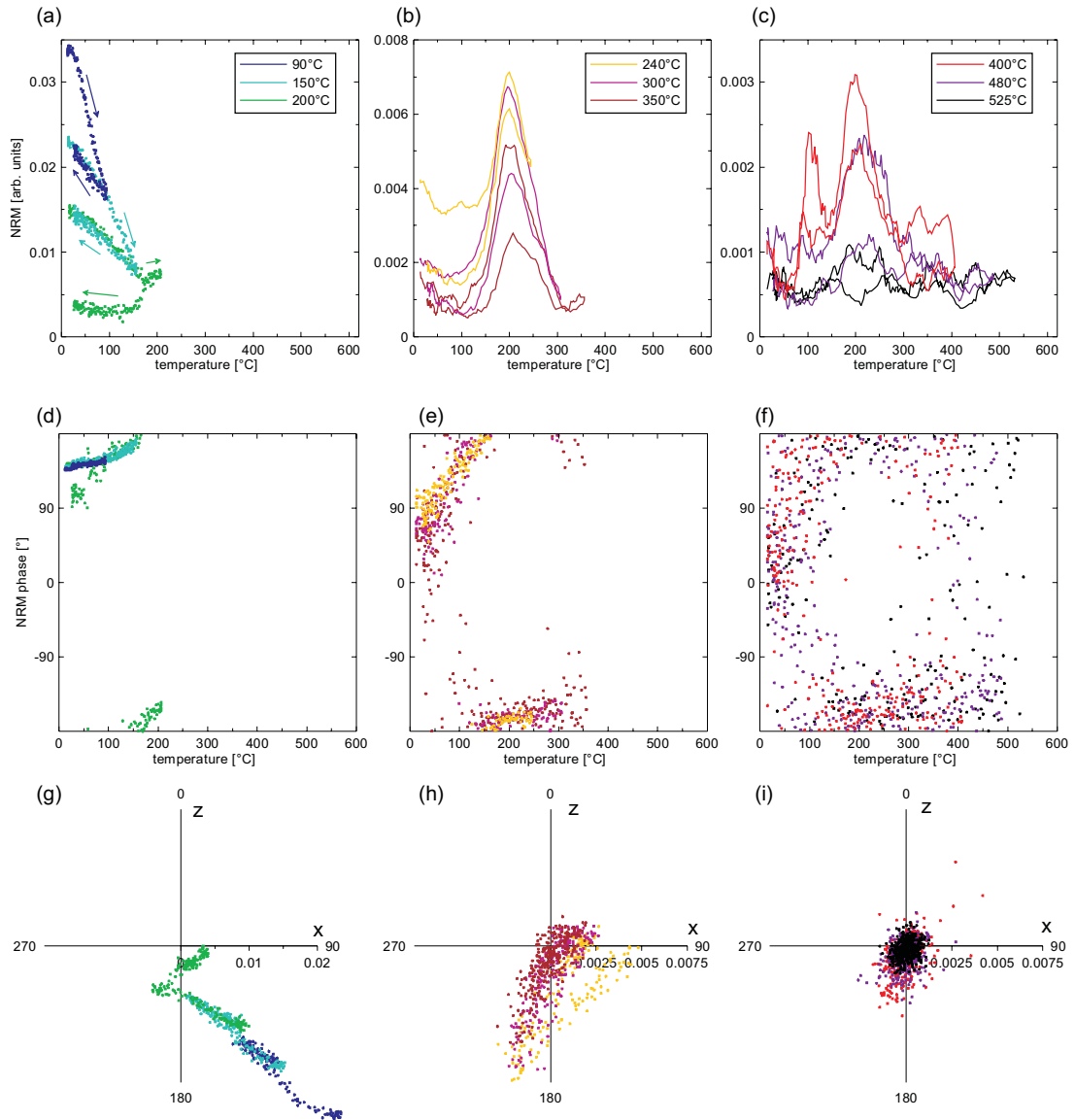


Figure 4.8: Results of sample O-1E. (a)-(c) NRM(T) intensity plots with progressively increasing maximum temperature. The data in panels (b) and (c) are smoothed by a running average over nine data points to reduce scatter. Note the difference in scale of magnetisation axes. (d)-(f) NRM direction versus temperature plot. (g)-(i) Pseudo-Zijderveld representation of the NRM direction.

4.3 Experiments with laboratory thermoremanent magnetisation

The NRM of the studied samples is unlikely to be solely a pure TRM. As shown in chapter 2, the remanence carriers in the basalt samples studied here have been subject to low-temperature oxidation. This potentially influences the primary TRM acquired after emplacement of the basalt. Moreover, the NRM is also contaminated by a viscous overprint, as mentioned in the discussion of NRM demagnetisation. To study the coupling mechanism between the two phases without any spurious influences, pTRMs in various fields and temperature intervals were imparted and studied by means of continuous thermal demagnetisation and alternating field (AF) demagnetisation. For acquisition of pTRMs a *Magnetic Measurements MMTD 20* thermal demagnetiser with built-in field coil was used.

First a pTRM($500\text{ }^{\circ}\text{C}, T_0$) (i.e. a magnetic field was applied from $500\text{ }^{\circ}\text{C}$ down to room temperature) was imparted. This pTRM was then continuously demagnetised to check whether coupling occurs when both magnetic phases are cooled in an external magnetic field through their blocking temperature range. This experiment was repeated in fields between 10 and $90\text{ }\mu\text{T}$ to test whether a certain threshold of field strength exists, above which interaction is suppressed. Figure 4.9 shows the results for sample O-1R. The characteristic feature of partial self-reversal – an increase of magnetisation during heating – is not visible regardless of the strength of the applied external field. The curve shape is similar for all field values and the TRM is approximately proportional to the applied external field during TRM acquisition. All curves show a kink at $100\text{ }^{\circ}\text{C}$ marking the temperature at which the low- T_b phase is demagnetised. This demonstrates, that an antiparallel coupling of the two remanence carrying phases either is already suppressed at external magnetic fields below the range of the Earth’s magnetic field ($30\text{--}60\text{ }\mu\text{T}$) or that the effect is masked by particles with low T_b which are not coupled to the high- T_b phase and thus also acquire a TRM in \vec{H}_{ext} direction. The latter interpretation is assumed to be more likely if the microscopic findings (chapter 3) are taken into account: The low- T_b phase consists of large multidomain particles and the coupling, regardless if controlled by exchange- or magnetostatic interaction, will not influence the whole grain but only parts ad-

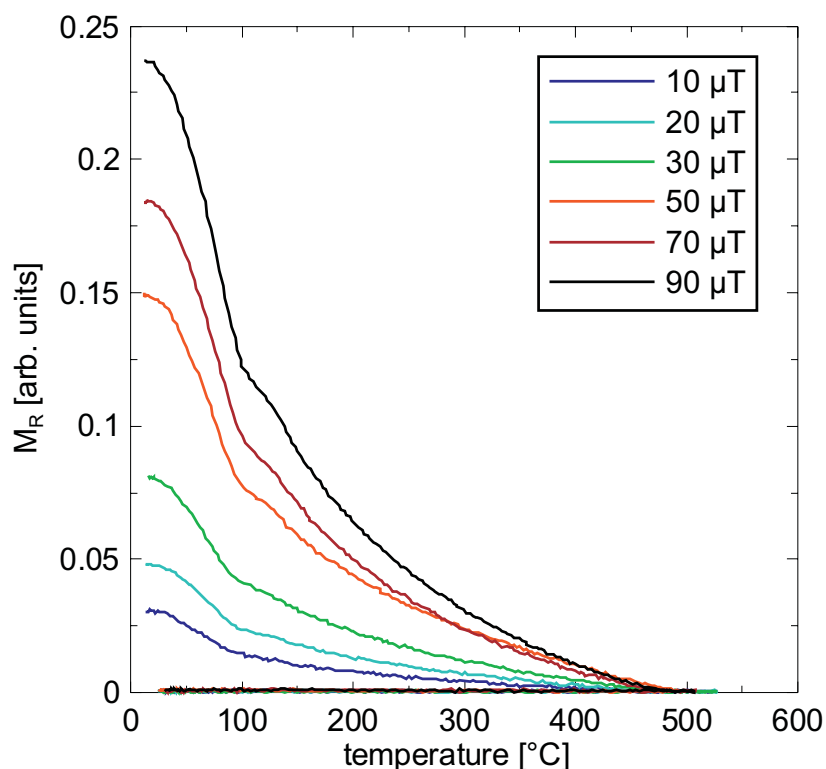


Figure 4.9: Continuous demagnetisation of TRM acquired in different applied magnetic fields for sample O-1R. The field strength is colour coded. The curve shape is independent of the applied field and the $TRM(T)$ values are roughly proportional to the applied field.

jacent to the high- T_b phase (see also the results of numerical models discussed in chapter 5). Taking also into account the findings of PETHERBRIDGE (1977) about the carriers of viscosity, it can be inferred that the antiparallel remanence in the case of self-reversal and the viscous remanence are both carried by the same magnetic phase.

Alternatively, the absence of partial self-reversal might also be explained by thermally induced alteration during the experiment which might affect the magnetomineralogy. To rule out this possibility, a pTRM($500^\circ\text{C}, 220^\circ\text{C}$) was imparted and the sample was cooled in zero field from 220°C to room temperature. This procedure ensures that the low- T_b phase ($T_C = 201^\circ\text{C}$) is only affected by the interaction with the high- T_b phase, whether magnetostatic or exchange coupled. The studied specimens had been heated several times to 600°C prior to the ex-

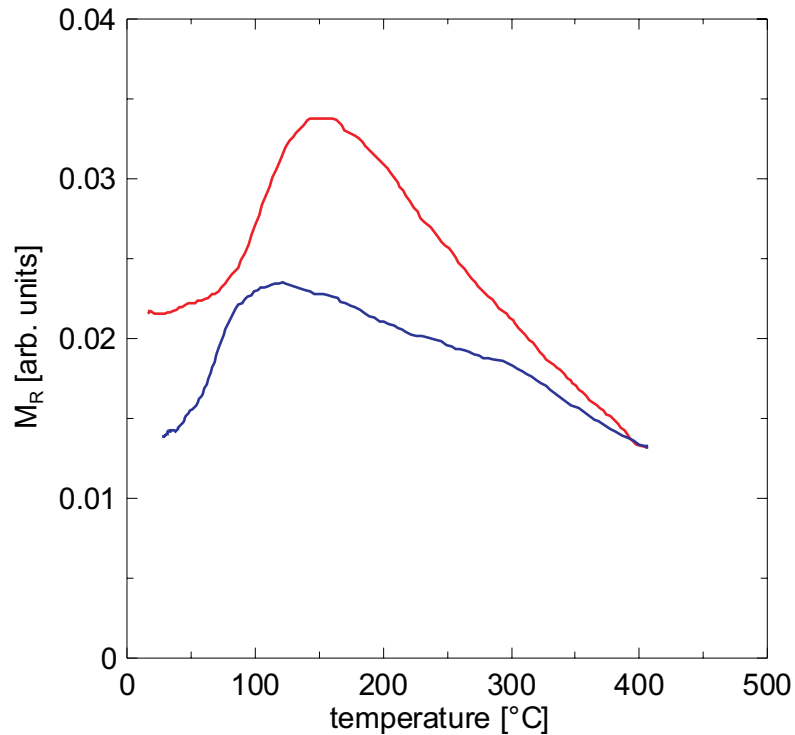


Figure 4.10: Continuous demagnetisation of pTRM(500 °C,220 °C) acquired at 25 μ T for sample O-1R. Red: heating, blue: cooling. Partial self-reversal is identified in both the heating and the cooling curve.

periment. Thus sufficient thermal stabilisation could be inferred. Results of the continuous thermal demagnetisation of this pTRM are plotted in Figure 4.10. The heating curve, measured again with the HOTSPIN, shows an increase in magnetisation up to 150 °C resembling the NRM(T) behaviour of this sample. The cooling curve displays the characteristic decrease in magnetisation. From this result two conclusions can be drawn:

- Firstly, heating does not change the magnetomineralogy to such an extent that self-reversal disappears.
- Secondly, self-reversal can be reproduced by laboratory thermoremanence. It is thus not a result of changes in titanomaghemite composition on geological timescales shifting the magnetic properties of the ore grains from Néel's P- or N-type to Q-type as discussed by SCHULT (1968). In this case the remanence direction might reverse due to modifications of the occu-

pancy of the magnetic sublattices in titanomagnetites/titanomaghemites in the course of low-temperature oxidation. In non-oxidised titanomagnetites the B- or octahedral sublattice has a higher spontaneous magnetisation than the A- or tetrahedral sublattice at room temperature. If, during low-temperature oxidation, cation vacancies are only formed on B-sites, the inverse magnetisation of the A-sublattice might eventually get stronger than the B-sublattice magnetisation. In such a case an “irreversible” self-reversal (PETERSEN AND BLEIL, 1973) not reproducible by imparting a laboratory TRM would be observed.

Similar experiments were performed for a range of samples that show self-reversal of the NRM to check the thermal stability of the magnetominerals responsible for the phenomenon. A pTRM(600 °C, 210 °C, 25 μ T) was imparted and then continuously demagnetised up to 200 or 300 °C to study whether self-reversal is reproducible after thermal treatment. Additionally, samples containing only one single magnetic phase were also included in the experiment to rule out that the increase in magnetisation during heating is caused by some pTRM acquisition artefact. Results are shown in Figure 4.11 and summarised in Table 4.1. Similar to sample O-1R most of the other samples with partially self-reversing NRM are able to acquire a reversed TRM in the low- T_b range. However, two of the Vogelsberg samples (V23 and V24) do not exhibit a peak in the HOT-SPIN heating/cooling curves. This is most likely due to chemical alteration of the remanence carriers.

The temperature of the peak in M_R lies always below the lower Curie temperature of the two-phase samples. This presents further evidence that the reversed TRM is carried by the magnetic phase which is responsible for the lower T_C determined by $M_S(T)$ measurements. This is also verified by results of samples where the lower Curie Temperature $T_C(1)$ is significantly above the minimum temperature of pTRM acquisition of 210 °C (Figure 4.12). The maximum in M_{pTRM} is preceded by an initial decrease of magnetisation during heating. For samples O-1G, O-1K and O-3E (Figures 4.12b, c and d) the maximum is more pronounced in the cooling run. This shows that part of the low- T_C phase with T_b above 210 °C is acquiring a thermoremanence parallel to H_{ext} and only particles with T_b below 210 °C are coupled to the high- T_C phase.

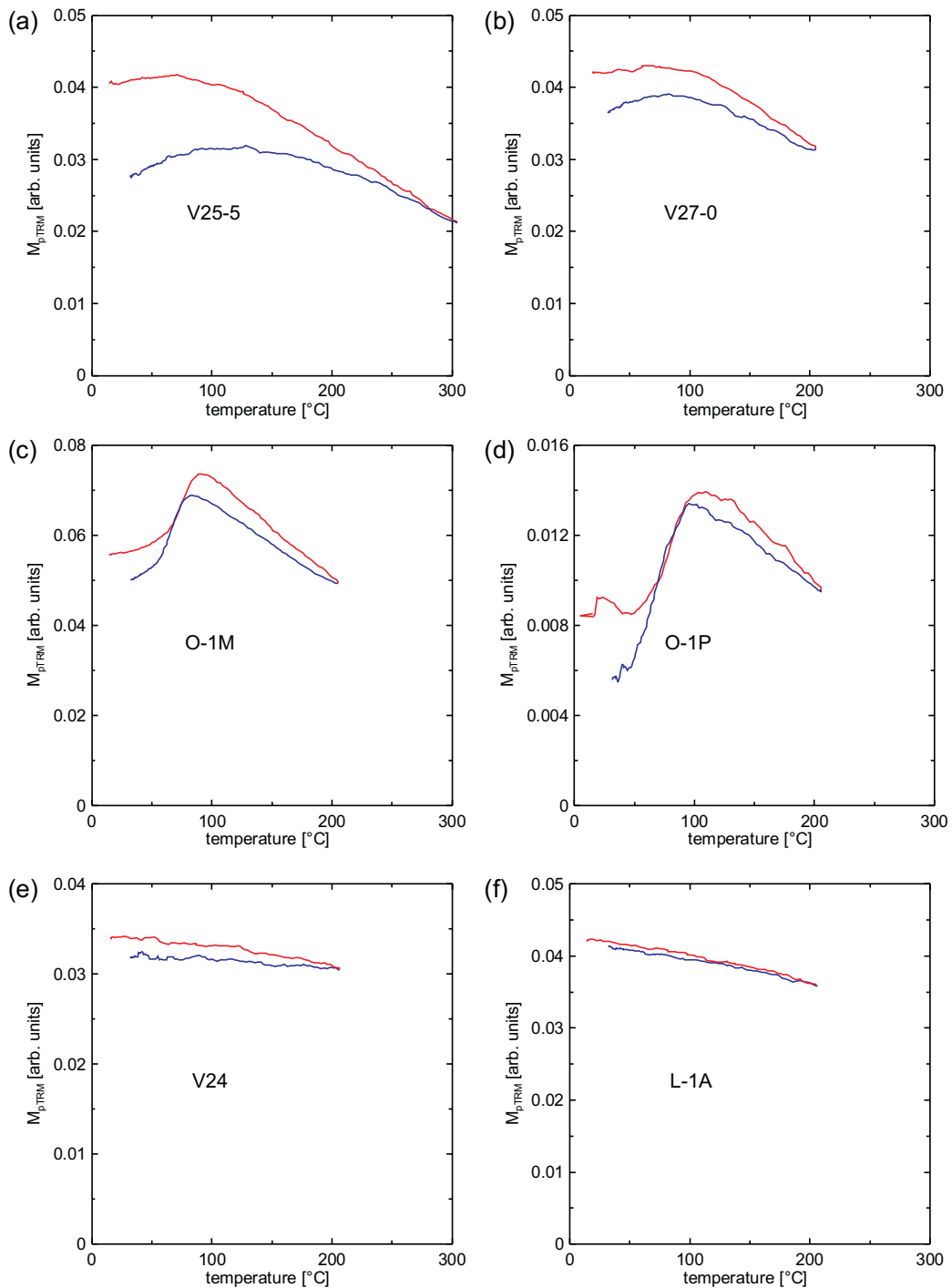


Figure 4.11: Continuous demagnetisation of pTRM(600 °C, 210 °C) acquired at 25 μ T. (a) and (b) show results of partially self-reversing Vogelsberg samples, (c) and (d) represent results from partially self-reversing Olby samples. (e) Vogelsberg sample with partially self-reversing NRM which is not reproducible by laboratory TRM. (f) Single phase sample L-1A.

Table 4.1: Results of pTRM(600 °C,210 °C,25 μ T) demagnetisation.

sample	NRM self-reversing	lab TRM self-reversing	temperature of M_R peak [°C]	$T_C(1)$ [°C]
O-1C	completely	partially	149	207
O-1E	completely	partially	195	260
O-1G	partially	partially	186 [†]	270
O-1K	partially	partially	173	268
O-1M	n/d [‡]	partially	92	194
O-1P	partially	partially	111	211
O-1R	partially	partially	105	201
O-1S	partially	partially	148	160
O-3E	no	partially	163	304
L-1A	no	no	–	–
L-1E	no	no	–	–
V23-1	partially	no	–	275
V24-6	partially	no	–	250
V25-5	partially	partially	69	191
V27-0	partially	partially	67	194
V28-6	partially	partially	\approx 130	208
V30-3	n/d	no	–	212

[†] temperature determined on cooling curve

[‡] not determined

In order to study the different coercivities of the two phases, the same pTRM(600 °C,210 °C,25 μ T) was imparted on the sample set once more and was then demagnetised by alternating field (AF) treatment with a *2G Enterprises* AF demagnetiser. The peak field was increased in steps from 1.5 to 200 mT and after each step the magnetisation was measured with a *2G Enterprises* cryogenic magnetometer. As demonstrated by the results of continuous thermal demagnetisation, the two phases carry antiparallel remanences after pTRM acquisition. If the coercivities of the two phases are different, it should be possible to isolate two antiparallel components using AF demagnetisation. Figure 4.13 shows results for six samples from both sampling locations Olby (O) and Vogelsberg (V). Magnetisation is initially increasing with increasing AF peak field and

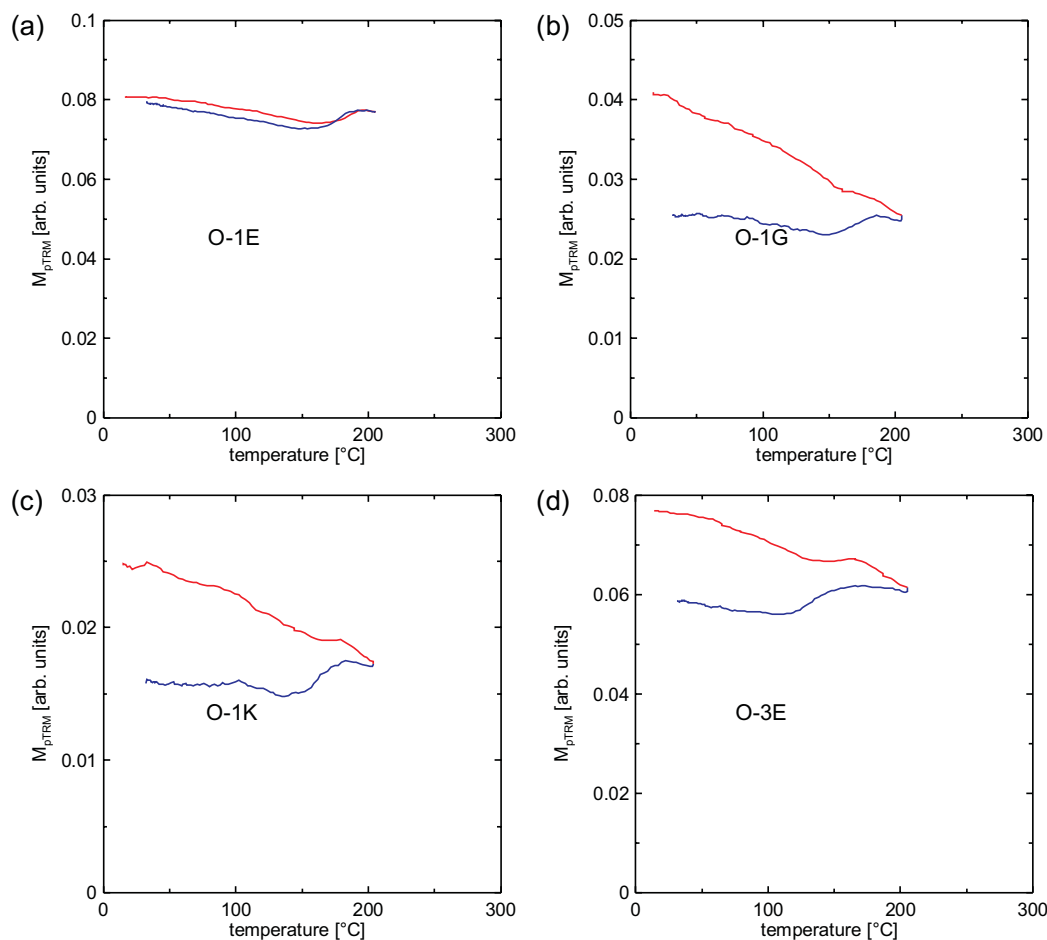


Figure 4.12: Continuous demagnetisation of pTRM(600 °C,200 °C) acquired at 25 μ T for samples with $T_C(1) > 210$ °C. The peak in magnetisation is preceded by an initial decrease of M_{pTRM} during heating. As the low- T_C phase is cooled in an external field between $T_C(1)$ and 210 °C, particles with T_b above 210 °C acquire a remanence in direction of H_{ext} .

reaches a maximum at peak fields below 10 mT. With rising peak fields magnetisation is decreasing until the samples are demagnetised. The initial increase in magnetisation is interpreted as demagnetisation of the antiparallel remanence component which is carried by the low- T_C phase followed by demagnetisation of the parallel remanence carried by the high- T_C phase. This is evidence for a marked contrast in coercivities of the two magnetic phases, with the low- T_C phase being magnetically softer and the high- T_C phase magnetically harder. Samples V27-0 and V28-6 show only a faintly visible increase in magnetisation of 0.2 and

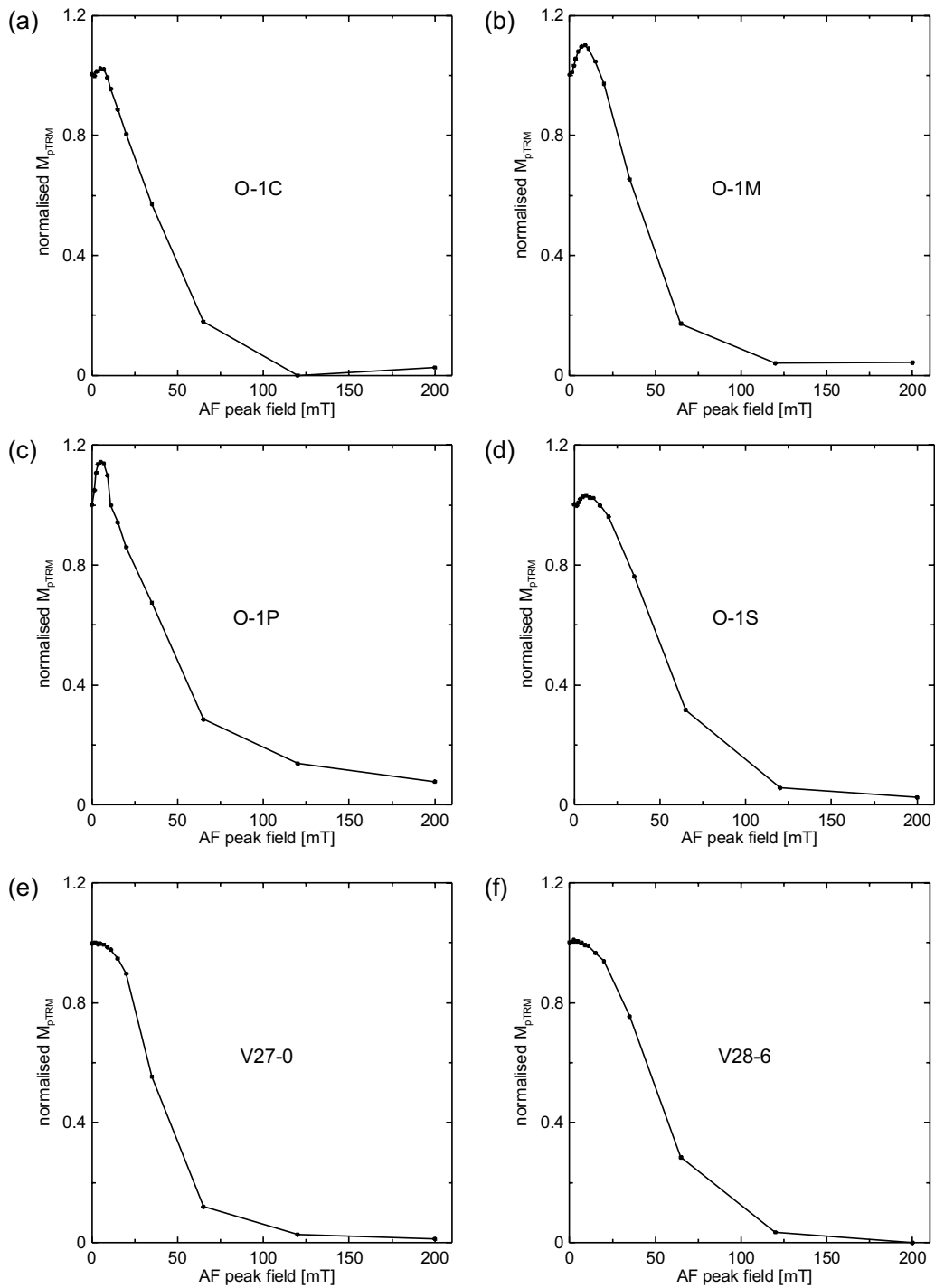


Figure 4.13: Alternating field demagnetisation of pTRM(600°C , 210°C , $25\ \mu\text{T}$). The pTRM was imparted in positive z direction in sample coordinates and the graphs represent the z component of magnetisation. All samples with a peak in M_{pTRM} during continuous thermal demagnetisation (Figure 4.11) also show an initial increase of magnetisation during AF demagnetisation.

0.7 %, respectively, after the first AF demagnetisation steps. This is probably due to overlapping coercivities of the two phases. Furthermore, the peak in magnetisation observed during continuous thermal demagnetisation (Figure 4.11) is much less pronounced for these two samples.

The finding of a low- T_b phase with low coercivity and a high- T_b phase with high coercivity supports results of rock magnetic experiments (chapter 2) assigning the lower Curie temperature to a non-oxidised or only slightly oxidised titanomagnetite mother phase and the higher Curie temperature to a daughter phase formed by low-temperature oxidation. ÖZDEMİR AND O'REILLY (1982) showed that in synthetic Al-substituted titanomagnetite single-domain grains H_C is increasing with increasing oxidation parameter z to a peak value at $z \approx 0.45 - 0.5$. Further oxidation results in a decrease of H_C . However, the authors note, that due to the synthetic nature and small grain size of the studied samples it is not possible to account for possible inhomogeneities as they occur in samples of the present study. These inhomogeneities in natural crystals are likely to increase internal stresses which in turn lead to a higher coercivity due to magnetoelastic anisotropy. In contrast to ÖZDEMİR AND O'REILLY (1982), RYALL ET AL. (1977) found an increase of the median destructive field (MDF) in AF demagnetisation by a factor of 2–3 as z increases from 0.5 to 0.8 for natural titanomaghemites in ocean basalts. A similar increase of MDF with low-temperature oxidation was also found by PETERSEN AND VALI (1987). An additional factor which might influence the variation of coercivity in the course of low-temperature oxidation was described by MOSKOWITZ (1980). He showed by theoretical calculations that the grain size thresholds between SP–SD, SD–two-domain (TD), and TD–PSD behaviour increase with increasing z . Therefore, particles with a given fixed grain size in the range of tens of microns change their domain state from PSD over TD to SD. Thus, their coercivity will increase during low-temperature oxidation.

4.4 The Laschamp event: Geomagnetic origin or self-reversal?

It is the matter of a long standing discussion if the reversed magnetisation of Laschamp and Olby samples is caused by a reversed geomagnetic field direction at the time of emplacement of the rocks or by self-reversal of magnetisation. HELLER AND PETERSEN (1982b) demonstrated that a reversed NRM is carried by the high- T_b component of the two phase samples from Olby. In contrast to that, the mean pole of the low- T_b remanence component is normal. However, data of individual samples are highly scattered about the Olby mean direction. Reverse, intermediate as well as normal remanence directions occur in the low- T_b interval. The high-temperature oxidised Laschamp samples containing only one single magnetic phase near magnetite all display a reverse NRM polarity as found earlier by BONHOMMET AND BABKINE (1967).

HELLER AND PETERSEN (1982a,b) concluded for the samples from Olby that the primary remanence was acquired in a normal geomagnetic field by the low- T_b phase (i.e. the non-oxidised primary titanomagnetite). The high dispersion is explained by strong viscous components which according to the authors are carried by superparamagnetic particles. In their view the low-temperature oxidised phase with a higher blocking temperature forms *after* acquisition of the primary remanence and acquires a reversed chemical remanent magnetisation (CRM) in the magnetostatic field of the low- T_b phase. This would imply that the reversed high-temperature component of the NRM is a pure artefact caused by self-reversal and not by a geomagnetic event.

The problem about this hypothesis is that it can not explain the reversed magnetisation of Laschamp samples. These have been subject to high-temperature oxidation (chapter 2 and 3) yielding a completely different magnetomineralogy. Thus, an analogous self-reversal mechanism as for the Olby samples cannot be invoked. Moreover, the primary titanomagnetite grains in Olby samples are in the magnetic multidomain range as shown by MFM observations in section 3.3. Therefore, the magnetostatic field of these grains is greatly reduced and presumably cannot account for the acquisition of a reversed CRM in the oxidised parts of the titanomagnetite particles. The MD size of the non-oxidised particles also

indicates that these grains are the carriers of the viscous magnetisation rather than SP particles as discussed by HELLER AND PETERSEN (1982b).

A third argument regards the change of magnetisation direction during low-temperature oxidation. If titanomaghemite as the product of low-temperature oxidation would acquire a CRM at ambient temperatures in the magnetostatic field of its mother phase, self-reversal due to magnetostatic interaction should occur very frequently especially in ocean floor basalts containing intermediately oxidised titanomagnetite grains. However, this is a very rare phenomenon (MATZKA, 2001). Instead, MARSHALL AND COX (1971), HALL (1977) and ÖZDEMİR AND DUNLOP (1985) demonstrated that titanomaghemite inherits the remanence direction of its mother phase in the course of low-temperature oxidation despite the application of deviating external fields of up to $100 \mu\text{T}$.

These arguments lead to the conclusion, that in samples from Olby the oxidised high- T_b (daughter) phase acquired a primary remanence parallel to the local field direction. Subsequently, the non-oxidised mother phase acquired a reverse magnetisation in the magnetostatic field of the daughter phase. This implies that oxidation took place during primary cooling of the lava flow at elevated temperatures above the blocking temperature of the titanomagnetite phase as indicated in chapter 3. The mode of oxidation thus probably ranges in-between low- and high-temperature oxidation.

A second implication is that the local geomagnetic field direction was indeed reversed, as both the high- T_b component of Olby samples and the single phase component of Laschamp samples show similar reversed remanence directions. Nevertheless, the question if the "Laschamp event" is a global or only local phenomenon is still not fully answered.

4.5 Conclusions

Complete and partial self-reversal is a phenomenon occurring in basalts containing titanomagnetite particles with two magnetic phases with markedly different magnetic properties. The NRM of most of these samples carries a significant viscous component in the low- T_b range. The low- T_b component is also the carrier of the fraction of remanence which is oriented antiparallel to the high- T_b remanence.

This reversed component is only identified after removal of the viscous overprint by heating and subsequent cooling of the sample in zero field. Using laboratory TRM, partially self-reversed remanence can only be imparted if the low- T_b phase is cooled in zero field. These findings lead to the conclusion, that in the case of unheated NRM and full TRM, partial self-reversal carried by the coupled low- T_b phase is either masked by low- T_b particles which are not coupled to the high- T_b phase, or, that the interaction field between the two phases is very weak (below the strength of the average Earth's magnetic field).

Regarding the actual mechanism of self-reversal, several authors (e.g. UYEDA, 1958; BANERJEE, 1966) have argued that the interaction fields of exchange coupling on the one hand and magnetostatic coupling on the other hand will differ by several orders of magnitude. In the case of exchange interaction values in the range of the molecular field (several Tesla) are expected, whereas the magnetostatic interaction field is supposed to be in the Millitesla range (HAAG ET AL., 1990a). Although these are only very crude estimates which itself vary by orders of magnitude in the literature, the observed very low field sufficient to suppress the phenomenon in the present study points clearly towards magnetostatic coupling as the cause of self-reversal in basalts. The geometric and mineral magnetic constraints of such an magnetostatic model will be discussed in detail in chapter 5.

Chapter 5

Numerical modelling of two-phase remanence acquisition

This chapter introduces a numerical model for the acquisition of thermoremanence in inhomogeneous ferrimagnetic particles. It has been shown in the experimental part of this work, that the remanence in samples displaying partial self-reversal is carried by inhomogeneous intergrowths of titanomagnetite as the mother phase and titanomaghemite formed by low-temperature oxidation as the daughter phase. The latter evolves preferentially along cracks pervading the grains and thus forms narrow ferrimagnetic bands with both a higher Curie temperature and higher magnetic stability compared to the mother phase. The two phases are in direct contact to each other; a fact which is making feasible both magnetostatic interaction and exchange coupling as the cause of self-reversal.

As PRÉVOT ET AL. (2001) have pointed out, superexchange interaction has an extremely short range. This makes it unlikely that this kind of interaction causes a substantial fraction of the comparatively large mother phase part of the grains being reversely magnetised. Superexchange interaction is basically a boundary layer phenomenon. However, the actual volume of the boundary layer potentially being subject to superexchange interaction between the two phases is very small compared to the total volume of the grain. The experimentally observed geometry of the two phases makes thus magnetostatic interaction much more favourable as the magnetostatic field is not confined to the boundary layer.

In order to quantitatively understand the experimentally observed two-phase arrangement causing the phenomenon of partial or complete self-reversal, a theoretical model was developed on the basis of observed magnetomineralogical and geometrical constraints. The model was mathematically formulated in cooperation with V. P. SHCHERBAKOV during his visit at the Munich Geophysics Section as a research fellow of the *Deutscher Akademischer Austauschdienst* (DAAD) in 2002 and will be described in the following sections.

5.1 The analytical model of a spherical two-phase grain

An earlier theoretical approach to this problem by STEPHENSON (1975) was based on the experimental findings of PETHERBRIDGE ET AL. (1974), who observed a decrease of room temperature saturation remanent magnetisation (SIRM) on cooling in synthetic titanomagnetites containing a minor amount of a magnetic phase with composition close to magnetite. STEPHENSON suggested that this decrease is due to magnetic screening of the magnetically hard magnetite phase (phase A, permeability μ_A) by the surrounding soft titanomagnetite phase (phase B, μ_B). The term screening in this context describes the effect that the magnetic field lines originating in the remanent magnetisation of phase A are refracted at the boundary to phase B due to the contrast in permeability. As $\mu_B > \mu_A$, the magnetic field lines will be concentrated in the surrounding phase B. Consequently, the stray field of the two-phase grain will be reduced when compared to the stray field of phase A alone. Experimentally, the total magnetisation is determined from the strength of the external stray field. Hence, the measured net magnetisation will also be reduced.

STEPHENSON (1975) considered a simple model of a sphere with permeability μ_A , remanent magnetisation M_{RA} and Curie temperature T_{CA} surrounded by a spherical shell with permeability $\mu_B = 1 + 4\pi\kappa$, where κ is the susceptibility, and Curie temperature $T_{CB} < T_{CA}$ (Figure 5.1). κ is assumed to be constant at temperatures below T_{CB} . At temperatures above T_{CB} κ is zero and thus $\mu_B = 1$.

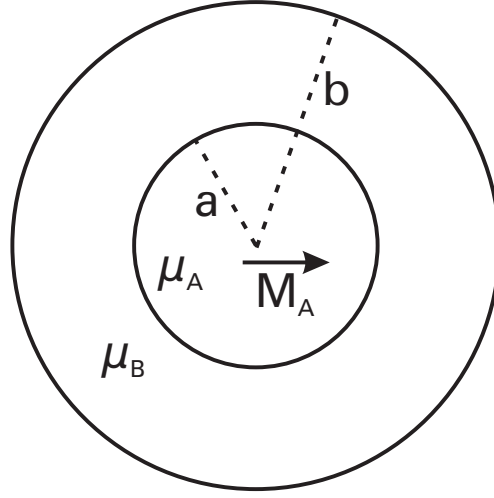


Figure 5.1: Two-phase model of a sphere with permeability μ_A surrounded by a spherical shell with permeability μ_B (redrawn after STEPHENSON (1975)).

If the remanence of phase A is blocked completely below some blocking temperature $T_{bA} > T_{CB}$, $M_{RA}(T)$ will be proportional to the temperature dependence of saturation magnetisation $M_{SA}(T)$ of the A-phase. The magnetic moment of the complete particle above T_{CB} is thus:

$$m(T) = m_0 m_{SA}(T), \quad T_{bA} > T > T_{CB} \quad (5.1)$$

with saturation moment $m_0 = (4\pi/3)a^3 R M_{SA}(T_0)$ (T_0 : room temperature), the ratio $R = M_{RA}/M_{SA}$ and $m_{SA}(T) = M_{SA}(T)/M_{SA}(T_0)$ being the saturation magnetisation normalised to the room temperature value.

STEPHENSON (1975) showed that due to the increase of μ_B below T_{CB} which results in effective screening of the moment m_0 , the total moment $m(T)$ is reduced to

$$m(T) = m_0 m_{SA}(T) \frac{9\mu_B + h(T)(1 - \sigma)(2\mu_B^2 - \mu_B - 1)}{(2\mu_B + 1)(\mu_B + 2) - 2\sigma(\mu_B - 1)^2}, \quad T < T_{CB} \quad (5.2)$$

with $\sigma = (a/b)^3$ and the reduced magnetic field

$$h(T) = \frac{3H_{\text{ext}}}{4\pi R M_S(T)} \quad (5.3)$$

where H_{ext} denotes the external magnetic field. For further calculations assume

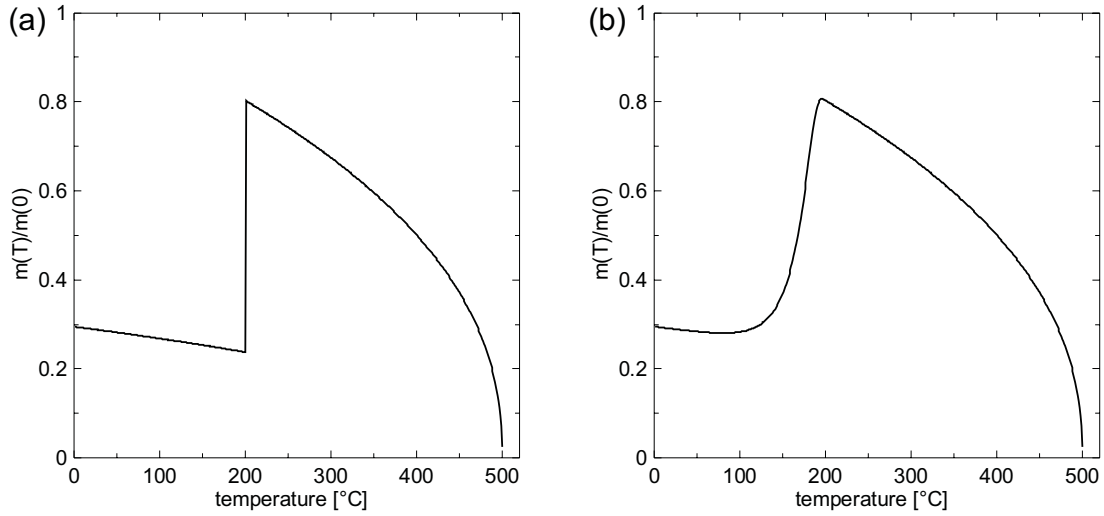


Figure 5.2: Results of modelled thermoremanence acquisition for the spherical two-phase grain. (a) $\mu_B(T) = 1 + 4\pi\kappa(T)$ is defined by a step function with $\kappa(T < T_{CB}) = 1$ and $\kappa(T > T_{CB}) = 0$. (b) $\mu_B(T)$ is defined by Equation 5.5.

now that T_{bA} is close to T_{CA} . The temperature dependence of saturation magnetisation of the A-phase is approximated by

$$M_{SA}(T) \propto \left(\frac{T_{CA} - T}{T_{CA}} \right)^\gamma \quad (5.4)$$

with $\gamma = 0.43$ for magnetite (DUNLOP AND ÖZDEMİR, 1997).

The analytical expression for $m(T)$ was evaluated using $T_{CA} = 500$ °C, $T_{CB} = 200$ °C, $M_{SA}(T_0) = 400$ e.m.u., $H_{ext} = 0.5$ e.m.u., $\sigma = (3/8)^3$, $R = 0.05$ (assuming the theoretical threshold for MD particles) and $\kappa = 1$. The result is shown in Figure 5.2a. The sudden decrease of magnetisation at T_{CB} similar to the experimental demagnetisation data in chapter 4 is clearly seen. Although STEPHENSON (1975) used this model to explain the decrease of SIRM on cooling it can also be applied to partial self-reversal of TRM as in both cases the A-phase will carry a stable TRM during the cooling process.

In natural samples the composition of the B-phase will slightly differ from grain to grain. Thus, the drop in $m(T)$ in reality will not be as sharp as in the model above. To account for this fact a temperature dependence of μ_B with a smooth increase in the vicinity of T_{CB} is assumed rather than a step function.

For this purpose the function $\mu_B(T)$ is introduced:

$$\mu_B(T) = 1 + 4\pi\kappa_0 \tanh^2 \frac{T_{CB} - T}{\Delta} \quad (5.5)$$

The *tangens hyperbolicus* function is used to describe phenomenologically the temperature dependence of κ and Δ is the adjusting parameter describing the width of the temperature interval where κ is increasing to its full value κ_0 . The result of the modified calculation with $\Delta = 50^\circ\text{C}$ is shown in Figure 5.2b.

The calculations show that the drop in magnetisation during cooling can be explained reasonably well with magnetic screening of the magnetic moment of a hard A-phase by a soft B-phase. Nevertheless, this model cannot account for a complete self-reversal, as the net magnetic moment cannot be reversed by magnetic screening.

Therefore, the STEPHENSON (1975) model is now extended by assigning a coercivity $H_C > 0$ to phase B. This leads to blocking of magnetic remanence if the temperature drops below a blocking temperature T_{bB} . If the saturation magnetisation M_{SB} of phase B grows faster than M_{SA} it is then possible that the reversely directed remanence M_{RB} outweighs M_{RA} resulting in a reversed net magnetisation of the particle.

To quantify this model, the right-hand side of Equation 5.2 is split into two terms to separate the contributions of the two phases:

$$m(T) = m_0 m_{SA}(T) \left[1 + \left(\frac{9\mu_B + h(T)(1 - \sigma)(2\mu_B^2 - \mu_B - 1)}{(2\mu_B + 1)(\mu_B + 2) - 2\sigma(\mu_B - 1)^2} - 1 \right) \right] \quad (5.6)$$

The blocking condition is introduced by stating that below T_{bB} the magnetic moments of both phases do not change their direction anymore and are both increasing proportionally to their respective M_S . Accordingly, Equation 5.6 is rewritten as

$$m(T) = m_0 \left\{ m_{SA}(T) + \frac{m_{SB}(T)}{m_{SB}(T_{bB})} m_{SA}(T_{bB}) \cdot \left[\frac{9\mu_B(T_{bB}) + h(T_{bB})(1 - \sigma)(2\mu_B(T_{bB})^2 - \mu_B(T_{bB}) - 1)}{(2\mu_B(T_{bB}) + 1)(\mu_B(T_{bB}) + 2) - 2\sigma(\mu_B(T_{bB}) - 1)^2} - 1 \right] \right\} \quad (5.7)$$

Analogous to $M_{SA}(T)$ (Equation 5.4) the temperature dependence of $M_{SB}(T)$ is defined as

$$M_{SB}(T) \propto \left(\frac{T_{CB} - T}{T_{CB}} \right)^{0.43} \quad (5.8)$$

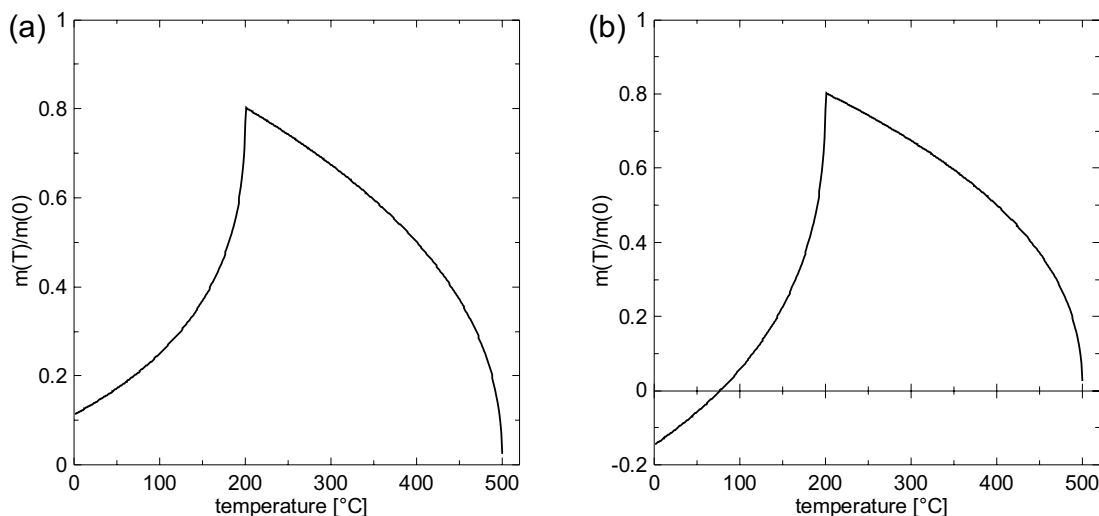


Figure 5.3: Results of modelled thermoremanence acquisition for the spherical two-phase grain with added blocking condition for phase B. (a) With $\kappa = 1$ only partial self-reversal develops. (b) If $\kappa = 2$ complete self-reversal is reached.

The blocking temperature of phase B was set to $T_{bB} = 150^\circ\text{C}$, all other parameters remained the same as for the previous calculations. The results are shown in Figure 5.3. If κ_0 is set to 1 only partial self-reversal is visible (Figure 5.3a). However, if κ_0 is increased to 2, complete self-reversal develops (Figure 5.3b). This can also be achieved by reducing Δ or increasing σ as will be shown in the next section.

5.2 Numerical model for arbitrary geometries

The analytical model developed in the previous section is only applicable to simple geometries like the spherical shell model and cannot account for the real situation in natural titanomagnetites. Inhomogeneities are likely to occur in natural titanomagnetite particles and a two phase arrangement responsible for self-reversal in the present case is caused by oxidation processes. The development of two distinct phases itself is manifestation of inhomogeneous alteration on the micrometre scale which is influenced by the presence of cracks or the proximity of grain boundaries. At the same time inhomogeneities may also evolve on the

sub-micrometre scale giving rise to a broad distribution of coercivities and thus blocking conditions. In order to fit a theoretical model to the experimentally observed data, a numerical approach is developed in the following.

The conventional micromagnetic approach takes into account magnetostatic, exchange, and magnetocrystalline energies to calculate the distribution of magnetisation vectors on the scale of domain wall width. This technique is computationally extremely time consuming and with today's computing power it is limited to a grain size below $\approx 2\mu\text{m}$. The particles in the present case are, however, in the size range of tens of microns and a classic micromagnetic approach is thus not feasible. On the other hand, to explain the self-reversal phenomenon it is not necessary to know the exact microscopic magnetisation structure of the particle but rather macroscopic properties like the net magnetisation of the whole grain. Thus the method is modified insofar, as the exchange and magnetocrystalline anisotropies are substituted by their macroscopic manifestations coercivity and susceptibility. The magnetostatic energy is accounted for by the demagnetising factor N_d . With the phenomenological approach of NÉEL (1955) the total energy of the grain can then be written as:

$$E = -MH_{\text{ext}} + \frac{M^2}{2\kappa} - N_d M^2 \pm MH_C \quad (5.9)$$

The minimum of Equation 5.9 is found at

$$M = \kappa \frac{H \pm H_C}{1 + N_d \kappa} \quad (5.10)$$

In the limit $\kappa \rightarrow \infty$ this is exactly NÉEL's (1955) hysteresis loop equation. For $H_C = 0$ it is the classical expression for the magnetisation of a multidomain grain in low fields. The plus and minus signs in Equations 5.9 and 5.10 correspond to the descending and ascending branch of the hysteresis loop, respectively.

To account for the three dimensional structure of the grain and for inhomogeneous distributions of self-demagnetising field (which is a vector field), coercivity and susceptibility, Equation 5.9 has to be transformed into a vectorial notation. For this purpose, also the coercivity H_C is written formally as a vector $\vec{H}_C = \{H_{Cx}, H_{Cy}, H_{Cz}\}$.

The resulting functional is then integrated over the volume of the grain and the total energy has to be minimised with respect to the magnetisation $\vec{M}(\vec{r})$ where

\vec{r} is the radius vector. For this purpose the volume of the grain is subdivided into a number of cells defined by a three-dimensional orthogonal grid of cubic volume elements. The number of subcubes is $N = n \times m \times l$, where n , m and l is the number of subcubes along the x -, y - and z -axis, respectively. The magnetisation \vec{M}_i ($i = 1, \dots, N$) of each subcube is assumed to be homogeneous. The total energy can now be summed up over the discrete set of N cells:

$$E = \sum_{i=1}^N \sum_{\alpha=x,y,z} [-M_{\alpha i} (H_{\text{ext}}^{\alpha} \pm H_{C\alpha}) + \frac{M_{\alpha i}^2}{2\kappa} + N_d \frac{M_{\alpha i}^2}{2} + \sum_{j>i}^N \sum_{\beta=x,y,z} V_{\alpha\beta ij} M_{\alpha i} M_{\beta j}] \quad (5.11)$$

where $V_{\alpha\beta ij}$ are the components of the matrix of magnetostatic interactions (FABIAN ET AL., 1996; SHCHERBAKOV AND SYCHEVA, 2001). For computation of the magnetostatic energy the Fast Fourier Transform (FFT) technique is used. The minimisation of total energy is performed using the conjugate gradient algorithm.

The blocking condition is taken after NÉEL (1955): If the total field acting on a single cell is below its coercivity H_C , this cell is regarded as being blocked. The blocking condition is thus:

$$|H_{C\alpha}| \geq |H_{\text{ext}}^{\alpha} + H_{\text{int}}| \quad (5.12)$$

with H_{int} being the internal field.

Phase A is blocked from the very beginning and the minimisation procedure ignores cells of phase B if the blocking condition is met. In analogy to the analytical model the magnetisation of blocked cells varies only proportional to $M_{\text{SB}}(T)$. The blocking condition described in Equation 5.12 is much closer to reality than the analytical model, as not the complete B-phase is blocked at a certain temperature. Blocking of each separate cell depends on the sum of interaction and external field for that cell, which in turn is dependent e.g. on the distance from phase A. As H_{int} is also dependent on temperature, a range of blocking temperatures will evolve.

Figure 5.4 shows results for the spherical two-phase model calculated on a $15 \times 15 \times 15$ grid. The following parameters are used: $T_{\text{CA}} = 500^\circ\text{C}$, $T_{\text{CB}} = 200^\circ\text{C}$, $M_{\text{SA}}(T_0) = 400$ e.m.u., $H_{\text{ext}} = 0.5$ e.m.u., $a/b = 3/8$, $R = 0.05$, $\kappa = 1$. Figure 5.4a was calculated with $\Delta = 30^\circ\text{C}$ and $H_C(T) = 0.01M_{\text{SB}}(T_0)$, Figure 5.4b with

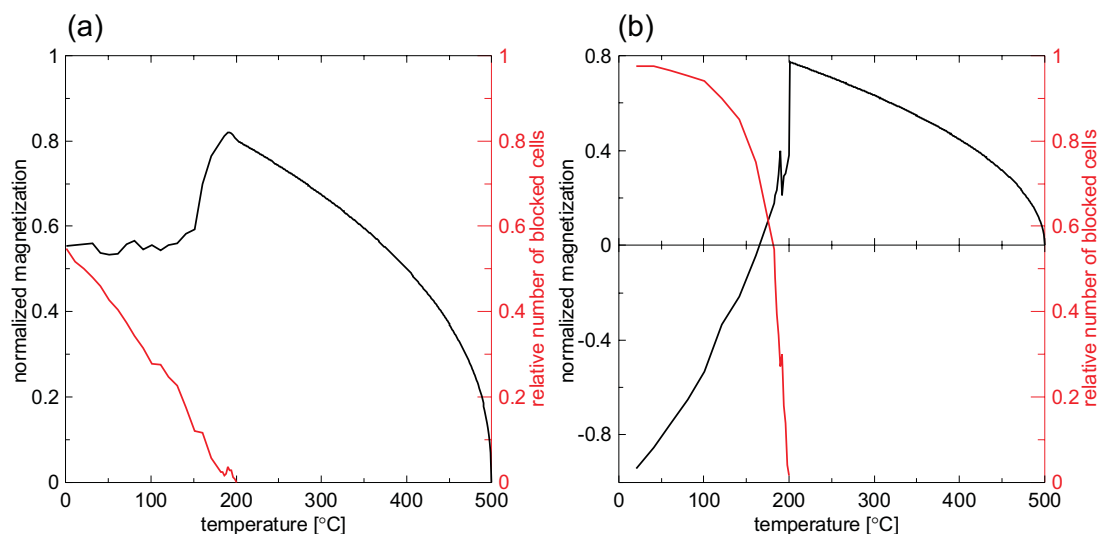


Figure 5.4: Results of numerical calculations for the spherical two-phase grain. (a) Only partial self-reversal develops if $H_C = 0.01M_{SB}(T_0)$ and $\Delta = 30^\circ\text{C}$. (b) If $H_C = 0.1M_{SB}(T_0)$ and $\Delta = 0$ self-reversal is reached. Red lines show the relative number of blocked cells.

$\Delta = 0$ and $H_C(T) = 0.1M_{SB}(T)$. The main difference is, that calculation (a) shows only partial self-reversal whereas in calculation (b) complete self-reversal takes place. This is due to the fact, that the blocking temperature spectrum is shifted to lower temperatures for lower H_C , which is also visible in the plot of the relative number of blocked cells (red line). This curve shows that for lower coercivities blocking starts right at T_{bB} and at room temperature still only about 55% of the cells are blocked. In contrast to that data for calculation (b) shows that 90% of cells are blocked already at 120°C . This fact enables complete self-reversal because the $M_{SB}(T)$ curve is much steeper at temperatures just below T_{bB} than at lower temperatures. As M_R of blocked cells is proportional to M_{SB} the decrease of total remanence is much more pronounced for high blocking temperatures.

The magnetic structure of calculation (b) at room temperature is shown in Figure 5.5. As expected, phase B has a strong component of \vec{M}_{RB} which is aligned with the external field and with \vec{M}_{RA} at positions near the axis of rotational symmetry. However, larger part of the phase B volume off the symmetry axis has a negative x -component (antiparallel to \vec{M}_{RA}) which causes the decrease of total M_R at temperatures below T_{CB} . This antiparallel component arises from

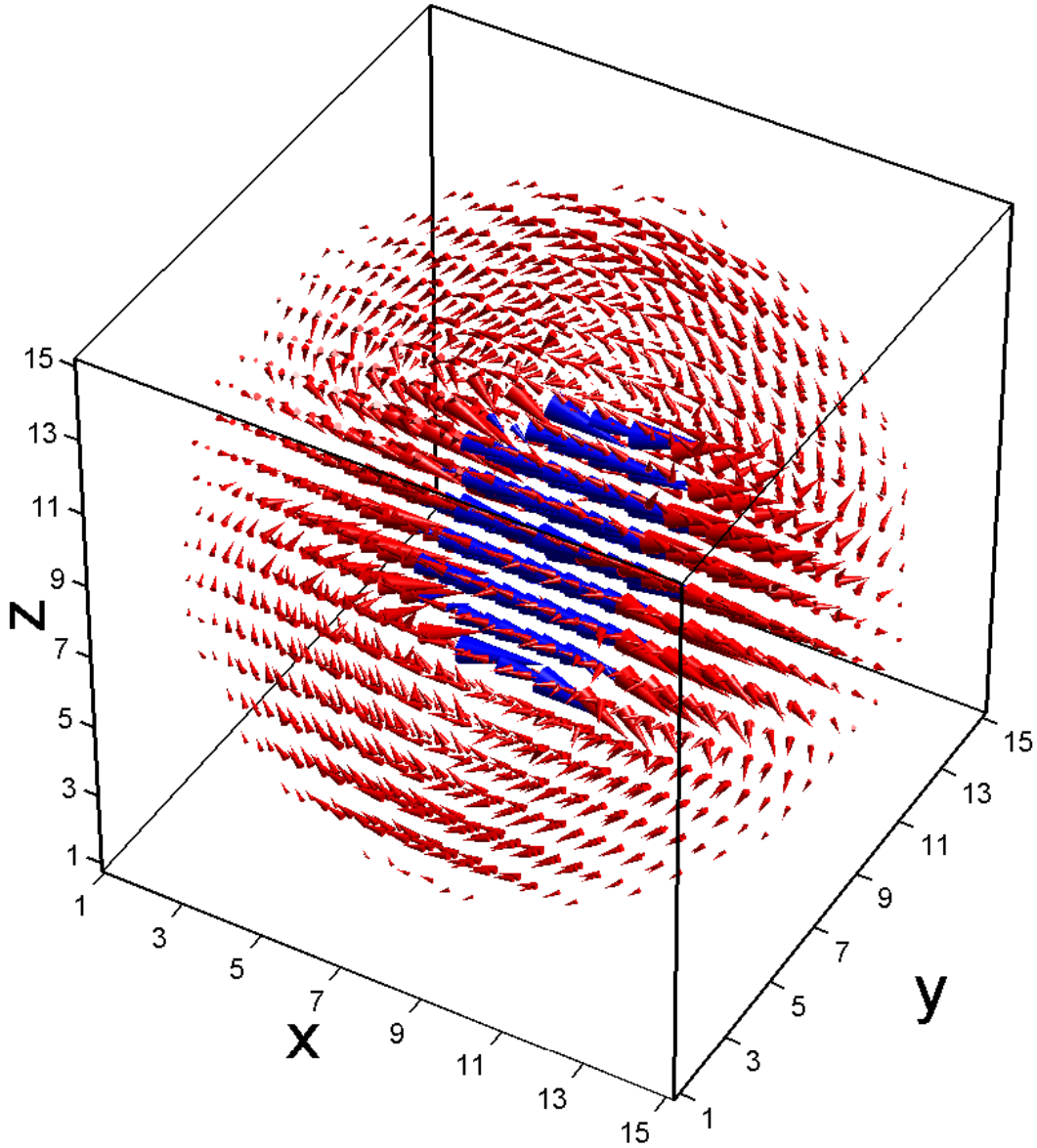


Figure 5.5: Magnetisation structure for the spherical two-phase grain resulting from the calculated remanence acquisition shown in Figure 5.4b. Magnetisation vectors of phase A are shown in blue, vectors of phase B in red. The external field is directed parallel to the x -axis.

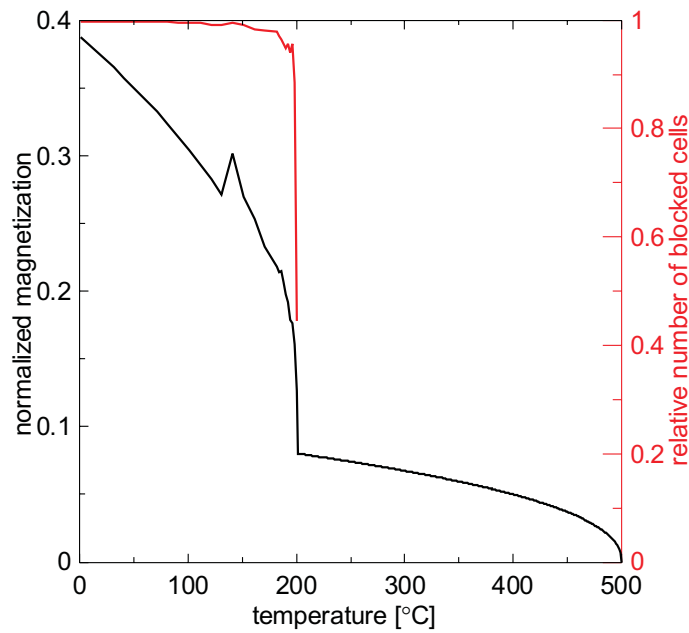


Figure 5.6: Result for spherical model with phase A consisting of one cell ($a/b = 1/16$). Further parameters $H_C(T) = 0.02M_{SB}(T)$, $H_{\text{ext}} = 0.05$ e.m.u, $\kappa = 1$. H_{ext} largely outweighs H_{int} and thus self-reversal is not observable.

the fact, that the reverse component of H_{int} outweighs the external field which is directed in positive x direction. As stated above, the strength of H_{int} is highly dependent on the distance between phase A and the respective cell and also on the total magnetic moment of phase A and thus its size.

To evaluate this dependence one more calculation was performed with phase A consisting only of a single cell in the centre of the sphere ($a/b = 1/16$). The result is shown in Figure 5.6. The $M_R(T)$ curve shows an increase in remanent magnetisation below T_{CB} rather than a decrease as for the previous calculations. This shows, that H_{ext} largely outweighs H_{int} . Thus, the x -component of the net magnetisation of phase B at room temperature points in direction of the external field and no self-reversal is observable. In terms of the experimentally observed grain geometry this means, that if phase A is very small in relation to phase B, only domains directly adjacent to phase A will acquire a reversed magnetisation, whereas the rest of grain is not influenced by H_{int} and will thus mask the self-reversal in thermal demagnetisation runs.

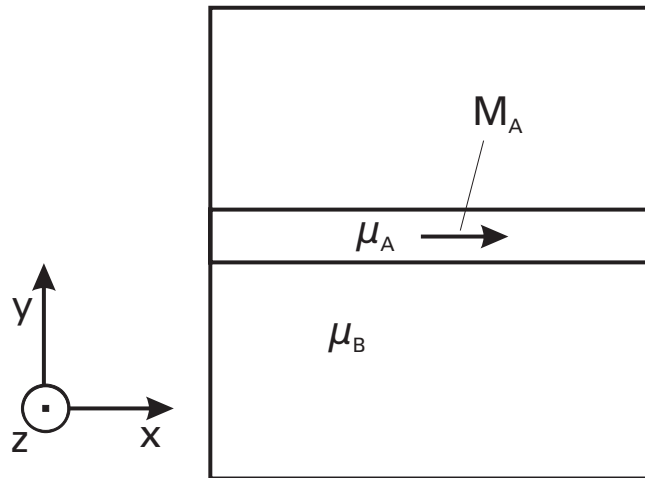


Figure 5.7: Simple rectangular model geometry. Phase A consists of a thin plate in the x - z plane inside the rectangular phase B grain. The external field is directed along the x axis.

To fit the numerical model to the microscopically observed distribution of phase A predominantly along linear cracks, a further model geometry shown in Figure 5.7 was calculated. In this case a thin layer of phase A is fitted in the centre of a rectangular phase B grain in the plane of the x and z axes. H_{ext} is directed along the x axis. These calculations are shown in Figure 5.8. Panel (a) shows two remanence acquisition curves for identical parameters with the exception of Δ . In case of $\Delta = 0^\circ\text{C}$ (causing a step function for the temperature dependence of κ) complete self-reversal develops whereas only a slight increase to $\Delta = 10^\circ\text{C}$ leads to partial self-reversal. As the number of blocked cells increases very steeply just below T_{CB} , a minor shift of T_{bB} towards lower temperatures is sufficient to cause a substantial change in room temperature remanence intensity. This shows that already a small delay in gaining the full value of κ leads to a significantly reduced reversed magnetisation of phase B which is probably another reason why complete self-reversal develops quite rarely in natural samples.

Panel (b) displays the remanence acquisition for reduced coercivity of phase B ($H_{\text{C}}(T) = 0.01M_{\text{SB}}(T)$) and a Δ of 50°C . As already seen for the spherical grain, reduced coercivity leads to a considerable shift of the blocking temperature spectrum towards lower temperatures. At room temperature only $\approx 50\%$ of the cells are blocked and thus only partial self-reversal develops.

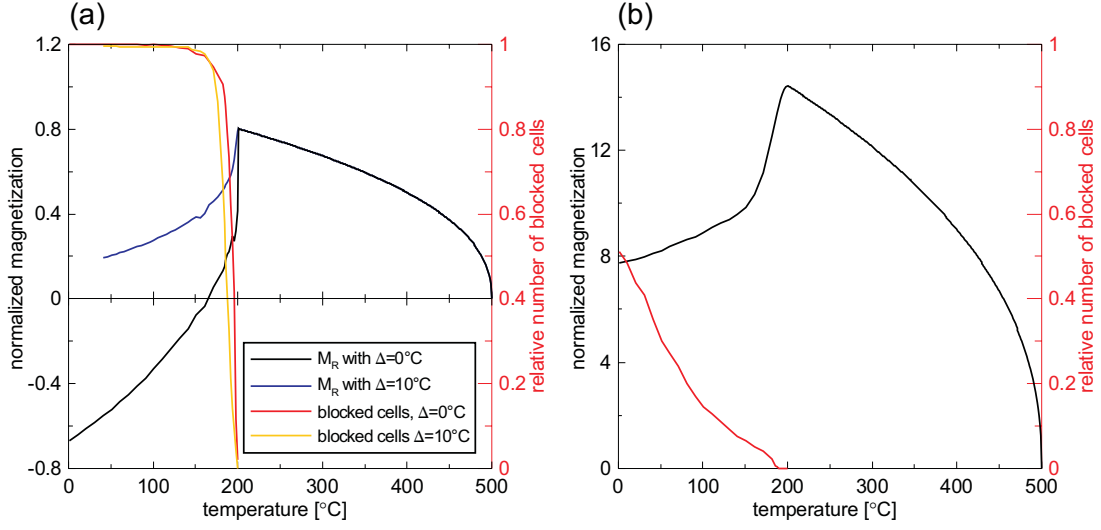


Figure 5.8: Results of numerical calculations for the rectangular two-phase grain. (a) Parameters: $T_{CA} = 500^\circ\text{C}$, $T_{CB} = 200^\circ\text{C}$, $M_{SA}(T_0) = 400$ e.m.u., $H_{\text{ext}} = 0.5$ e.m.u., $R = 0.05$, $\kappa = 1$ and $H_C(T) = 0.1M_{SB}(T)$. Black remanence curve corresponds to $\Delta = 0^\circ\text{C}$, blue curve to $\Delta = 10^\circ\text{C}$. (b) Calculation for lower $H_C(T) = 0.01M_{SB}(T)$ and $\Delta = 50^\circ\text{C}$.

The magnetic structure for the grain of Figure 5.8a displaying complete self-reversal is shown in Figure 5.9. As the phase A layer extends to both x - z grain surfaces there are no phase B cells with an x -component of magnetisation in direction of the external field. In contrast to the spherical two-phase grain all phase B cells have thus a reversed x -component of remanence which makes the layered geometry much more favourable for self-reversal. One has to keep in mind, though, that this grain model has a reduced symmetry compared to the spherical grain. If the external field and thus \vec{M}_{RA} is oriented perpendicular to the phase A layer, self-reversal is not possible as all moments (or cells) will have a predominant magnetisation component in the direction of H_{ext} . Considering a bulk sample with many grains where the phase A layers are randomly oriented, the ability for self-reversal will be greatly reduced. This favours partial self-reversal rather than complete self-reversal as only a certain part of phase B particles will carry a reversed remanence.

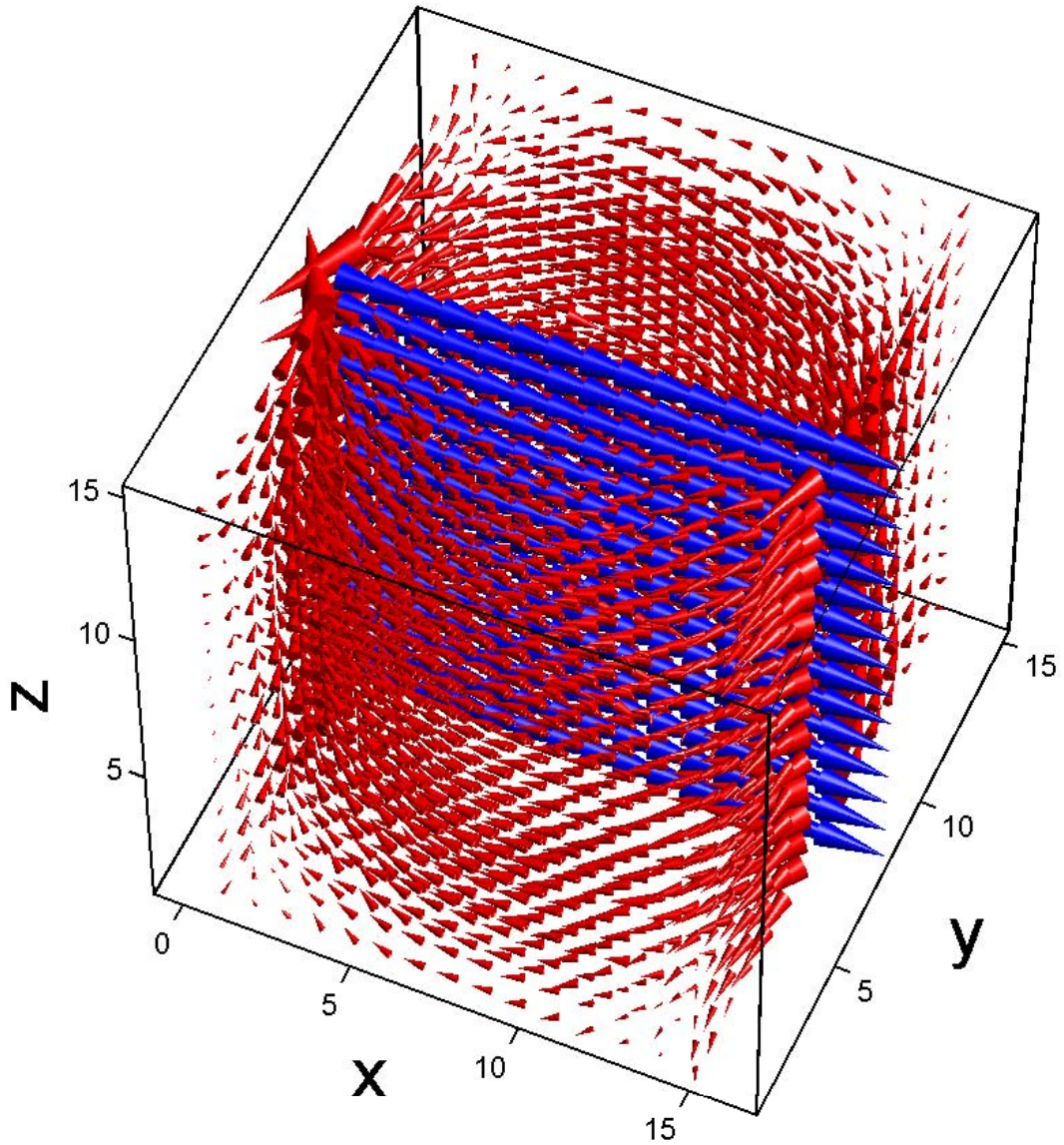


Figure 5.9: Magnetisation structure for the rectangular two-phase grain resulting from the calculated remanence acquisition shown in Figure 5.8a. Magnetisation vectors of phase A are shown in blue, vectors of phase B in red. The value of magnetisation $|\vec{M}_{RB}|$ for phase B cells (represented by the size of the cones) is scaled by the factor 1.5 compared to phase A. The external field is directed parallel to the x -axis.

5.3 Conclusions

The calculations of this chapter show, that the microscopically determined grain configuration is capable of causing partial and complete self-reversal. The two phases are coupled magnetostatically. The special geometry with the two phases being in close contact to each other can evolve by low-temperature oxidation of the primary phase (phase B) which is transforming titanomagnetite into titanomaghemite (phase A) and is preferentially advancing along cracks. Maghemitisation will also increase the Curie temperature and the coercivity thus yielding the necessary magnetic parameters for phase A for the mechanism of self-reversal to occur.

Chapter 6

Detection of self-reversal and MD effects in Thellier experiments

Absolute palaeointensity estimates determined on rocks carrying a thermoremanent magnetisation (TRM) are vital for the reconstruction of the ancient geomagnetic field and, by implication, the behaviour of the geodynamo in the geological past. Among the many proposed experimental procedures the THELLIER AND THELLIER (1959) method and its modifications proved to be the most successful. This method relies on the assumption that the intensity of a TRM is proportional to the strength of the applied magnetic field in which it was acquired. Thus, if the natural remanent magnetisation (NRM) carried by a rock sample is a pure TRM acquired in an unknown ancient field H_n , its intensity M_{NRM} can be compared to the intensity M_{TRM} of a laboratory TRM which is acquired in a known laboratory field H_{lab} . The ancient field strength is then given by:

$$H_n = \frac{M_{\text{NRM}}}{M_{\text{TRM}}} \cdot H_{\text{lab}} \quad (6.1)$$

In order to obtain several independent estimates of the palaeointensity, to identify possible viscous overprints and to analyse the result statistically, the experiment is performed in successive double heating steps: First the sample is partially demagnetised by heating it to a temperature T_i ($i = 1, \dots, n$) and cooling it in zero field. After measuring the remaining NRM, the sample is heated again to T_i and cooled in the applied laboratory field to impart a partial TRM (pTRM). Then the pTRM intensity is determined. Each value of remaining NRM is then

plotted versus the respective pTRM gained. In the ideal case, these points lie on a straight line with slope $-H_n/H_{lab}$.

Besides the proportionality of applied field and TRM intensity, two more basic assumptions known as Thellier's laws have to be fulfilled:

- Independence of partial thermoremanences (pTRM): A pTRM acquired between T_1 and T_2 (pTRM(T_1, T_2)) with $T_1 > T_2$) must not be changed by heating the sample to a temperature below T_2 and must be completely demagnetised by heating the sample above T_1 .
- Additivity of pTRMs. The sum of separate pTRMs, pTRM(T_1, T_2) + pTRM(T_2, T_3) ($T_1 > T_2 > T_3$) equals the pTRM over the joint temperature interval pTRM(T_1, T_3).

Main causes for the violation of these laws are chemical alteration, which can be detected by pTRM checks introduced by COE (1967), thermoremanence carried by multidomain (MD) particles and, as will be shown, also the presence of partially self-reversed TRM. For the reliability of the obtained results it is of crucial importance to assess the influence of these effects.

6.1 Relevant properties of multidomain and partially self-reversed thermoremanence

MD remanence, causing a difference between blocking and unblocking temperatures (T_b and T_{ub} respectively) and thus giving rise to a so-called MD tail (SHASHKANOV AND METALLOVA, 1972), invalidates Thellier-Thellier experiments if $T_b > T_{ub}$. In this case, linearity of the NRM-TRM plot is destroyed (FABIAN, 2001). As SHCHERBAKOV ET AL. (1993) pointed out, MD pTRM is also dependent on the thermal prehistory of the sample. One of the main consequences is that the law of additivity in the case of MD particles is in fact valid for a regular pTRM, i.e. the maximum temperature of pTRM acquisition is reached by cooling the sample from its Curie temperature T_C in zero field. The pTRM used in Thellier-Thellier experiments, however, is of the pTRM* type, i.e. the maximum temperature of pTRM acquisition is always reached by heating the

sample from room temperature and the sample is never heated beyond that temperature. SHCHERBAKOV ET AL. (1993) showed that additivity does not hold for pTRM* applied to MD samples. Thus, it should be possible to distinguish between MD and SD grains by checking the validity of the law of additivity of pTRM*.

So far, determination of the domain state for the selection of suitable samples for Thellier-Thellier experiments relies usually on hysteresis measurements using the theoretical limits of the H_{CR}/H_C and the M_{RS}/M_S ratio (DAY ET AL., 1977). However, interpretation of these data is not straightforward, as natural samples often consist of mixtures of SD, MD or SP particles. Moreover, the results depend not only on domain state but also on factors like internal stress of the grains (DUNLOP, 2002).

On the other hand, detection of MD remanence is hitherto pursued by measuring the tail of pTRMs. MCCLELLAND AND BRIDEN (1996) proposed to check for MD behaviour by introducing additional heating steps to the Thellier-Thellier experiment. In this modified procedure the sample is demagnetised by heating to a temperature $T_i > T_0$ and subsequent cooling in zero field, then a pTRM*(T_i, T_0) is imparted followed by a demagnetisation of this pTRM* by heating the sample again to T_i and cooling it in zero field. This test was later used for a modified Thellier technique (MT3) by LEONHARDT ET AL. (2000) to exclude samples dominated by MD particles and more recently by RIISAGER AND RIISAGER (2001). However, although there is a MD tail resulting from pTRM* as well, it is nonetheless much smaller than the tail of a regular pTRM (SHCHERBAKOVA ET AL., 2000).

Another domain state criterion based on the observation of a tail of a regular pTRM was proposed by SHCHERBAKOV ET AL. (2001). The authors introduced the parameter A_a which is the tail of pTRM(T_1, T_2) normalised to pTRM(T_1, T_2) intensity. However, as they also pointed out, the disadvantage of this criterion is the need to heat the samples to T_C , potentially causing serious chemical alteration, in order to acquire a regular pTRM. Another drawback is the fact, that this test can only be performed on sister samples of the sample used for the Thellier-Thellier experiment, as the NRM is completely demagnetised.

The failure of the law of additivity in the case of samples exhibiting partial self-reversal is caused by the fact that these samples contain two magnetic phases with different blocking and unblocking temperature spectra which are interacting under certain circumstances. If a pTRM* over the blocking temperature range of the low- T_C phase is imparted, this phase carries a remanence in the direction of H_{ext} . However, if a pTRM* in the T_b interval of the high- T_C phase is imparted, the low- T_C phase acquires a remanence which is directed antiparallel to the high- T_C remanence (see chapter 4). The same applies for the demagnetisation of a total TRM to a temperature at or above the maximum T_{ub} of the low- T_C phase. This indicates that the two phases are not independent of each other and that the low- T_C phase can acquire a parallel or antiparallel thermoremanence depending on the thermal treatment. As the Thellier-Thellier experiment consists of heating steps with and without applied external field, partial self-reversal will seriously affect the obtained results.

In order to detect MD effects and the coupling of two different magnetic phases during Thellier-Thellier experiments, a check is proposed which makes use of the failure of the law of additivity for the case of MD pTRM* (KRÁSA ET AL., 2003) and for partially self-reversed thermoremanence.

6.2 Sample description and experimental methods

In order to evaluate the efficiency of the test, complete Thellier-Thellier experiments plus the additivity checks at various temperature intervals were performed on basalt samples exhibiting partial self-reversal and on synthetic magnetite samples of different grain sizes. Seven commercially available synthetic samples were used for this study: Three pseudo single-domain (PSD) samples with a grain size below $1\mu\text{m}$ (threshold for PSD particles according to DUNLOP AND ÖZDEMIR (1997)) and three MD samples (grain size up to $12.1\mu\text{m}$) from *Wright Industries Inc.* (New York) and one SD sample which was obtained by reducing fine-grained maghemite (average grain size $0.023\mu\text{m}$) available from *Alfa Aesar* (Karlsruhe). The properties of these samples are summarised in Table 6.1.

Table 6.1: Grain size and rock magnetic parameters of synthetic samples.

Type	name	d_n [μm]	d_m [μm]	T_C [$^\circ\text{C}$]	T_V [K]	M_{RS}/M_S	H_{CR}/H_C	S_d/SIRM @920 mT [%]	
Alfa Aesar	MGH1	0.023	-	577	120	0.19	2.03	2.1	
	3006	W1	-	0.7	578	117	0.06	4.54	3.6
	4000	W2	0.5	< 0.5	578	116	0.14	2.44	2.3
	31182	W3	-	0.5	582	126	0.07	3.54	2.8
	33093	W4	7	5.7	586	126	0.03	5.90	0.8
	42093	W5	11	8.3	577	126	0.03	5.09	0.3
	112982	W6	-	12.1	583	115	0.02	8.37	0.04

Samples W1–W6 were obtained from *Wright Industries Inc.* Nominal grain size (d_n) is the size given by the manufacturer. The mean grain size (d_m) was determined on SEM pictures by picking 500 grains for each sample and using a log-normal fit. S_d : viscous decay coefficient.

In order to diminish intergrain magnetostatic interaction, the samples were dispersed in CaF_2 to obtain a magnetite content of about 3 weight-%. To avoid major chemical changes during the Thellier-Thellier experiment, the samples were sealed in evacuated quartz glass tubes and were heated for 3 hours to 700°C to stabilise them thermally. For the experiments a laboratory total TRM($700^\circ\text{C}, 20^\circ\text{C}$) in a field of $60 \mu\text{T}$, resembling the NRM of a natural sample and thus simply called NRM in the following, was then imparted. The laboratory field used for pTRM* acquisition during the Thellier-Thellier experiment was also $60 \mu\text{T}$.

The rock magnetic characterisation of the samples was performed by measuring hysteresis parameters, $M_S(T)$ curves and, as a proxy for SP grains, the viscous decay coefficient defined as $S_d = (\text{IRM}_{t_0} - \text{IRM}_t) / \log(t/t_0)$ (WORM, 1999) with a Variable Field Translation Balance (VFTB). Additionally, low-temperature saturation IRM (LTSIRM) warming curves were measured with an MPMS. All samples show a sharp Verwey transition (Figure 6.1) and Curie temperatures between 577 and 586°C (Table 6.1). The grain size of the samples is also reflected in the LTSIRM plot, where the magnitude of the change in magnetisation at the Verwey transition increases with increasing grain size. This dependence is valid up to a grain size of $\approx 10\mu\text{m}$ (HEIDER ET AL., 1992). The grain size dependence might also be an artefact caused by a certain small degree of oxidation and thus non-stoichiometry of the samples. Due to their larger surface-to-volume ratio,

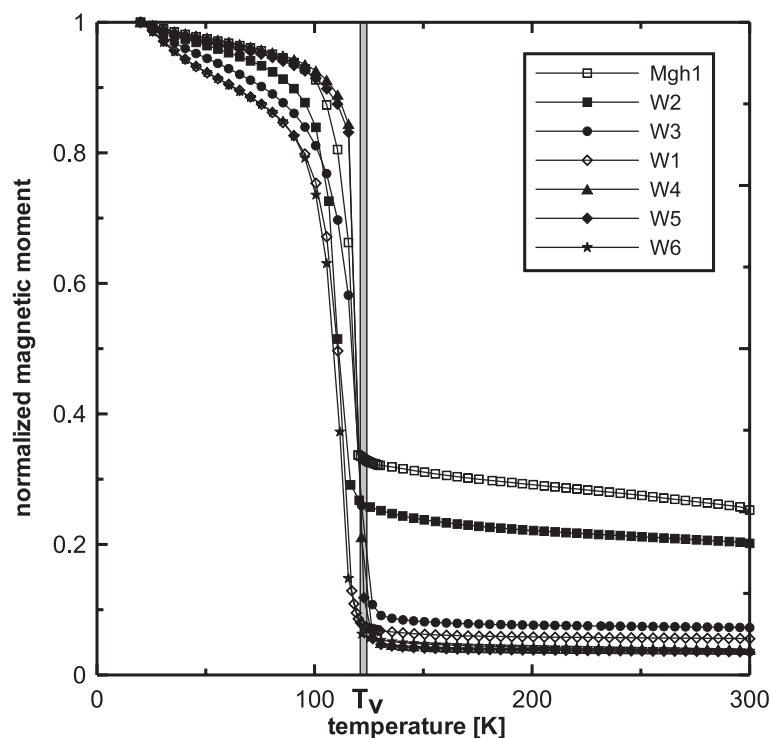


Figure 6.1: Low-temperature SIRM warming curves of the synthetic samples. T_V marks the temperature interval of the Verwey transition for pure magnetite (MUXWORTHY, 1999). T_V of the samples shows only minor deviations probably due to a small degree of maghemitisation.

smaller grains will be affected to a higher extent by oxidation than larger grains. However, the small deviations of T_V from the value of pure stoichiometric magnetite (120–124 K, MUXWORTHY (1999)) for all samples imply that the degree of oxidation is negligible.

Although having a grain size in the SD range, sample MGH1 shows a M_{RS}/M_S ratio well below the theoretical value of 0.5 for uniaxial anisotropy. This might either be due to particle interactions caused by incomplete separation of the grains or to a certain content of superparamagnetic (SP) grains (DUNLOP, 2002). As a rough estimate, published data from WORM (1999) shows that for a significantly decreased M_{RS}/M_S ratio (below 0.4) caused by SP grains, S_d/IRM exceeds 7%. In contrast to WORM (1999) who used an IRM acquired at 78 mT, the decay of *saturation* IRM (SIRM) was determined in the present work. This results in a considerably larger decay coefficient according to WORM (1999). For the samples

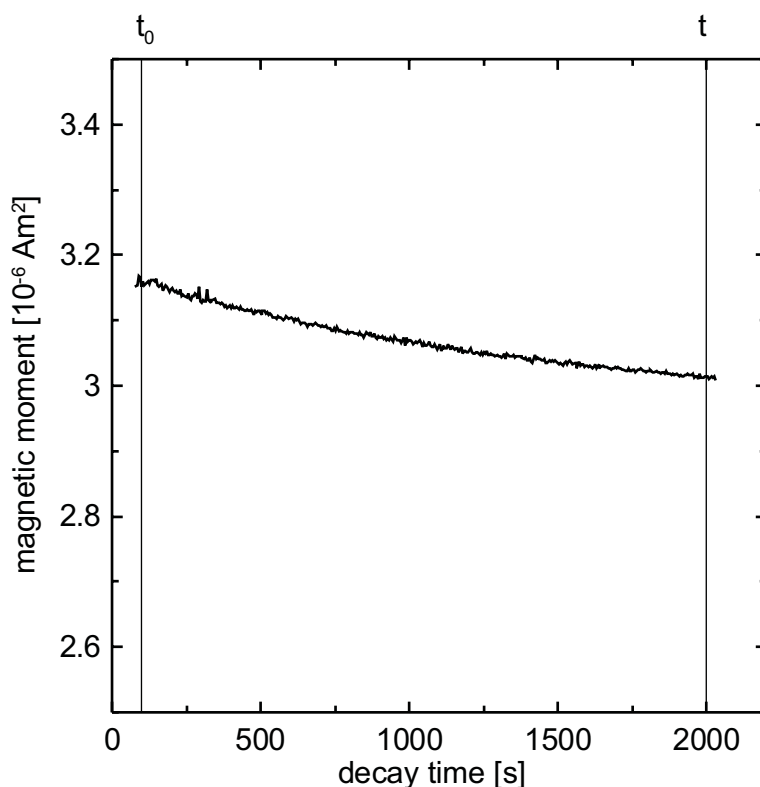


Figure 6.2: Viscous decay curve of SIRM at room temperature for sample W1 with the highest value of $S_d/\text{SIRM} = 3.6\%$. $S_d = (\text{IRM}_{t_0} - \text{IRM}_t) / \log(t/t_0)$ was calculated with $t_0 = 100$ s and $t = 2000$ s (vertical lines).

used in this study however, the maximum S_d/SIRM never rises above 3.6 % (Table 6.1 and Figure 6.2). This value is even lower than the above mentioned threshold for the IRM(78 mT) viscous decay. Thus, it can be concluded that incomplete grain separation is the main cause for the reduced $M_{\text{RS}}/M_{\text{S}}$ ratio in the grain size range of sample MGH1 and that the contribution of SP particles can be neglected.

For this investigation the modified THELLIER AND THELLIER (1959) experiment after COE (1967) with additional tail checks after MCCLELLAND AND BRIDEN (1996) referred to as MT3 (LEONHARDT ET AL., 2000) was used. In order to check the additivity of two certain pTRMs* an additional demagnetisation step is introduced: In the course of the Thellier-Thellier experiment the two pTRMs* (pTRM*(T_1, T_0) and pTRM*(T_2, T_0) with $T_1 > T_2$ and T_0 : room

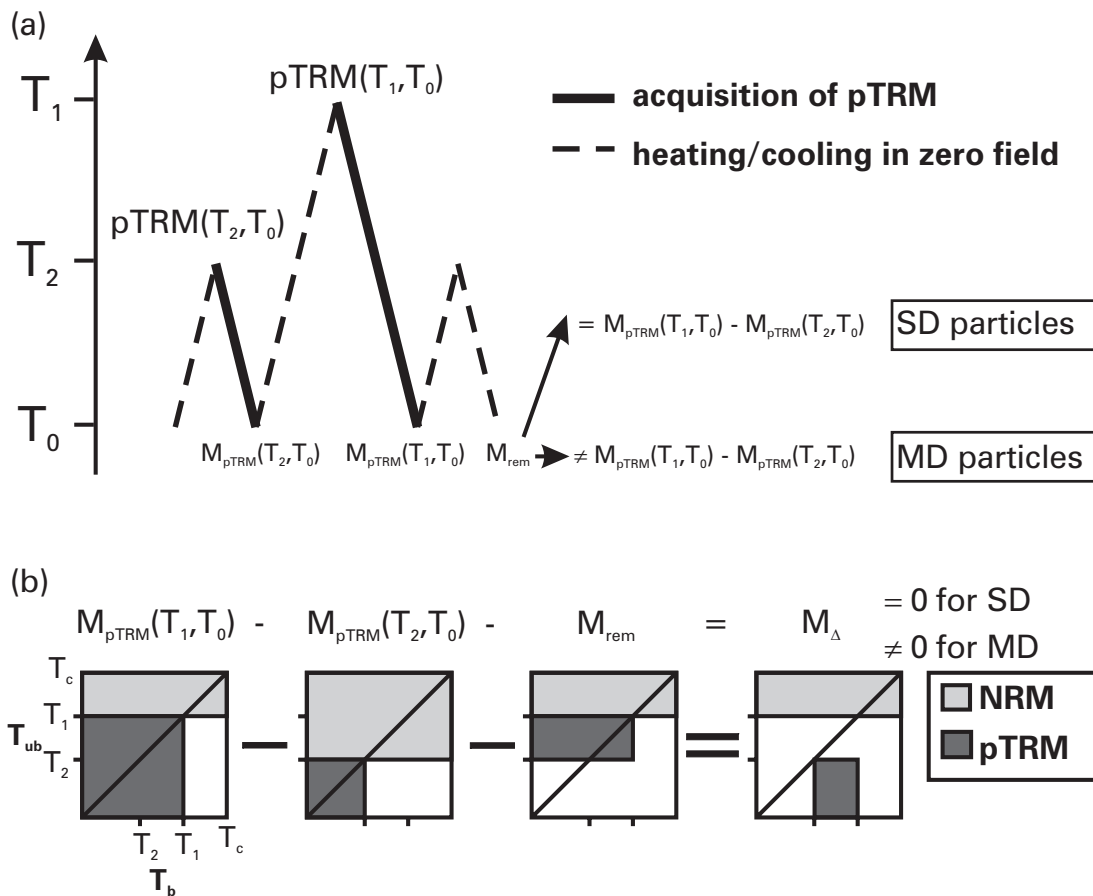


Figure 6.3: Scheme of the proposed additivity check. (a) Sketch of the experimental procedure. (b) Diagram equation of the proposed additivity check using the phenomenological representation of FABIAN (2000). The equation shows that the additivity check error M_{Δ} is only caused by remanences with $T_{\text{ub}} < T_b$. See text for further details.

temperature) are imparted on the sample. The acquired pTRM*(T_1, T_0) is then partly demagnetised by heating in zero field up to temperature $T_2 < T_1$ and the remaining remanence M_{rem} is measured. If the law of additivity is valid, then $M_{\text{rem}} = M_{\text{pTRM}}(T_1, T_0) - M_{\text{pTRM}}(T_2, T_0)$ is fulfilled. In case of MD remanence, the remaining remanence will be less than the difference of the two separate pTRMs*. The value of deficiency is referred to as M_{Δ} .

Figure 6.3 visualises the procedure by using the phenomenological model of FABIAN (2000). Failure of the test in the case of MD remanence is caused by MD

particles having an unblocking temperature T_{ub} below their respective blocking temperature T_b . The procedure is not sensitive to particles with $T_{ub} > T_b$. However, DUNLOP AND ÖZDEMİR (2000) showed that there is a symmetry of high- T_{ub} and low- T_{ub} tails in MD magnetite, i.e. the distribution function of unblocking temperatures $f(T_{ub})$ has always a high- T as well as a low- T tail. Moreover, only remanences with $T_{ub} < T_b$ cause a non-linearity in the NRM-TRM plots (FABIAN, 2001).

For potentially self-reversing samples T_1 and T_2 should lie in the T_b range of the high- T_C and low- T_C phase, respectively. In this case, measurement of $pTRM^*(T_2, T_0)$ will yield the remanence value for the low- T_C phase magnetised in H_{ext} direction and after acquisition of $pTRM^*(T_1, T_0)$ both phases will be magnetised parallel to H_{ext} . In the subsequent AC step up to T_2 the low- T_C phase will be demagnetised and, in the absence of a H_{ext} , will acquire a reversed remanence during cooling due to the coupling to the high- T_C phase. Thus, the measured M_{rem} should be substantially smaller than the difference $M_{pTRM}(T_1, T_0) - M_{pTRM}(T_2, T_0)$. In this study three different values for T_1 (340°C, 500 °C and 610 °C) and 220 °C for T_2 were used for the experiments on various basalt samples.

6.3 Results

The results of the Thellier-Thellier experiments are shown in Figure 6.4 and Table 6.2. The NRM-TRM plots include the pTRM checks and the additivity checks (AC) which are displayed in an analogous manner. As the remaining remanence M_{rem} after the AC step should equal the difference between $pTRM^*(T_1, T_0)$ and $pTRM^*(T_2, T_0)$, the measured M_{rem} is plotted as a filled square and a horizontal line starting at $pTRM^*(T_1, T_0)$. The length of this line represents the value of M_{rem} .

The sample MGH1 shows the expected behaviour for SD samples: A linear NRM-TRM plot, positive tail checks and also positive ACs. The pTRM checks confirm that no alterations have occurred. All other samples show a varying degree of concave curvature of the NRM-TRM plots potentially causing erroneous palaeointensity estimates. According to FABIAN (2001) this curvature is caused

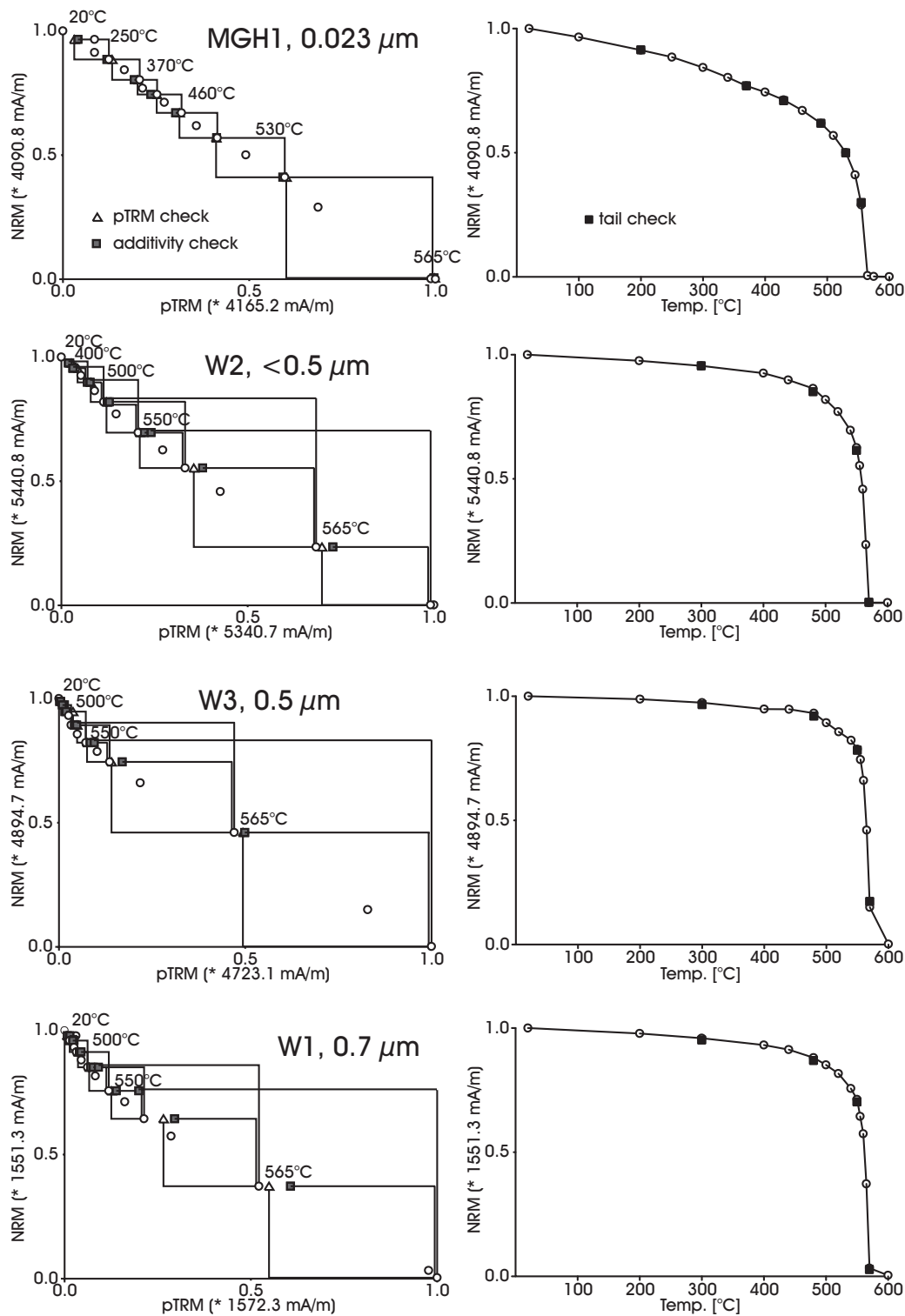


Figure 6.4: Results of the Thellier experiments. Each additivity check is plotted as a filled square and a horizontal line starting at $pTRM^*(T_1, T_0)$. The value of M_{rem} is represented by the length of this horizontal line. MGH1 and W1 to W6 are synthetic samples, Olby 1S is a basalt sample exhibiting partial self-reversal. (*continued on next page*)

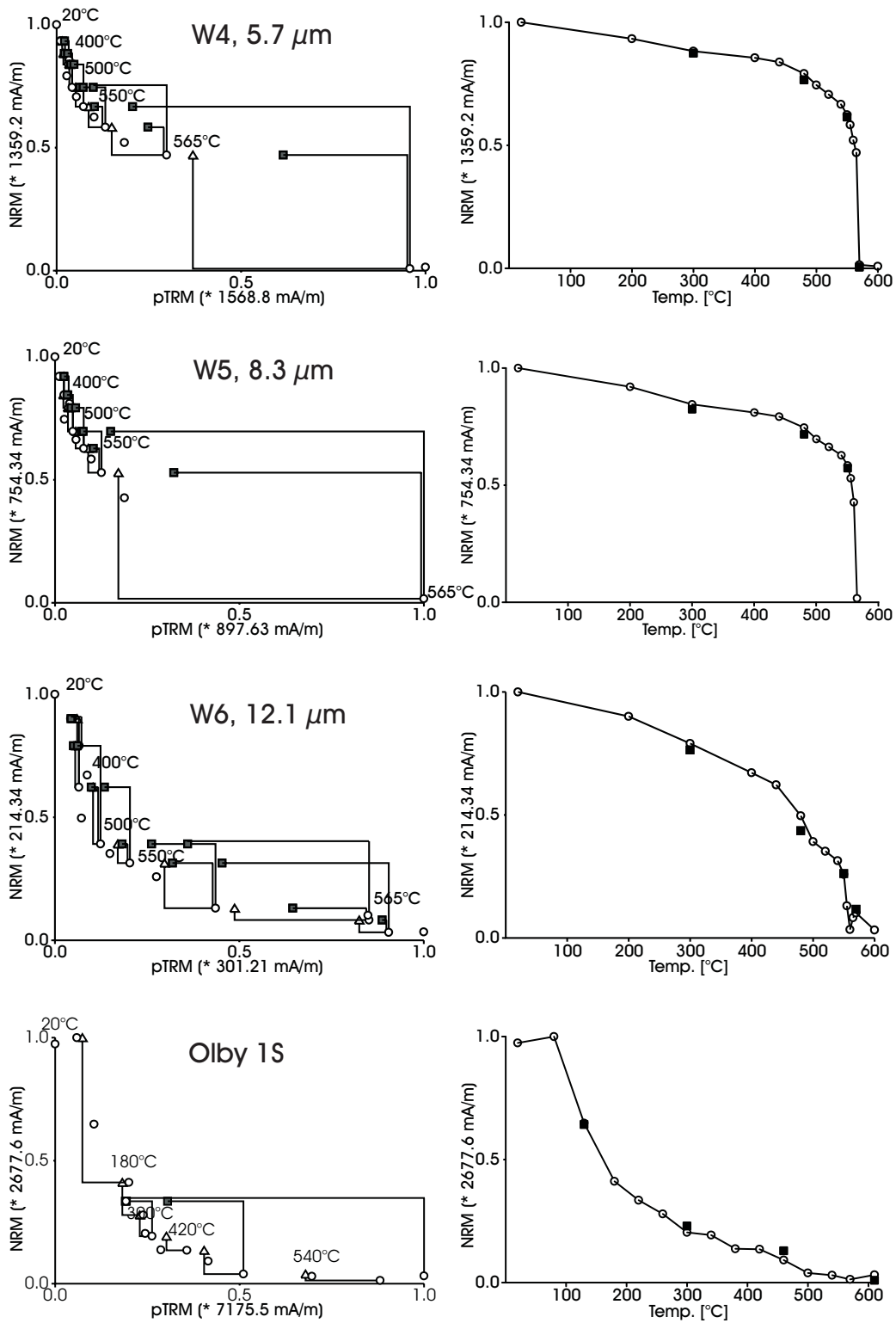


Figure 6.4: (continued)

Table 6.2: Results of the palaeointensity experiment.

sample	max. AC error M_{Δ} [%]	max. pTRM check error [%]	max. tail check error [%]	TRM [mA/m]	NRM [mA/m]	Q_{nt} error [%]	$\Delta F/F$ [%]
Synthetic samples							
MGH1	1.6	1	0.97	4133	4091	-1.0	1.6
W2	3.1	2	1.3	4968	5441	8.7	7.0
W3	3.7	2	2.3	4413	4895	9.8	8.4
W1	9.2	5	1.2	1475	1551	4.9	12.0
W4	27.8	7	2.6	1361	1359	-0.15	35.0
W5	16.4	5	3	825	754	-9.4	48.2
W6	21.3	10	6.1	222	214	-3.7	66.9
Basalt samples							
V25-5	8.6	18	9.2	3634	740	–	–
O-1C	18.1	9	3.9	6511	4715	–	–
O-1K	17.4	9	0.99	5772	7850	–	–
O-1R	27.4	13	3.4	5450	3991	–	–
O-1S	32.2	17	3.8	5438	2678	–	–

AC error and pTRM check error are normalised to the total TRM, the tail check error is normalised to the NRM. The TRM value is the magnetisation after the last pTRM acquisition step and after correction of the pTRM check error with the method of VALET ET AL. (1996). This correction was also carried out before calculating the AC error. Q_{nt} error indicates the deviation from the expected KOENIGSBERGER (1936) ratio Q_{nt} of 1. The last column shows the deviation of the palaeointensity estimate from the expected value of 60 μ T determined on the near linear high-temperature part of the NRM/TRM plot.

by remanences having a $T_{ub} < T_b$. As already mentioned in the previous section, these remanences also cause failure of the AC.

Only sample W6 with the largest grain size shows a tail check error exceeding the threshold of 5% of the NRM given by LEONHARDT ET AL. (2000). Despite sealing them in evacuated quartz glass tubes, *Wright* samples show a certain degree of chemical alteration as can be seen from the pTRM checks. This error seems to increase with increasing grain size and is largest in the case of sample W6 (10% of total TRM), in the case of the other samples it never exceeds 7%. This dependence on grain size might be caused by the fact, that thermal stabilisation by heating the samples takes longer for larger grains. A pTRM check error indicates that alteration of existing or the formation of new particles with a T_b in

the temperature range of the pTRM check took place. This does not only affect the acquired remanence but also the loss of remanence during the AC. Thus, the ACs are also biased by chemical alteration. In order to determine the true AC error, the data were corrected for alteration by the method of VALET ET AL. (1996) using the pTRM check errors.

The ACs show no significant deviations for sample MGH1 confirming the law of additivity for the SD sample. The rest of the samples displays AC errors which are increasing with grain size.

From the basalt sample set, six samples were excluded due to their strong viscous overprint. The remaining five samples with a single directional component show a concave curvature in the NRM-TRM plots as is also seen for the synthetic MD samples. Representative data for the basalt samples is shown in Figure 6.4 (sample O-1S). All samples show high pTRM check errors of 9% or more. After performing the VALET ET AL. (1996) alteration correction the samples display AC errors between 8.6 and 32.2%. However, in some cases M_{rem} is larger than $M_{\text{pTRM}}(T_1, T_0) - M_{\text{pTRM}}(T_2, T_0)$ after pTRM check correction especially for $T_1 = 610^\circ\text{C}$. This is in contradiction to the above discussed theory whereupon both in the case of MD behaviour as well as partial self-reversal M_{rem} should always be smaller than the difference of the two pTRMs*. The results indicate that during thermal treatment a new magnetic phase develops in the upper blocking temperature range between 500°C and 610°C . In contrast, the magnetic mineralogy in the low- T_b interval seems not to change during heating above 500°C . The AC should in that case match the pTRM*($220^\circ\text{C}, 0^\circ\text{C}$) value without correction for the high-temperature alteration. However, as the blocking temperature range of newly formed magnetominerals in most cases can not be determined unequivocally, the results on basalts show, that the VALET ET AL. (1996) correction has to be used with care. Strictly spoken, it can only be applied, if the temperature interval covered by the additivity check and the pTRM check are identical.

6.4 Conclusions

A modified Thellier-Thellier experiment is introduced here. When tested on synthetic samples carrying a laboratory thermoremanent magnetisation, it shows that the proposed additivity check is capable of identifying remanence carried by multidomain particles. A palaeointensity determination for samples W1, W4, W5 and W6 using the low-temperature or high-temperature part of the NRM-TRM plot would yield a significantly too high or too low palaeointensity estimate, respectively (Table 6.2). The result for sample W1 implies that already PSD sized particles can cause wrong palaeointensity estimates due to failure of the law of additivity. The measurements on basalt samples from this study exhibiting partial self-reversal indicate, that samples displaying this peculiar phenomenon can be identified by the additivity check and can be excluded from further interpretation. The efficiency of the test was also shown for natural samples from the Siberian Trap Basalts by HEUNEMANN ET AL. (2003).

In the case of chemical alterations the data can under certain circumstances (matching AC and pTRM check intervals) be corrected using the method of VALET ET AL. (1996). In this case the ACs have to match the respective pTRM values after check correction to yield a positive result. However, the reliability of palaeointensity estimates obtained by this correction method is limited as the unblocking and blocking temperature spectra of newly formed or destroyed remanence carriers are generally not known.

In the absence of chemical alteration or after correction for alteration the KOENIGSBERGER (1936) ratio ($Q_{nt} = \text{NRM}/\text{TRM}$) yields correct palaeointensity estimates for the synthetic samples within an error margin of maximum 10% (Table 6.2). This was already shown in the numerical approach to Thellier-Thellier experiments by FABIAN (2001).

Sample W1 is the sample with the smallest grain size where the error of a palaeointensity estimate in the near linear part of the NRM-TRM plot in the temperature interval between 550 °C and 600 °C exceeds 10%. As this sample shows a maximum AC error of 9.2% of total TRM, a value of 7% as the limit for a positive AC is proposed here. If the check error exceeds this threshold, palaeointensity estimates will suffer from significant errors.

The failure of the pTRM tail check to detect MD behaviour for all samples apart from sample W6 can be attributed to the fact, that pTRM* has a much smaller tail than a regular pTRM as already discussed in section 6.1.

Chapter 7

Summary

One of the main goals of current palaeomagnetic research is the attempt to acquire high-resolution data on palaeodirections *and* -intensities in order to obtain detailed information about the Earth's magnetic field in the geological past. The material best suited for such studies are basaltic rocks. For these high-quality directional investigations and especially for palaeointensity determinations, a profound knowledge about the stability, magnetomineralogical character and the domain state of the carriers of remanence is imperative.

The emphasis of the present work was placed on the investigation of basalts exhibiting partial self-reversal of natural remanent magnetisation (NRM). This phenomenon is not an exotic rarity but a widespread characteristic of many basaltic rocks. However it remains usually unnoticed by routine palaeomagnetic measurements as it requires special techniques for its detection.

In a first step, a large number of basaltic rocks was screened for the occurrence of partial self-reversal. The only way to detect this phenomenon unequivocally is the continuous measurement of the temperature dependence of natural remanent magnetisation at elevated temperatures. Then, for the following detailed investigation, samples exhibiting partial or (in some cases) complete self-reversal were selected. These originate from Olby (France), where self-reversal has been shown to occur by HELLER (1980), and from a flow of the Vogelsberg volcanics (Germany).

The magnetomineralogy of these samples was studied by rock magnetic methods as well as microscopic and microanalytical techniques. As a novel method in rock magnetism, magnetic force microscopy (MFM) was applied for investigations of the magnetic microstructure of the ore grains. This technique provides a spatial resolution and sensitivity hitherto unattainable by classical domain imaging methods.

The peculiarities of remanence acquisition of self-reversing samples were analysed by imparting laboratory induced thermoremanent magnetisations (TRM) and comparing their demagnetisation behaviour to that of the NRM.

On the basis of the experimental work a numerical model was developed which shows that, from the physical point of view, the observed magnetomineralogy is capable of causing self-reversal.

The present work provides new insights into the mechanisms and magnetomineralogical prerequisites of partial and complete self-reversal:

- The phenomenon is caused by two magnetic phases with different blocking temperatures T_b which are magnetically coupled. The lower T_b corresponds to the primary titanomagnetite (mother phase) crystallising from the basaltic magma. The remanence with higher T_b is carried by titanomaghemite (daughter phase) evolving from the primary titanomagnetite by partial low-temperature oxidation. The daughter phase forms narrow bands ($\approx 5\mu\text{m}$ wide) along cracks in the otherwise unaffected mother phase particles. This yields a close side-by-side assemblage of titanomagnetite and titanomaghemite with markedly different magnetic properties in one and the same grain. By applying the various microscopic techniques on identical grains, it was possible to directly correlate magnetomineralogy with magnetic domain structure.
- Numerical calculations of remanence acquisition demonstrate that two-phase particles with the experimentally observed geometry and magnetic properties are able to acquire a partially or completely self-reversed remanent magnetisation. This proves that the two magnetic phases present in the studied samples are coupled by magnetostatic interaction.

- The experimental results indicate that the low-temperature oxidation process responsible for the formation of the second magnetic phase takes place at temperatures at or above the T_b of this daughter phase during primary cooling. This titanomaghemite phase is thus carrying a stable remanence in direction of the ambient magnetic field. Although the original titanomagnetite as the mother phase is in a strict sense the primary magnetic mineral, it does not carry the primary magnetic remanence but is at least in part magnetostatically coupled to the titanomaghemite. Therefore, its remanence is – at least in part – antiparallel to the external field.
- MFM domain observations present evidence that the mother phase is in the magnetic multidomain range. Hence, its magnetic remanence is not stable and is replaced by a viscous overprint acquired at ambient temperatures. In contrast, the daughter phase has a higher coercivity due to oxidation induced stresses and an increased domain width.

Regarding the samples from Olby, these magnetomineralogical investigations directly lead to new arguments in favour of the existence of the Laschamp geomagnetic event: As the high- T_b daughter phase carries a stable remanence in direction of the external magnetic field, the local geomagnetic field direction was indeed reversed at the time of emplacement in contrast to the conclusions of HELLER AND PETERSEN (1982a,b).

Due to their complex magnetomineralogy and remanence acquisition, samples exhibiting partial or complete self-reversal are not suitable for palaeointensity determinations. In order to identify and exclude such samples in the course of such experiments, a modification of the existing THELLIER AND THELLIER (1959) method is proposed. Additionally, this new procedure is also able to detect remanence carried by multidomain (MD) particles. The method substantially improves the reliability and quality of palaeointensity estimates as multidomain behaviour is among the most common reasons for erroneous results in Thellier-type palaeointensity determinations.

Bibliography

- AGABEKOV, V. A. AND METALLOVA, V. V., 1972. Partial Self-Reversal of Partial Thermoremanent Magnetization in Natural Titanomagnetites. *Izv. Phys. Solid Earth*, 3:44–49.
- AMBATIELLO, A. AND SOFFEL, H. C., 1996. Kerr Microscopy of Small Synthetic Ti-Rich Titanomagnetite Grains. *Geophys. Res. Lett.*, 23(20):2807–2810.
- ANGENHEISTER, G. AND TURKOWSKY, C., 1964. Die Verteilung der induzierten und natürlichen remanenten Magnetisierung innerhalb einiger Basaltlagen des Vogelsberges. *Boll. Geofis. Teor. ed Appl.*, 6:285–295.
- APPEL, E. AND SOFFEL, H. C., 1984. Model for the Domain State of Ti-Rich Titanomagnetites. *Geophys. Res. Lett.*, 11:189–192.
- APPEL, E. AND SOFFEL, H. C., 1985. Domain State of Ti-Rich Titanomagnetites Deduced from Domain Structure Observations and Susceptibility Measurements. *J. Geophys.*, 56:121–132.
- APPEL, E., 1987. Stress Anisotropy in Ti-Rich Titanomagnetites. *Phys. Earth Planet. Int.*, 46:233–240.
- BANERJEE, S. K., 1966. Exchange Anisotropy in Intergrown Magnetite and Hematite. *Geophys. J. R. astr. Soc.*, 10:449–450.
- BJERREGAARD, L., GEELS, K., OTTESEN, B. AND RÜCKERT, M., 1992. *Metallurgy Guide*. Struers A/S, Rødovre, 3. ed.
- BOL'SHAKOV, A. S., DASHEVSKAYA, D. M. AND MEL'NIKOV, B. N., 1973. Partial Self-Reversal of the Magnetization in Kovdor Magnetites. *Izv. Phys. Solid Earth*, 6:103–109.

- BONHOMMET, N. AND BABKINE, J., 1967. Sur la présence d'aimantations inversées dans la Chaîne des Puys. *C.R. Acad. Sc. Paris*, 264:92–94.
- BONHOMMET, N. AND ZÄHRINGER, J., 1969. Paleomagnetism and Potassium Argon Age Determinations of the Laschamp Geomagnetic Polarity Event. *Earth Planet Sci. Lett.*, 6:43–46.
- BUDDINGTON, A. AND LINDSLEY, D., 1964. Iron-Titanium Oxide Minerals and Synthetic Equivalents. *J. Petrol.*, 5:310–357.
- CARMICHAEL, I. S. E. AND NICHOLLS, J., 1967. Iron-Titanium Oxides and Oxygen Fugacities in Volcanic Rocks. *J. Geophys. Res.*, 72(18):4665–4687.
- COE, R. S., 1967. The Determination of Paleointensities of the Earth's Magnetic Field with Emphasis on Mechanisms Which Could Cause Non-Ideal Behavior in Thellier's Method. *J. Geomag. Geoelec.*, 19:157–179.
- CREER, K. M., PETERSEN, N. AND PETHERBRIDGE, J., 1970. Partial Self-Reversal of Remanent Magnetization and Anisotropy of Viscous Magnetization in Basalts. *Geophys. J. R. astr. Soc.*, 21:471–483.
- CREER, K. M. AND PETERSEN, N., 1969. Thermochemical Magnetization in Basalts. *Z. Geophys.*, 35:501–516.
- DAY, R., FULLER, M. AND SCHMIDT, V. A., 1977. Hysteresis Properties of Titanomagnetites: Grain-Size and Compositional Dependence. *Phys. Earth Planet. Int.*, 13:260–267.
- DUNLOP, D. AND ÖZDEMİR, Ö., 1997. *Rock Magnetism: Fundamentals and Frontiers*. Cambridge Studies in Magnetism. Cambridge University Press, Cambridge.
- DUNLOP, D. AND ÖZDEMİR, Ö., 2000. Effect of Grain Size and Domain State on Thermal Demagnetization Tails. *Geophys. Res. Lett.*, 27(9):1311–1314.
- DUNLOP, D., 2002. Theory and Application of the Day Plot (M_{RS}/M_S Versus H_{CR}/H_C) 1. Theoretical Curves and Tests Using Titanomagnetite Data. *J. Geophys. Res.*, 107(B3):EPM 4–1–EPM 4–22.

- FABIAN, K., KIRCHNER, A., WILLIAMS, W., HEIDER, F., LEIBL, T. AND HUBER, A., 1996. Three-Dimensional Micromagnetic Calculations for Magnetite Using FFT. *Geophys. J. Int.*, 124:89–104.
- FABIAN, K., 2000. Acquisition of Thermoremanent Magnetization in Weak Magnetic Fields. *Geophys. J. Int.*, 142:478–486.
- FABIAN, K., 2001. A Theoretical Treatment of Paleointensity Determination Experiments on Rocks Containing Pseudo-Single or Multi Domain Magnetic Particles. *Earth Planet Sci. Lett.*, 188:45–58.
- GALLAGHER, K. J., FEITKNECHT, W. AND MANNWEILER, U., 1968. Mechanism of Oxidation of Magnetite to γ -Fe₂O₃. *Nature*, 217:1118–1121.
- HAAG, M., HELLER, F., ALLENSPACH, R. AND ROCHE, K., 1990a. Self-Reversal of Natural Remanent Magnetization in Andesitic Pumice. *Phys. Earth Planet. Int.*, 65:104–108.
- HAAG, M., HELLER, F. AND ALLENSPACH, R., 1988. Magnetic Interaction in Self-Reversing Andesitic Pumice in Relation to Iron Alloys. *J. de Phys.*, 49(12):2065–2066.
- HAAG, M., HELLER, F., CARRACEDO, J. C. AND SOLER, V., 1990b. Remanent Magnetization of Andesitic and Dacitic Pumice from the 1985 Eruption of Nevado Del Ruiz (Colombia) Reversed Due to Self-Reversal. *J. Volcanol. Geotherm. Res.*, 41:369–377.
- HALGEDAHL, S. L., 1987. Domain Pattern Observations in Rock Magnetism: Progress and Problems. *Phys. Earth Planet. Int.*, 46(1-3):127–163.
- HALL, J. M., 1977. Does TRM Occur in Oceanic Layer 2 Basalts? *J. Geomag. Geoelec.*, 29:411–419.
- HARGRAVES, R. AND PETERSEN, N., 1971. Notes on the Correlation between Petrology and Magnetic Properties of Basaltic Rocks. *Z. Geophys.*, 37:367–382.
- HAVARD, A. D. AND LEWIS, M., 1965. Reversed Partial Thermo-Magnetic Remanence in Natural and Synthetic Titanomagnetites. *Geophys. J. R. astr. Soc.*, 10:59–68.

- HEIDER, F., DUNLOP, D. J. AND SOFFEL, H. C., 1992. Low-Temperature and Alternating Field Demagnetization of Saturation Remanence and Thermoremanence in Magnetite Grains (0.37 μm to 5 mm). *J. Geophys. Res.*, 97:9371–9381.
- HELLER, F., MARKERT, H. AND SCHMIDBAUER, E., 1979. Partial Self-Reversal of Natural Remanent Magnetization of an Historical Lava Flow of Mt. Etna (Sicily). *J. Geophys.*, 45:235–257.
- HELLER, F. AND PETERSEN, N., 1980. Self-Reversal of NRM in the Basalts from Olby and Laschamp (Auvergne, France). *Geophys. J. R. astr. Soc.*, 61(1):212–212.
- HELLER, F. AND PETERSEN, N., 1982a. The Laschamp Excursion. *Phil. Trans. R. Soc. Lond.*, 306:169–177.
- HELLER, F. AND PETERSEN, N., 1982b. Self-Reversal Explanation for the Laschamp/Olby Geomagnetic Field Excursion. *Phys. Earth Planet. Int.*, 30:358–372.
- HELLER, F., 1980. Self-Reversal of Natural Remanent Magnetization in the Olby-Laschamp Lavas. *Nature*, 284:334–335.
- HEUNEMANN, C., KRÁSA, D., GUREVITCH, E. L., SOFFEL, H. C. AND BACHTADSE, V., 2003. Directions and Intensities of the Earth's Magnetic Field During a Reversal: Results from the Permo-Triassic Siberian Trap Basalts, Russia. *Earth Planet Sci. Lett.*, submitted.
- HOFFMANN, V., SCHÄFER, R., APPEL, E., HUBERT, A. AND SOFFEL, H., 1987. First Domain Observations with the Magneto-Optical Kerr Effect on Ti-Ferrites in Rocks and Their Synthetic Equivalents. *J. Magn. Magn. Mat.*, 71(1):90–94.
- KAKOL, Z., SABOL, J. AND HONIG, J. M., 1991a. Cation Distribution and Magnetic Properties of Titanomagnetites $\text{Fe}_{3-x}\text{Ti}_x\text{O}_4$ ($0 \leq x < 1$). *Phys. Rev. B*, 43:649–654.

- KAKOL, Z., SABOL, J. AND HONIG, J. M., 1991b. Magnetic Anisotropy of Titanomagnetites $\text{Fe}_{3-x}\text{Ti}_x\text{O}_4$, $0 \leq x \leq 0.55$. *Phys. Rev. B*, 44:2198–2204.
- KLERK, J., BRABERS, V. A. M. AND KUIPERS, A. J. M., 1977. Magnetostriction of the Mixed Series $\text{Fe}_{3-x}\text{Ti}_x\text{O}_4$. *J. de Phys.*, 38(C-1):87–189.
- KNELLER, E., 1962. *Ferromagnetismus*. Springer, Berlin, Göttingen, Heidelberg.
- KOENIGSBERGER, J. G., 1936. Die Abhängigkeit der natürlichen remanenten Magnetisierung bei Eruptivgesteinen von deren Alter und Zusammensetzung. *Beitr. Angew. Geophys.*, 5:193–246.
- KRÁSA, D., HEUNEMANN, C., LEONHARDT, R. AND PETERSEN, N., 2003. Experimental Procedure to Detect Multidomain Remanence During Thellier-Thellier Experiments. *Phys. Chem. Earth*, 28(16–19):681–687.
- KRÁSA, D., 2002. Partial Self-Reversal of the NRM in Basalts: Identifying the Responsible Mineral Phases. *IRM Quarterly*, 12(2):3–4.
- LAWSON, C. A., NORD, JR., G. L. AND CHAMPION, D. E., 1987. Fe—Ti Oxide Mineralogy and the Origin of Normal and Reverse Remanent Magnetization in Dacitic Pumice Blocks from Mt. Shasta, California. *Phys. Earth Planet. Int.*, 46(1-3):270–288.
- LEONHARDT, R., HUFENBECHER, F., HEIDER, F. AND SOFFEL, H. C., 2000. High Absolute Paleointensity During a Mid Miocene Excursion of the Earth's Magnetic Field. *Earth Planet Sci. Lett.*, 184(1):141–154.
- MARKOV, G. P., SHCHERBAKOV, V. P., BOLSHAKOV, A. S. AND VINOGRADOV, Y. K., 1983. On the Temperature-Dependence of the Partial Thermoremanent Magnetization of Multidomain Grains. *Izv. Phys. Solid Earth*, 19(8):625–630.
- MARSHALL, M. AND COX, A., 1971. Effect of Oxidation on the Natural Remanent Magnetization of Titanomagnetite in Suboceanic Basalt. *Nature*, 230:28–31.

- MATZKA, J., KRÁSA, D., KUNZMANN, T., SCHULT, A. AND PETERSEN, N., 2003. Magnetic State of 10-40 Ma Old Ocean Basalts and Its Implications for Natural Remanent Magnetization. *Earth Planet Sci. Lett.*, 206(3-4):541–553.
- MATZKA, J., 2001. *Besondere magnetische Eigenschaften der Ozeanbasalte im Altersbereich 10 bis 40 Ma*. Ph.D. thesis, Ludwig-Maximilians-Universität, München.
- MCCLELLAND, E. AND BRIDEN, J., 1996. An Improved Methodology for Thellier-Type Paleointensity Determination in Igneous Rocks, and Its Usefulness for Verifying Primary Thermoremanence. *J. Geophys. Res.*, 101(B10):21995–22014.
- MCCLELLAND, E. AND SUGIURA, N., 1987. A Kinematic Model of TRM Acquisition in Multidomain Magnetite. *Phys. Earth Planet. Int.*, 46:9–23.
- MEIKLEJOHN, W. H. AND BEAN, C. P., 1956. New Magnetic Anisotropy. *Phys. Rev.*, 102(5):1413–1414.
- MEIKLEJOHN, W. H. AND BEAN, C. P., 1957. New Magnetic Anisotropy. *Phys. Rev.*, 105(3):904–913.
- MEIKLEJOHN, W. H. AND CARTER, R. E., 1960. Exchange Anisotropy in Rock Magnetism. *J. Appl. Phys.*, 31:164–165.
- MEIKLEJOHN, W. H., 1962. Exchange Anisotropy - a Review. *J. Appl. Phys.*, 33(3):1328–1335.
- METCALF, M. AND FULLER, M., 1987a. Domain Observations of Titanomagnetites During Hysteresis at Elevated Temperatures and Thermal Cycling. *Phys. Earth Planet. Int.*, 46(1-3):120–126.
- METCALF, M. AND FULLER, M., 1987b. Magnetic Remanence Measurements of Single Particles and the Nature of Domain Patterns in Titanomagnetites. *Geophys. Res. Lett.*, 14(12):1207–1210.
- MORIN, F. J., 1950. Magnetic Susceptibility of $\alpha\text{Fe}_2\text{O}_3$ and $\alpha\text{Fe}_2\text{O}_3$ with Added Titanium. *Phys. Rev.*, 78:819–820.

- MOSKOWITZ, B. M. AND HALGEDAHL, S. L., 1987. Theoretical Temperature and Grain-Size Dependence of Domain State in $x = 0.6$ Titanomagnetite. *J. Geophys. Res.*, 92(B10):10667–10682.
- MOSKOWITZ, B. M., 1980. Theoretical Grain Size Limits for Single-Domain, Pseudo-Single Domain and Multidomain Behavior in Titanomagnetite ($x = 0.6$) as a Function of Low-Temperature Oxidation. *Earth Planet Sci. Lett.*, 47:1285–1293.
- MUXWORTHY, A. R., 1999. Low-Temperature Susceptibility and Hysteresis of Magnetite. *Earth Planet Sci. Lett.*, 169(1-2):51–58.
- NAGATA, T., UYEDA, S. AND AKIMOTO, S., 1952. Self-Reversal of Thermo-Remanent Magnetism of Igneous Rocks. *J. Geomag. Geoelec.*, 4:22–38.
- NAGATA, T. AND UYEDA, S., 1959. Exchange Interaction as a Cause of Reverse Thermoremanent Magnetism. *Nature*, 184:890.
- NAGATA, T., 1961. *Rock Magnetism*. Maruzen Company Ltd., Tokyo, 2. ed.
- NÉEL, L., 1948. Propriétés magnétiques des ferrites; ferrimagnétisme et antiferromagnétisme. *Ann. Géophys.*, 12:137–198.
- NÉEL, L., 1949. Théorie du traînage magnétique des ferromagnétiques en grains fins avec applications aux terres cuites. *Ann. Géophys.*, 5:99–136.
- NÉEL, L., 1951. L'inversion de l'aimantation permanente des roches. *Ann. Géophys.*, 7:90–102.
- NÉEL, L., 1955. Some Theoretical Aspects of Rock Magnetism. *Advances Phys.*, 4:191–243.
- O'REILLY, W., 1984. *Rock and Mineral Magnetism*. Blackie, Glasgow, London.
- ÖZDEMİR, Ö. AND DUNLOP, D. J., 1985. An Experimental Study of Chemical Remanent Magnetizations of Synthetic Monodomain Titanomaghemites with Initial Thermoremanent Magnetizations. *J. Geophys. Res.*, 90(B13):11513–11523.

- ÖZDEMİR, Ö. AND O'REILLY, W., 1982. Magnetic Hysteresis Properties of Synthetic Monodomain Titanomaghemites. *Earth Planet Sci. Lett.*, 57(2):437–447.
- OZIMA, M. AND FUNAKI, M., 2003. Hemoilmenite as a Carrier of SRTRM in Dacitic Pumice from Akagi, Ontake and Sambe Volcanoes, Japan. *Earth Planet Sci. Lett.*, 213(3-4):311–320.
- OZIMA, M. AND OZIMA, M., 1967. Self-Reversal of Remanent Magnetization in Some Dredged Submarine Basalts. *Earth Planet Sci. Lett.*, 3:213–215.
- PARRY, L. G., 1982. Magnetization of Immobilized Particle Dispersions with Two Distinct Particle Sizes. *Phys. Earth Planet. Int.*, 28(3):230–241.
- PETERSEN, N. AND BLEIL, U., 1973. Self Reversal of Remanent Magnetization in Synthetic Titanomagnetites. *Z. Geophys.*, 39:965–977.
- PETERSEN, N., EISENACH, P. AND BLEIL, U., 1979. Low Temperature Alteration of the Magnetic Minerals in Ocean Floor Basalts. In: Talwani, M., Harrison, C. G. A. and Hayes, D. (Eds.), *Deep Drilling Results in the Atlantic Ocean: Ocean Crust*, vol. 2 of *Maurice Ewing Series*, pp. 169–209. American Geophysical Union, Washington.
- PETERSEN, N. AND VALI, H., 1987. Observation of Shrinkage Cracks in Ocean Floor Titanomagnetites. *Phys. Earth Planet. Int.*, 46:197–205.
- PETERSEN, N., 1976. Notes on the Variation of Magnetization within Basalt Lava Flows and Dikes. *Pageoph*, 114:177–193.
- PETHERBRIDGE, J., CAMPBELL, A. L. AND HAUPTMAN, Z., 1974. Magnetic Behaviour of Some Partially Unmixed Titanomagnetites. *Nature*, 250:479–480.
- PETHERBRIDGE, J., 1977. A Magnetic Coupling Occuring in Partial Self-Reversal of Magnetism and Its Association with Increased Magnetic Viscosity in Basalts. *Geophys. J. R. astr. Soc.*, 50:395–406.
- PETROVA, G. N. AND TRUKHIN, V. I., 1961. Spontaneous Changes in H_C of Particular Cycles of Magnetization Observed During Cooling of Ferromagnetic Minerals. *Izv. Phys. Solid Earth*, 6:584–588.

- PRÉVOT, M., HOFFMAN, K. A., GOGUITCHAICHVILI, A., DOUKHAN, J.-C., SHCHERBAKOV, V. AND BINA, M., 2001. The Mechanism of Self-Reversal of Thermoremanence in Natural Hemoilmenite Crystals: New Experimental Data and Model. *Phys. Earth Planet. Int.*, 126:75–92.
- RAMDOHR, P., 1955. *Die Erzminerale und ihre Verwachsungen*. Akademie-Verlag, Berlin.
- READMAN, P. W. AND O'REILLY, W., 1972. Magnetic Properties of Oxidized (Cation-Deficient) Titanomagnetites (Fe,Ti,□)₃O₄. *J. Geomag. Geoelec.*, 24(1):69–90.
- RIISAGER, J. AND RIISAGER, P., 2001. Detecting Multidomain Magnetic Grains in Thellier Paleointensity Experiments. *Phys. Earth Planet. Int.*, 125:111–117.
- ROBERTS, A. P., CUI, Y. L. AND VEROSUB, K. L., 1995. Wasp-Waisted Hysteresis Loops - Mineral Magnetic Characteristics and Discrimination of Components in Mixed Magnetic Systems. *J. Geophys. Res.*, 100(B9):17909–17924.
- RUGAR, D., MAMIN, H. J., GUETHNER, P., LAMBERT, S. E., STERN, J. E., MCFADYEN, I. AND YOGI, T., 1990. Magnetic Force Microscopy - General Principles and Application to Longitudinal Recording Media. *J. Appl. Phys.*, 68(3):1169–1183.
- RYALL, J. C. AND ADE-HALL, J. M., 1975. Laboratory-Induced Self Reversal of Thermoremanent Magnetization in Pillow Basalts. *Nature*, 257:117–118.
- RYALL, P. J. C., HALL, J. M., CLARK, J. AND MILLIGAN, T., 1977. Magnetization of Oceanic Layer 2 — Results and Thoughts after DSDP Leg 37. *Can. J. Earth Sci.*, 14:684–706.
- SCHMIDT, P. W. AND CLARK, D. A., 1985. Step-Wise and Continuous Thermal Demagnetization and Theories of Thermoremanence. *Geophys. J. R. astr. Soc.*, 83(3):731–751.
- SCHÖNENBERGER, C. AND ALVARADO, S. F., 1990. Understanding Magnetic Force Microscopy. *Z. Phys. B – Condensed Matter*, 80:373–383.

- SCHULT, A., 1968. Self-Reversal of Magnetization and Chemical Composition of Titanomagnetites in Basalts. *Earth Planet Sci. Lett.*, 4(1):57–63.
- SCHULT, A., 1976. Self-Reversal above Room Temperature Due to N-Type Magnetization in Basalt. *J. Geophys.*, 42:81–84.
- SHASHKANOV, V. A. AND METALLOVA, V. V., 1972. Violation of Thellier's Law for Partial Thermoremanent Magnetization. *Izv. Phys. Solid Earth*, 8:180–184.
- SHCHERBAKOVA, V. V., SHCHERBAKOV, V. P. AND HEIDER, F., 2000. Properties of Partial Thermoremanent Magnetization in Pseudosingle Domain and Multidomain Magnetite Grains. *J. Geophys. Res.*, 105(B1):767–781.
- SHCHERBAKOV, V. P., MCCLELLAND, E. AND SHCHERBAKOVA, V. V., 1993. A Model of Multidomain Thermoremanent Magnetization Incorporating Temperature-Variable Domain Structure. *J. Geophys. Res.*, 98:6201–6216.
- SHCHERBAKOV, V. P. AND SYCHEVA, N. K., 2001. Numerical Modeling of the Domain Structure in Magnetite grains of Submicron Sizes. *Izv. Phys. Solid Earth*, 37(4):334–344.
- SHCHERBAKOV, V., SHCHERBAKOVA, V., VINOGRADOV, Y. AND HEIDER, F., 2001. Thermal Stability of pTRMs Created from Different Magnetic States. *Phys. Earth Planet. Int.*, 126:59–73.
- SOFFEL, H. AND PETERSEN, N., 1971. Ionic Etching of Titanomagnetite Grains in Basalts. *Earth Planet Sci. Lett.*, 11:312–316.
- SOFFEL, H., 1966. Stress-Dependence of the Domain Structure of Natural Magnetite. *Z. Geophys.*, 32:63–77.
- STEPHENSON, A., 1975. The Observed Moment of a Magnetized Inclusion of High Curie Point within a Titanomagnetite Particle of Lower Curie Point. *Geophys. J. R. astr. Soc.*, 40:29–36.
- SYONO, Y., 1965. Magnetocrystalline Anisotropy and Magnetostriction of $\text{Fe}_3\text{O}_4\text{--Fe}_2\text{TiO}_4$ Series, with Special Application to Rock Magnetism. *Jap. J. Geophys.*, 4:71–143.

- TAUXE, L., MULLENDER, T. A. T. AND PICK, T., 1996. Potbellies, Wasp-Waists, and Superparamagnetism in Magnetic Hysteresis. *J. Geophys. Res.*, 101(B1):571–583.
- TAUXE, L., 1998. *Paleomagnetic Principles and Practice*, vol. 17 of *Modern Approaches in Geophysics*. Kluwer Academic Publishers, Dordrecht, Boston, London.
- TAYLOR, R. W., 1964. Phase Equilibria in the System FeO-Fe₂O₃-TiO₂ at 1300 °C. *Am. Mineral.*, 49:1016–1030.
- TEPLYAKOV, V. V., ZVEGINTSEV, A. G. AND ZHESTKOVA, L. I., 1973. Magnetic Properties of Synthesized Titanomagnetites. *Izv. Phys. Solid Earth*, 9:108–110.
- THELLIER, E. AND THELLIER, O., 1959. Sur l'intensité du champ magnétique terrestre dans le passé historique et géologique. *Ann. Géophys.*, 15(3):285–376.
- THOUVENY, N. AND CREER, K. M., 1992. Geomagnetic Excursions in the Past 60 ka: Ephemeral Secular Variation Features. *Geology*, 20(5):399–402.
- TUCKER, P. AND O'REILLY, W., 1980. Reversed Thermoremanent Magnetization in Synthetic Titanomagnetites as a Consequence of High Temperature Oxidation. *J. Geomag. Geoelectr.*, 32:341–355.
- UYEDA, S., 1958. Thermo-Remanent Magnetism as a Medium of Palaeomagnetism, with Special Reference to Reverse Thermo-Remanent Magnetism. *Jap. J. Geophys.*, 2:1–123.
- VALET, J.-P., BRASSART, J., LE MEUR, I., SOLER, V., QUIDELLEUR, X., TRIC, E. AND GILLOT, P.-Y., 1996. Absolute Paleointensity and Magnetomineralogical Changes. *J. Geophys. Res.*, 101(B11):25029–25044.
- VERNET, G., RAYNAL, J. P., FAIN, J., MIALLIER, D., MONTRET, M., PILLEYRE, T. AND SANZELLE, S., 1998. Tephrostratigraphy of the Last 160 ka in Western Limagne (France). *Quaternary International*, 47-8:139–146.

- VERWEY, E. J., 1939. Electronic Conduction of Magnetite (Fe_3O_4) and Its Transition Point at Low Temperature. *Nature*, 144:327–328.
- WIMMENAUER, W., 1974. The Alkaline Province of Central Europe and France. In: Sørensen, H. (Ed.), *The Alkaline Rocks*, pp. 238–271. John Wiley & Sons, London, New York, Sydney, Toronto.
- WORM, H. U., 1999. Time-Dependent IRM: A New Technique for Magnetic Granulometry. *Geophys. Res. Lett.*, 26(16):2557–2560.
- WRIGHT, T. L. AND WEIBLEN, P. W., 1968. Mineral Composition and Paragenesis in Tholeiitic Basalt from Makaopuhi Lava Lake, Hawaii (Abstract). *Geological Society of America - Special Paper*, 115:242.
- ZIJDERVELD, J. D. A., 1967. A. C. Demagnetization of Rocks: Analysis of Results. In: Collinson, D. W., Creer, K. M. and Runcorn, S. K. (Eds.), *Methods in Palaeomagnetism*, pp. 254–286. Elsevier, Amsterdam, New York.

Acknowledgements

First of all, I would like to thank my supervisors Nikolai Petersen and Thomas Kunzmann for their advice and guidance throughout the thesis and their encouragement to present and publish my results. Nikolai Petersen stimulated my interest in the field of magnetic petrology and his door was always open for questions of all kinds. Thomas Kunzmann was patient enough to guide me through the wonders and mysteries of microprobe analysis.

Heinrich Soffel is thanked for his advice and helpful suggestions on magnetic domain imaging.

Thanks are due to Axel Schult who provided me with many insights into the phenomenon of self-reversed magnetisation.

I very much appreciated working together with Valera Shcherbakov. His knowledge about micromagnetic theory and numerical calculations was indispensable for the theoretical part of this work.

I am indebted to Friedrich Heller, who provided the samples from Olby and Laschamp and gave me the opportunity to perform low-temperature measurements in the Zürich laboratory.

Karl Fabian is thanked for many inspiring discussions on the nature of multidomain thermoremanences.

Special thanks are given to Christoph Heunemann, Jürgen Matzka, Roman Leonhardt, Maria Antretter, Alexander Zwing, Jenny Tait, and Valerian Bach-tadse and all other members of the "Munich Gang" for many fruitful discussions during and after work hours. I appreciate, that all of you are not just stimulating colleagues but also great friends. Thank you, Christoph, for two unforgettable field trips into the wilderness of northern Siberia.

H. Reichl, A. Mayer, G. Hesberg, A. Hornung, H. Spitzfaden and H. Khek are doing an indispensable job in transforming hardly decipherable draft sketches into working instruments. Many thanks to all of them. I would also like to thank Manuela Weiss for keeping the laboratory in Niederlippach in such a good shape. Frau Schröer is thanked for their constant patience and help in solving administrative puzzles.

I thank Riccarda Wagner and Yannik Behr for performing some of the laboratory measurements.

The MFM observations and some of the rock magnetic measurements were done in the course of a visiting fellowship at the Institute of Rock Magnetism (IRM) in Minneapolis. Sincere thanks to all of the IRM staff for their continuous support during my stay. The IRM is funded by the Keck Foundation, the National Science Foundation and the University of Minnesota.

Part of the MFM observations was also carried out at the Institute of Experimental Physics, University of Saarbrücken. I would like to thank Jiandong Wei for his help with the measurements.

Many thanks to my parents for their constant support and interest in my work.

Finally, I would like to express my thanks to Kathinka for her patience and support.

This project was funded by the Deutsche Forschungsgemeinschaft (DFG) in the framework of the priority programme "Geomagnetic variations" (grants Pe173/12-1 & 2).

Curriculum Vitae

17. Juli 1974 geboren in Neustadt a. d. Waldnaab als viertes Kind von Marie und Dr. Zdeněk Krása
- Sept. 80 bis Sept. 84 Besuch der Grundschule Parkstein
- Sept. 84 bis Sept. 91 Besuch des Gymnasiums in Neustadt a. d. Waldnaab
- Sept. 91 bis Juli 93 Besuch des Kepler-Gymnasiums in Weiden/Opf.
- Juli 93 Erwerb der allgemeinen Hochschulreife
- Nov. 93 bis Jan. 00 Studium der Geophysik an der Ludwig-Maximilians-Universität München (LMU)
- Nov. 96 Erwerb des Vordiploms in Geophysik
- März 98 und Apr. 98 Praktikum bei der Firma Western Geophysical in London, GB
- Januar 00 Erwerb des Diploms in Geophysik
 Titel der Diplomarbeit: "Gesteinsmagnetische, röntgen-diffraktometrische und mikroskopische Untersuchungen zum Oxidationsmechanismus von Titanomagnetiten in Ozeanbasalten", Betreuer: Prof. Dr. N. Petersen
- Jan. 00 bis März 00 wissenschaftliche Hilfskraft am Institut für Geophysik der LMU im Rahmen des DFG-Projekts So72/63-2
- seit April 00 wissenschaftlicher Angestellter am Institut für Geophysik der LMU im Rahmen des DFG Schwerpunktprogramms "Erdmagnetische Variationen", Thema: "Palaeointensity measurement of the Earth's magnetic field and partial self-reversal of natural remanent magnetization of basalts" (Pe173/12-1 & 2)
- März 02 Visiting Fellowship zum Thema "Partial self-reversal of the NRM in basalts: Identifying the responsible mineral phases" am Institute for Rock Magnetism der Universität von Minnesota, Minneapolis, USA